

THE STUDY OF THE LOWER IONOSPHERE AT LOW LATITUDE

Thesis

Presented by

S.P.GUPTA

to the

Gujarat University Ahmedabad

for the Ph.D. degree.

043



B3717

Physical Research Laboratory

Ahmedabad - 9.

January 1970

STATEMENT

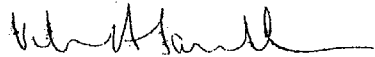
The work presented in this thesis is based on the results obtained from the rocket borne Langmuir probe and plasma noise probe studies over Thumba near geomagnetic equator. Working under the guidance of Prof.V.A.Sarabhai and Prof.Satya Prakash at the Physical Research Laboratory, the author was responsible for the design and development of the plasma noise probe that was employed to study the fluctuations in Langmuir probe current which is termed as plasma noise in the thesis. The necessary telemetry system which includes subcarrier oscillators and band pass filters as per I.R.I.G. specifications was developed by the author. A spectrum analyser was also developed to study the spectrum of the observed plasma noise. The author also made improvements in the Langmuir probe system.

The author took active part in extensive testing and checking of the Langmuir probe and plasma noise probe system prior to launching. He was also responsible for analysing the data and interpreting the experimental results.

The Langmuir probe was employed to determine the electron density and electron temperature while the plasma noise probe was used to study the Langmuir probe current fluctuations with amplitudes as low as 0.05% in the frequency range 70 Hz to 1 KHz. Fluctuations with frequencies less than 70 Hz can be studied directly from the telemetry record of the Langmuir probe current. These measurements of ionospheric irregularities have been interpreted in terms of processes taking place in the equatorial

ionosphere. Many conclusive results have come out from the present study.

The results presented in the thesis contain probably the first in situ measurements of equatorial E region irregularities with scale sizes of the order of a few meters. They also contain probably the first systematic in-situ measurements of disturbances created in the medium by a moving rocket. It is believed that ion acoustic waves are generated in the wake of a vehicle moving through the ionosphere, but so far no in-situ measurements were available. The present results therefore provide fresh insights into plasma instabilities in the equatorial ionosphere and the disturbances produced by the rocket.


Prof. V.A. Sarabhai
Director
Physical Research Laboratory
Navrangpura
Ahmedabad-9

S. P. Gupta
S. P. Gupta
Author

January 24, 1970

ACKNOWLEDGEMENT

The author is indebted deeply to Professor Satya Prakash for the guidance, supervision and encouragement, he gave throughout the period of the work. Prof.V.A.Sarabhai took keen interest in guidance and gave valuable advice for which author expresses sincere gratitude to him.

It is a great privilege to thank Prof.K.R.Ramanathan and Prof.F.R.Pisharoty for valuable discussions and suggestions. Thanks are due to Dr.B.H.Subbaraya for going through the manuscript of the thesis and suggesting many improvements.

Sincere thanks are expressed to Mr.H.G.S. Murthy, Director, Thumba Equatorial Rocket Launching Station and his colleagues Messrs A.P.J.Abdul Kalam, R.Aravamudan, D.Easwardas, P.P.Kale, B.Ramakrishna Rao and G.Madhavan Nair whose enthusiastic cooperation made rocket launchings successful. The author is also thankful to Dr.B.V.Krishnamurthy for providing ionograms.

Acknowledgements are also due to National Aeronautics and Space Administration, U.S.A. for supplying the Nike-Apache rockets. Thanks are also due to Atomic Energy Commission, Government of India and Indian National Committee for Space Research for financial assistance. The author is very grateful to Ministry of Education, Government of India for the award of a scholarship.

It is a particular pleasure to express gratitude to Messrs N.S. Savalgi for preparing payload circuitry, R.I. Patel for his help in data analysis, and C.L.Gajjar for making mechanical parts of the payload.

S.P. Gupta
S.P. GUPTA.

LIST OF CONTENTS

Chapter I

Introduction

1.1	The equatorial D region.	2
1.2	The equatorial E region.	3
1.3	The equatorial electrojet.	4
1.4	Electric field in the equatorial E region.	6
1.5	Equatorial electrojet irregularities.	7
1.6	Necessity of the present study.	8

Chapter II

Production Mechanisms of equatorial electrojet irregularities.

2.1	The cross-field instability.	19
2.2	The two stream instability.	21
2.3	Plasma turbulence.	24

Chapter III

Experimental techniques. Theory of Langmuir probe and Plasma noise probe.

3.1	Ground based techniques.	30
3.2	Rocket and satellite borne techniques.	32
3.3	Langmuir probes used for ionospheric studies.	33
3.4	Theory of Langmuir probe.	34
3.5	Electron temperature from first derivative of Langmuir probe characteristic.	40

3.6	Langmuir probe for ionospheric studies.	41
3.7	Small scale irregularities measurement by Plasma noise probe.	45
3.8	Theory of Plasma noise probe.	46
3.9	Sampling of irregularities by moving rocket.	47
3.10	Environmental conditions around the moving rocket.	51
3.11	Production of disturbances in Plasma by moving rocket.	53

Chapter IV

Instrumentation

4.1	The conventional Langmuir Probe system.	55
4.2	The present system.	57
4.3	Description of the Langmuir Probe and Plasma noise probe.	59
4.4	Electrode Geometry.	60
4.5	Probe electronics.	61
4.6	Sweep circuit.	62
4.7	Electrometer amplifier.	65
4.8	Plasma noise amplifier.	70
4.9	Electronic differentiation of Langmuir Probe characteristic.	72
4.10	Subcarrier Oscillator.	72
4.11	Power supply.	75
4.12	Spectrum analyser.	76
4.13	Wiring of the payload circuits.	76
4.14	Dotting of the payload.	77
4.15	Telemetry requirements.	78

4.16	Mounting and fixing of the payload and probe.	80
4.17	Pre-launch testing.	81

Chapter V

Experimental results

Summary of Langmuir Probe and Plasma noise probe flights.

5.1	Nike - Apache 10.11	85
5.2	Nike - Apache 10.13	91
5.3	Nike - Apache 20.07	96
5.4	Nike - Apache 20.08	97

Chapter VI

Discussion of experimental results.

6.1	Ionisation irregularities	100
6.2	Summary of the results	108
6.3	Discussion	110
6.4	Irregularities due to rocket motion.	123
6.5	Equatorial D region electron density.	127
6.6	The equatorial E-region during afternoon hours.	129
6.7	The equatorial E region during evening twilight.	129
6.8	The E region over Thumba around mid-night	131
6.9	Electron temperature in the equatorial E region.	134

Chapter VII

Summary and conclusions

138

References

i to viii

List of Figures

		<u>Page</u>
Figure 1	Simplified picture of one mode of operation of the instability.	20 (a)
Figure 2	Typical Langmuir Probe characteristic.	36 (a)
Figure 3	Schematic representation of the sampling process of irregularities by moving rocket. Lines indicate the irregularity wave fronts while arrow indicates the rocket.	48
Figure 4	Schematic representation of the disturbed regions in the vicinity of the moving bodies of various shapes From Alpert 1965)	53 (a)
Figure 5	Contact Potential versus time after launch for day and night flights.	53 (b)
Figure 6	Rocket borne Langmuir Probe system (a) Conventional system (b) Present system.	56 (a)
Figure 7	Functional diagram of the Langmuir and Plasma noise probe system.	58 (a)
Figure 8	Nose tip electrode photograph.	61 (a)
Figure 9	Block diagram of sweep generator.	62
Figure 10	Circuit diagram of sweep generator.	63 (a)
Figure 11	Various wave forms at different terminals of the sweep circuit.	64 (a)
Figure 12	Block diagram of 100% current feedback amplifier.	66
Figure 13	Electrometer amplifier circuit.	67 (a)
Figure 14	Zero marker and resistance to Thyrite switching circuit.	68 (a)
Figure 15	Calibration curves of electrometer amplifier	70 (a)

Figure 16	Plasma noise probe amplifier circuit.	70 (b)
Figure 17	Phase inverter and detector circuit.	71 (a)
Figure 18	Subcarrier Oscillator circuit.	73 (a)
Figure 19	Input voltage versus frequency curve of Subcarrier Oscillator	74 (a)
Figure 20	Characteristic curve of band-pass filter.	
Figure 21	Voltage regulator circuit.	75 (b)
Figure 22	Plasma noise probe data recording system using spectrum analyser.	76 (a)
Figure 23	Response curve of spectrum analyser.	76 (b)
Figure 24	Photograph of wired circuit.	77 (a)
Figure 25	Photograph of Langmuir probe and Plasma noise probe layload.	77 (b)
Figure 26	Installation of Langmuir Probe, Plasma noise probe and Telemetry system in a Nike-Apache rocket.	80 (a)
Figure 27	Integrated payload block diagram.	81 (a)
Figure 28	Control box for monitoring the payload from block house.	81 (b)
Figure 29	Sketch diagram of nose tip electrode.	85 (a)
Figure 30	Electron density profile for evening flight 10.11.	89 (a)
Figure 31	A semilog plot of electron current versus probe voltage.	89 (b)
Figure 32	Electron temperature for evening flight 10.11.	89 (c)
Figure 33	Percentage fluctuations in probe current for evening flight 10.11.	91 (a)

Figure 34	Electron density profile for evening flight 10.13.	94 (a)
Figure 35	Percentage fluctuations in probe current in frequency range 70 Hz to 1 KHz.	95 (a)
Figure 36	Amplitude of irregularities in various scale sizes in arbitrary units.	95 (b)
Figure 37	Typical curve for log - log plot of percentage amplitude and frequency for Plasma noise.	96 (a)
Figure 38	Spectral index values for flight 10.13.	96 (b)
Figure 39	Electron density profile for mid-day flight 20.07.	97 (a)
Figure 40	Electron temperature for mid-day flight 20.07.	97 (b)
Figure 41	Percentage fluctuations in probe current in frequency range 70 Hz to 1 KHz for mid-day flight 20.07.	98 (a)
Figure 42	Electron density profile for mid-night flight 20.08.	98 (b)
Figure 43	Electron temperature for mid-day night flight 20.08.	98 (c)
Figure 44 a)	Percentage fluctuations in (30-300 meters scale size,) probe current and electron density, (ascent) profile for flight 20.08.	99 (a ₁)
b)	Percentage fluctuations in (30-300 meters scale size) probe current and electron density, (descent) profile for flight 20.08.	99 (a ₂)
Figure 45	Percentage fluctuations in probe current in frequency range 70 Hz to 1 KHz for flight 20.08.	99 (b)
Figure 46	Spectral index values for flight 20.08.	99 (c)

Figure 47 (a)	Telemetry record obtained at 87 Km.	103 (a)
Figure 47 (b)	Telemetry record obtained at 96 Km.	104 (a)
Figure 47 (c)	Telemetry record obtained at 171 Km.	104 (b)
Figure 48 (a)	Spectrum analyser output record at 87 Km.	105 (a)
Figure 48 (b)	Spectrum analyser output record at 96 Km.	105 (b)
Figure 48 (c)	Spectrum analyser output record at 171 Km.	124 (a)

CHAPTER - I

INTRODUCTION

The equatorial ionosphere has many characteristic features some of which arise due to the presence of the earth's magnetic field which is nearly horizontal. The author has studied some of the special features of lower region of the equatorial ionosphere i.e upto 180 kms.

The lower ionosphere is mainly due to the ionisation of the neutral particles through ultraviolet radiations, X-rays and particle radiations from the sun and the cosmic rays. Near the equator only particles with energies greater than 15 Bev can reach the lower ionosphere and hence the equatorial ionosphere is mainly due to ultraviolet radiations and X-rays from the sun. This makes the interpretation of the phenomena occurring near the equator much easier than that at high latitude.

The interaction of charged particles with the horizontal magnetic field leads to various geomagnetic and ionospheric phenomena, unique to this region. The enhanced conductivity at 100 km associated with the special magnetic field configuration at the equator results in a strong daytime equatorial electrojet current. Even during night time when electron density is comparatively very small a weak current flows in the reverse direction. In the equatorial E-region we encounter various types of plasma instabilities

which are difficult to simulate in the laboratory. This region can be effectively used to study some of the plasma instabilities not yet detected and explored.

The author has carried out a study of equatorial D and E regions over Thumba using a modified Langmuir probe. A plasma noise probe was developed to make in situ measurements of irregularities of sizes as low as 1.0 meter in the D and E regions of the ionosphere. Amplitudes as low as 0.05% were measured for small scale irregularities in the range 1 meter to 15 meters. This enables the study of irregularities spectrum. Some of these irregularities in scale size of 3 meters have been studied by other workers using backscatter techniques at Jicamarca, Peru, near the magnetic equator.

The following describes some of the important features of the lower ionosphere near the vicinity of the equator.

1.1 The equatorial D region: It is usually considered the lowest portion of the ionosphere and ranges in altitude from about 50 to 85 km. The region below 60 km is sometimes called the C region because of its cosmic ray origin. Over equator the C region is almost absent due to a large reduction in the high energy particle flux. In the D region the motion of the electrons is dominated by collisions with neutral particles giving rise to a large radiowave absorption. This absorption provides a powerful tool for making measurements

of the D region electron density by radiowave technique. It is generally believed that during solar quiet period the ionisation in the D region is produced due to ionisation of nitric oxide by Lyman alpha (1216 \AA). However, during periods of increased solar activity the flux of kilo volt X-rays ($2-8 \text{ \AA}$) increases by an order of magnitude, while the Lyman alpha flux remains essentially constant. Above some level of activity it can be expected that the production of D region ionisation by solar X-rays will exceed the Lyman alpha nitric oxide contribution. At any given time however it is difficult to evaluate the relative importance of these two ionising sources because the nitric oxide concentration is not known with certainty.

1.1.1 D-region irregularities: D region irregularities have been observed by Clemsha (1963) during day light hours. As the neutral density is very large compared to electron density the dynamical properties of D region irregularities are governed by the motion of neutral constituents. Clemsha has observed that between 80 to 90 km altitude region there is no tendency for field alignment while there is a slight tendency for field alignment above 90 km. These irregularities are discussed in detail in the Chapter II.

1.2 The day time equatorial E region: The E region extends from 85 to 150 km. Unlike D region the radio wave absorption in this region is low as the collision frequency

of electron with neutrals is small. In E-region the electron density follows closely the $(\cos \gamma)^{\frac{1}{2}}$ law where γ is the solar zenith angle and is called a Chapman layer.

The equatorial E layer is similar to that of temperate latitude E region except the presence of electrojet current. The electrojet gives rise to irregularities which are not observed in the mid-latitudes. These irregularities are responsible for non blanketing type equatorial Es (Bowles and Cohen 1962).

1.2.1 The night time equatorial E region: During the night time the E region electron density as high as 10^4 ele/cc have been observed both over the coast of Peru (Aikin and Blumle, 1968) and over Thumba (Satya Prakash et al 1970) in the height range 95 to 115 km. A valley in 120 km region with electron density around 10^2 - 10^3 ele/cc has also been observed. Such high electron densities around 100 km can't be explained on the basis of scattered Lyman α and Lyman β radiations (Ogawa et al 1966).

1.3 The equatorial electrojet: The equatorial electrojet is an enhanced current system within a narrow belt of a few degrees of the geomagnetic latitude. This enhanced current arises due to enhanced electrical conductivity in the 100 km region. In the presence of a primary east-west electric field and horizontal magnetic field directed northward, a vertical polarisation field is set up due to the disparity between the

electron and ion mobilities. This polarization field known as Hall field is responsible for enhanced conductivity.

The westward drift of electrons during day time is believed to reverse the direction during night time. The experimental evidence of the night time flow direction was given by Balsley (1966, 1969 a, b).

During the early periods the primary experimental evidence for the existence of the equatorial current system was obtained from the observations of daily variation in the earth's magnetic field by ground based magnetometers, situated in the vicinity of geomagnetic equator. The direct measurements of the electrojet were carried out by Singer et al (1959) using rocket borne magnetometers. The extensive measurements for the vertical, latitudinal and longitudinal behaviour of the electrojet were carried out by many workers, [Maynard^{& Cahill} (1965), Davies et al (1966), Sastry (1968)]. Recent measurement of the current density at the height of maximum flow is $\approx 5 \text{ amp/km}^2$ over Thumba and $\approx 10 \text{ amp/km}^2$ over the coast of Peru.

1.3.1 Equatorial electrojet model: Suguira and Cain (1966) derived the electrojet model as the difference of current which will explain the deviations from the normal magnetic field. This is expressed in terms of 48 coefficients and the corresponding Legendre terms. Other related parameters being taken from standard atmospheric models.

The value of primary east-west electric field was calculated to be 2.4 mv/meter. In addition to that they have shown that conductivity values for Indian zone is lesser by 60% to that of American zone. This may explain the observed current density which is nearly twice over American zone as compared to Indian zone if it is assumed that primary east-west field is same for both the places.

Various problems of Sq current systems and the equatorial electrojet have been reviewed by Onwumechill (1967). It was thought earlier that the electrojet is a simple intensification of the world wide Sq current system, near the geomagnetic equator. Recently OGBENI et al (1967) have shown that all the experimental results can't be explained by this model of electrojet.

Untiedt (1967) introduced a model of equatorial electrojet involving meridional currents. This model yields stronger currents and gives larger width of electrojet compared to previous models.

1.4 The electric field in the equatorial E region: The electric field around 100 km altitude have been estimated from the measurement of the horizontal drift velocity of irregularities embedded in the equatorial electrojet (Balsley 1967, 1969 b). Balsley suggests that during certain period the velocity of the irregularities is a measure of electron drift velocity which in turn can be related to the east-west

electric field through the following expression given by Sugaira and Cain,

$$E_y \simeq -10^{-6} V_e, \text{ Volts/meter} \quad 1$$

A drift velocity V_e of electrons of the order of 300 m/sec will correspond to an electric field $E_y = 0.3 \text{ m V/m}$.

The observations of Balsley (1969 b) show that during the night time the electron drift velocity is comparable to those during the day time and is of the order of 300 m/sec. This favours the theoretical calculation of Maeda et al (1963), that the driving electric field has comparable magnitude during the day time and night time. Although the direction of the field during the night time is opposite to that during the day time.

The electric field measurements carried out over Thumba around 200 km altitude during evening twilight using Barium cloud technique. Haerendal et al (1968) gives the value of about 0.5 mv/meter for east-west field and 2.8 mv/meter for vertical field.

1.5 The equatorial electrojet irregularities: It has been realised for some time that certain scatter echo configurations noted on conventional ionograms near the vicinity of the equator were associated with the electrojet current variations, (Matshushita 1962). These configurations are due to irregularities embedded in the electrojet and are known as equatorial 'sporadic E'.

The irregularities of sizes 3 meters have been studied by backscatter radar at Jicamarca (dip 1°N). Rocket borne Langmuir probes and plasma noise probe were flown over Thumba to make in situ measurements. The sizes studied lie in the range 1.0 to 15 meters (Satya Prakash et al 1968, 1969 a*, 1969 b, 1970). As shown by backscatter radar study, these irregularities have been found to be associated with field aligned plane waves having their wave fronts oriented parallel to magnetic field lines and velocity vector perpendicular to it, (Cohen and Bowles 1967).

These waves are presumed to be of small amplitude, so that many waves moving in variety of directions and having a variety of wave lengths could be present in the same volume simultaneously. The density amplitudes of the order of 3% has been estimated by Weinstoke (1968) from the coherent backscatter measurements from these irregularities.

Two types of irregularities are known to exist in the equatorial electrojet (Balsley 1967). Type one which occurs when electron drift velocity exceeds the ion thermal velocity. Farley (1963) developed two stream instability theory to explain their production mechanism. While the type two exist during most of the periods.

1.6 Necessity of the present study: Many of the phenomena in the lower ionosphere over equator have not been

completely understood. Some of the features which require further study and in situ measurements are given in the following text.

In addition to those measurements carried out by rocket borne probes, it becomes necessary to study the disturbances produced by a moving rocket if the results of the in situ measurements are to be interpreted correctly.

1.6.1 The equatorial E region irregularities: The equatorial E region irregularities have been studied at Jicamarca for quite some time with backscatter radar. Only recently in situ measurements of these irregularities were made by Satya Prakash et al (1969 a) over Thumba. The radar measurements have shown that strong irregularities are present in the 100 km region most of the time. These are plane waves with their wavefronts mostly aligned along the magnetic field lines. The horizontal movements of these irregularities depend on the time of the day and have been observed to be in westward direction during day while mostly in eastward direction during most of the night time, (Palsley 1969 b). The radar operating at a single frequency resolves the one Fourier component of irregularities whose sizes are about half the wavelengths of exploring e.m. wave. The above conclusions are based on the study of scale sizes of the order of 3 m. The irregularities of

different scale sizes can't be studied by the radar technique, as many radars operating at different frequencies would be required for such a study. Even to study one scale size the backscatter technique is quite complicated. If various sizes are to be studied then the system will become too cumbersome and expensive.

The spectrum of these waves and its relationship with other ionosphere parameters has now been studied with rocket borne probes in order to examine their production mechanism. Plasma noise probe incorporated with Langmuir probe has proved very useful tool for such studies and is complementary to the backscatter radar studies. While the rocket borne plasma noise probe enables the study of the spectrum of the irregularities, the coherent backscatter radar gives the direction of the motion of irregularities and the large scale structure.

The presently known mechanisms responsible for the electrojet irregularities are the cross-field instability, the two stream instability and the plasma turbulence. The conditions and the time at which different irregularities are likely to operate are as follows.

1. The two-stream instability operates when the velocity of the stream of electrons exceeds that of the ion acoustic waves in the medium. This condition is likely

to be realized during noon hours when the electrojet current is maximum.

2. The cross-field instability requires the gradients in the electron density and electric field to be in the same direction. Such a condition can be realized both in the day time and the night time.

3. The plasma turbulence requires large shear in electron drift velocity and which can be realized during most of the time of the day as well as of night, both above and below the region where the Hall conductivity is a maximum.

The present knowledge of these irregularities is based on the ground based measurements. However in situ measurements of the secondary irregularities like those discussed in this thesis will greatly help in establishing the importance of various mechanisms responsible for the generation of these instabilities.

A few rocket borne plasma-noise probes have been flown from Thumba during different periods of the day and night. The spectrum of ionospheric irregularities have been studied by the author in the scale size $\frac{V_R}{f}$ where V_R is rocket velocity and f is the frequency, ranging from 70Hz-1KHz

1.6.2 D region irregularities: A few ground based experimental measurements suggest that D region irregularities can give rise to the scattering of V.H.F (30 MHz to 100 MHz) radio wave, (Davies 1965). Due to small electron densities in this region and relatively large absorption, the D region irregu-

larity measurement with ground based radio techniques are quite difficult. Langmuir probe and plasma noise probe are recently employed to study D region irregularities over Thumba by the author, (Satya Prakash et. al 1969 a, 1970). Thus the study of D region irregularities and their spectrum will reveal about the nature of forces responsible for D region irregularities and will indirectly help in locating the region where such forces are operative.

1.6.3 The equatorial E region: Unlike the study of the E region at high latitude the study of the equatorial E region can't be carried out with the conventional ground based techniques. This is mainly due to the presence of the equatorial type of E_s for most of the time of the day and night. The in situ measurements are therefore necessary for the study of E region.

One of the problems which still remains unsolved is the night time source of ionization for the E region. Electron densities as high as 10^4 electrons/cc around 105 km have been observed both at high latitude and at equator. Also a valley around 120 km with an electron density as low as 10^2 /cc has been observed in both the regions.

These observations indicate that a similar mechanism is operative during night time hours over the equator as well as over the mid-latitude. The night time fluxes of scattered Lyman alpha and Lyman beta radiation can't account

for the observed high electron density. Vertical downward drift from the F region into the E region has also been suggested as a possible mechanism. However, this mechanism has not been studied on a quantitative basis due to lack of sufficient data (Aikin & Blumle 1968, Smith 1966, Satya Prakash et al 1970).

During evening twilight periods a valley around 125 km just starts developing and occasionally an E_2 layer is also observed around 135 km. (Satya Prakash et al 1968). The above authors pointed out that this layer is due to high electron temperatures and some more studies are necessary to establish the source of such high electron temperatures. It was also pointed out that the higher electron temperature in this region is likely to be due to electric currents present in the altitude region during evening twilight.

Electron temperature measurements over equator are very few, (Satya Prakash et al 1968 , 1969a.). Electron temperature measurements are necessary at different period of the day as well as during night to study the nature of heat sources.

1.6.4 Study of the disturbances produced by moving rocket or satellite: The interaction of a moving body ^{with} a low density plasma (ionosphere) needs to be studied if the results of measurements by a

variety of direct measurement devices on space vehicles are to be correctly interpreted. This problem has been the subject of number of theoretical studies. On the other hand, ground based measurements of these irregularities have yet been carried out. Singer and Walker(1965) Alpert et al(1965) have carried out theoretical investigation of the effects produced by moving rocket or satellite in the earth's ionosphere. However, no adequate theory is yet available which can explain the nature of these disturbances taking into account the rocket velocity, the body potential and body dimensions. Gurvich and Titavesky (1965) have shown that in the wake region of moving satellite ion acoustic waves are generated with frequencies lying in the range $0.1\omega_e$ to $1.0\omega_e$ where ω_e is the ion plasma frequency in radians.

The first systematic measurements of these ion acoustic waves produced by a moving rocket using a Langmuir probe and plasma noise probe, in the frequency range around 1 KHz, during evening twilight hours were made in the range 155 to 175 km by Satya Prakash et al (1969 a). It is necessary to study the spectrum of these waves and thus correlate the experimental results with the existing theories, for various probe geometries and probe potentials. The author has studied the spectrum of these waves by rocket borne langmuir probes and plasma noise probes. These oscillations

were observed near rocket apogee when the probes were able to record these fluctuations due to the subsonic motion of the rocket. The results are presented in this thesis.

The study presented in this thesis is based on the following measurements carried out over Thumba using modified Langmuir probe and plasma noise probe.

- 1) D region electron density profile and irregularities during afternoon hour and evening twilight hours.
- 2) The electron density and the electron temperatures of equatorial E region at midday evening and midnight hours.
- 3) The spectrum of the electron density irregularities in the 100 km and 145 km altitude region during midday, evening and midnight.
- 4) The spectra of plasma ion acoustic waves due to disturbance from the rocket motion observed near the rocket apogee.

1.6.5 Synopsis of the thesis: The thesis is organised in 7 chapters. The first chapter describes some of the special features of equatorial ionosphere between 50 to 150 km region.

Pertinent mechanisms for the generation of equatorial electrojet irregularities are treated in Chapter II. The cross-field instability, the two-stream instability and the

plasma turbulence in a collision dominated low density magnetoionic media are treated in some detail.

In Chapter III the various techniques to study lower ionosphere are described. The basic principles of Langmuir probe in regard to the electron density and the temperature measurements are discussed. A brief review of various forms of Langmuir probe is also given. The principles of the plasma-noise probe capable of studying the irregularities of scale sizes as low as one meter and amplitude as low as 0.05% of background electron density are described. The disturbances created by moving rocket are also discussed.

Chapter IV deals with the development and instrumentation of modified Langmuir probe and Plasma noise probe. Various circuits including sweep circuit, electrometer amplifier, audio frequency amplifier, subcarrier oscillators and band-pass filters are described. The prelaunch checking and testing of the whole payload are described in detail. The results of electron density, electron temperature and Plasma irregularities are presented in Chapter V.

Chapter VI includes discussion of results described in Chapter V in relation to presently known theories. The inadequacies of the presently known theories have also been discussed. In the last Chapter VII, conclusions drawn from the above studies are presented.

CHAPTER- II

PRODUCTION MECHANISMS OF EQUATORIAL ELECTROJET IRREGULARITIES

It is now believed that the day time configuration of sporadic E echoes on equatorial ionograms is produced by electron density irregularities closely associated with electrojet. Various authors have noted that equatorial sporadic E echoes and electrojet current show a close correlation. The configuration due to sporadic E on the equatorial ionogram is so strong that the regular E layer reflections are blurred making it difficult to determine the E region electron density profile from the ionograms. V.H.F. coherent backscatter radar experiments over Jicamarca (dip 1° N) have established that there are almost always strong scattering irregularities present in the 100 km region, (Balsley 1969 a, b, Cohen et al 1962, Cohen and Bowles 1963).

The drift of the E region large scale irregularities of the order of 100 meter over Thumba have been measured during day time with the space antenna technique operating at 2.2 MHz by Deshpande and Rastogi (1966). A westward drift of about 80 meters/sec was observed during day time. There are some observations which indicate that even during twilight and night time hours large scale irregularities are present in equatorial E region. In the thesis the author calls large scale irregularities for sizes 30 to 300 meters and small scale for sizes 1 to 15 meters. An understanding of the

physical characteristics of these irregularities is important for the purpose of studying the physics of electrojet which is related to physics of ionospheric plasma. Various theories have been proposed for generation mechanism of these irregularities but none of these can explain all the observed features of the irregularities.

An ionised gas is capable of sustaining various types of oscillatory motions and waves. Both longitudinal and transverse waves can be excited in plasma by different type of instabilities. In the presence of a magnetic field hydromagnetic waves are generated whose frequencies are less than ion cyclotron frequency (Stix 1960, Sptizer 1962). In the equatorial electrojet the irregularities are generated by some kind of instability. Farley (1963) has shown that there is ample reason to believe that electrojet should generate a type of two stream instability. Such instabilities are familiar in the field of plasma physics and they lead to the spontaneous formation of one or more types of wave disturbance.

There is another type of instability called cross-field instability which was investigated theoretically by Simon (1963) for a laboratory plasma. Its possible application to the formation of sporadic E irregularities in the ionosphere has been studied by Tsuda et al (1966, 1969). Partially ionised plasmas with gradients in ionisation density

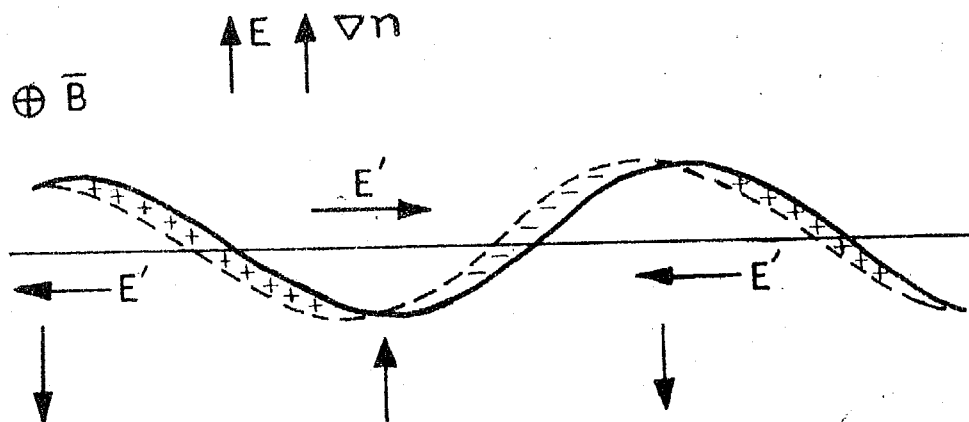
in the direction of electric field and both perpendicular to magnetic field are subject to cross field instability. The other possible cause of ionospheric irregularities may be plasma turbulence. Turbulence in neutral atmosphere between an altitude region 80 to 110 km is observed by Elamont and his group (1961). The neutral turbulence can be imparted to charged particle through collisions and can give rise to ionospheric irregularities. In the electrojet region the electron drift may give rise to plasma turbulence which may not be related to neutral gas turbulence (Balsley 1969)^C. The cross-field instability, two stream instability and plasma turbulence which may be operating in electrojet region will be discussed in detail.

2.1 Cross-field instability: Partially ionised plasma that contain a magnetic field and gradient in ionisation density are subject to a unique type of instability under the influence of an ambient electric field. This instability can give rise to growing irregularities in ionization density that are field aligned along the direction of the magnetic field. Such mechanism can be examined for ionosphere with appropriate properties. In the ionosphere the electric fields are generally present along with gradients of electron density which frequently display the presence of field aligned irregularities.

The instability was first investigated theoretically by Simon (1963) and its possible application to the formation

of sporadic E irregularities in the ionosphere has been studied by Tsude et al (1966). One mode in which the instability can operate has been discussed by Tsude et al and is illustrated in fig.1 . The horizontal line represents an unperturbed contour of constant electron density, and the steady density gradient and electric field are both directed upward. The magnetic field is directed into the paper. If now the density is perturbed by a small amplitude the $E \times B$ drifts of ions and electrons will carry them both to the left. Since the Hall mobility of the ions is always less than that of the electrons, the space charge will appear giving rise to small scale electric fields E' directed alternatively to left and right. The corresponding $E' \times B$ drifts will then carry the enhanced regions downward and the depleted regions upward, so that they both appear to grow in amplitude against the background density. Obviously, if either the electric field or the steady density gradient were reversed in direction, the perturbations would tend to disappear and we would have a stable situation. The frequencies involved in this type of instability are of the order of 10 Hz, having scale sizes about 100 meters (Tsuda et al 1969).

A different mode of operation applies if the steady electric field in above figure is directed towards the right instead of upward. The Pedersen mobilities of the ions and electrons produce same space charge potential with similar



SIMPLIFIED PHYSICAL PICTURE OF ONE MODE
OF OPERATION OF THE CROSS FIELD INSTABILITY

FIG.1

results, (Reid 1968). This mode produces large scale irregularities at greater altitudes in the ionosphere i.e spread F irregularities.

For a given gradient in background electron density and for a given value of electric field there is a lower limit for scale size of irregularities that can exist in a particular region of ionosphere. This limit is given by

$$\lambda_{\min} \propto \left(\frac{1}{\mathcal{L} E_{oz}} \right)^{\frac{1}{2}}$$

2

where $\mathcal{L} = \frac{1}{ne} \frac{\partial ne}{\partial z}$ and E_{oz} vertical polarization field.

Tsuda et al (1969) give the value of λ_{\min} for $\mathcal{L} = 1 \text{ km}^{-1}$ and $E_{oz} = 1 \text{ m.volt/meter}$. equal to 100 meters. Thus for smaller scale sizes large electric field and large \mathcal{L} are required.

2.2. The two stream instability: When a beam of electron traverses in plasma, the plasma becomes unstable and consequently wave type disturbances grow. The energy required for the growth of the wave is taken from the streaming electrons. In a collisionless plasma the instability develops if the drift velocity of the streaming electrons exceed their thermal velocity. The waves thus generated move with velocities equal to electron thermal velocity and their frequencies are of the order of electron plasma frequency (Buneman, 1959, Penrose 1960). In the presence of the magnetic field, hydromagnetic waves are generated whose frequencies are less than the ion cyclotron frequency and velocity of the order of electron thermal velocity.

A collision dominated magnetoionic plasma can develop instability if the electron drift velocity exceeds the ion thermal velocity, (Farley 1963, Buneman 1963). The waves are known as ion acoustic waves. They move with a velocity of the order of ion thermal velocity. Such conditions are satisfied in equatorial electrojet over Jicamarca during noon hours. When the drift velocity of westward drifting electrons exceed the ion thermal velocity. These are plane waves moving perpendicular to the magnetic field lines with their wavefronts aligned at various angles to the vertical.

For equatorial electrojet the general drift of electrons over Peru is of the order of 600 m/sec, while over Thumba it is only of the order of 300 m/sec. It can thus be seen that while the threshold for the two stream instability will be reached over Peru, it may not exceed over Thumba. Therefore it will be worth confirming whether the type I irregularities are present over Indian zone. The above value for the general drift of electrons has been derived from the formula $J = n_e e v_e$ where n_e is electron density and v_e drift velocity, J current density and e electronic charge. The value of J over Peru has been measured and found to be 10 Amp/km² while over Thumba 5 Amp/km². The electron density for both the places was found to be of the order of 10^5 ele/cc

(Davis et al 1966, Aikin and Blumle 1968, Maynard and Cahill 1965, Satya Prakash et al 1970).

The irregularities of this type have been studied at Jicamarca with 50 MHz radar. The irregularities thus studied are 3 meters in size perpendicular to the magnetic field. They are present only during noon hours. These are known as type one irregularity. During other periods the irregularities were of different nature and have been called type II. Following are the main features of the irregularities, (Cohen and Bowles 1967).

Type I irregularities:

1. The strength of the scattered signal for these irregularities is closely associated with the strength of the electrojet.
2. The maximum scattered power is received in east-west plane i.e. echoes are aspect sensitive.
3. The Doppler shift associated with echoes is independent of angle between the beam and the jet current. The sign depends whether one is looking east or west. To explain this result Bowles et al (1960, 1963) suggested that the irregularities were plane waves moving in all directions in vertical plane with their wavefronts aligned at various angles, with respect to vertical.

in the E layer. Turbulence in the neutral gas around 100 km region is supposed to be one of the cause of ionospheric E region irregularities, (Blamont and DeJager 1961).

The turbulence criterion for an incompressible and isotropic fluid is satisfied if the ratio of dynamical force to the viscous force is much larger than unity. This ratio is called the Reynold number and is denoted by

$$Re = \frac{L \cdot V}{Y} \quad 3$$

V is streaming velocity, Y the kinematic viscosity and L is the size of the largest eddy. For a given L, V and Y, the Reynold number can be calculated for neutral turbulence.

Let L = 1 km, V = 250 meter/sec, Y = 50 meters²/sec at 100 km altitude which gives Reynold No. = 5000.

The electron drift velocity gradients play an important part to generate plasma turbulence. This electron drift velocity profile will be similar to the conductivity profile or the vertical electric field profile. The mean electron flow in the electrojet has been shown to be confined by fairly well established boundries. The horizontal electron velocity is large at the centre of the electrojet while at boundries it is small. Somewhere between these two limits strong velocity shear should exist. These velocity shears have an obvious counter part in the confined neutral flow within a tube. But the underlying forces are quite different in plasma turbulence compared to neutral one, (Balsley 1969^c).

The Reynold number can be calculated for electron gas and can be compared with neutral gas values. The value of kinematic viscosity can be taken equal to the diffusion coefficients, (Booker 1956). The diffusion coefficient is given by $\frac{KT}{m\gamma} = \frac{(\text{Thermal velocity})^2}{\text{collision frequency}}$ (Chapman and Cowling 1960). Where K Boltzman's constant, T temperature, m mass and γ is collision frequency of particle. In the ionosphere at 100 km the electron thermal velocity is $V_e = 10^7$ cm/sec and collision frequency $\gamma_e = 10^5$ /sec. The electron diffusion coefficient will be $D_o = 10^5$ meter²/sec.

In the presence of magnetic field the diffusion coefficient of electron gas in east west direction is given by Pedersen diffusion coefficient.

$$D_p = \frac{D_o \gamma_e^2}{\gamma_e^2 + \omega_e^2} \approx \frac{D_o}{\left(\frac{\omega_e}{\gamma_e}\right)^2} = 5.0 \text{ meter}^2/\text{sec.} \quad 4$$

Since $\frac{\omega_e}{\gamma_e} \approx 140$ at 100km

ω_e is electron cyclotron frequency. If Hall field is also considered the diffusion coefficient for electron gas is given by pressure diffusion coefficient $D_o = \frac{KT_e}{m_e \gamma_e} = 10^5 \text{ m}^2/\text{sec.}$

For calculating the value of Reynold number for electron gas, the Pedersen diffusion coefficient should be used for kinematic viscosity value. Using the value of kinematic viscosity equal to 5 meter²/sec and other parameter same as written on previous page the value of Reynold

number comes to be 5×10^4 which is larger by order of magnitude as the corresponding value of neutral gas. Thus the presence of magnetic field makes plasma turbulence more plausible in electrojet.

2.3.1 Spectrum of eddies produced due to turbulence: For an eddy produced by turbulence the energy $E(K)$ contained in an eddy of wave number K can be represented by $E(K) \propto K^n$, (5)

n is the spectral index and is of the order of $-5/3$ for neutral turbulence, (Batchelor 1956). The size of the smallest eddy is given by $\lambda_K = \frac{1}{K_0} = \left(\frac{L_0}{R_e}\right)^{3/4}$. Where L_0 (6) is the largest scale size, R_e is Reynold number and λ_K is Kolomogorov microscale. For ionospheric conditions the value of Reynold number goes on decreasing with altitude due to increase of diffusion coefficient and hence the kinematic viscosity. The net result is that the Kolomogorov microscale value increases with altitude. The smallest scale size of the irregularity which can exist in the neutral atmosphere is a few times the mean free path of the particles. The mean free path values versus altitude are shown in table I. For example at 100 km the mean free path of neutral gas molecules is 22 cm, hence the smallest eddy size produced by neutral turbulence will be more than a few meters.

TABLE - 1

Altitude km	Electron density per cc	Mean free path cm		Debye length cm	Frequency ratio	
		Neutral molecules	Electrons		$\frac{\omega_e}{\nu_e}$	$\frac{\omega_i}{\nu_i}$
70	3×10^2	0.1	0.6	9	0.4	4×10^{-4}
80	10^3	0.4	2.4	5.0	1.6	10^{-3}
90	10^4	3.0	18.0	1.5	23	6×10^{-3}
100	10^5	22.0	1.3×10^2	0.5	140	4×10^{-2}
110	1.5×10^5	100.0	6×10^2	0.4	6×10^2	2×10^{-1}
120	1.5×10^5	6×10^2	3.6×10^3	0.4	2×10^3	1
140	2×10^5	2.6×10^3	1.6×10^4	0.40	5×10^3	2.5
150	2×10^5	10^4	6×10^4	0.5	1.4×10^4	10

Important parameters at 100 km altitude

Radius of gyration of electron = 2 cm
 Radius of gyration of ions = 5.0 meter
 $T_e = T_i = 500^\circ K$

Ion acoustic velocity 360 meters/sec

$\omega_e = \frac{eB}{m_e c} = 7 \times 10^6$ Radians/sec

$\omega_i = \frac{eB}{m_i c} = 120$ Radians/sec.

CHAPTER - III

EXPERIMENTAL TECHNIQUES

Theory of Langmuir probe and plasma noise probe:- The earth's ionosphere has been the subject of experimental investigations for many decades. The earlier work utilised the ground based radio technique. Other ground based technique known as optical technique like air glow provides information about the composition of the upper atmosphere. But in all the ground based techniques neither the ionisation, neutral atmosphere nor the causative solar radiation could be directly measured. Thus it is not surprising to note the highly speculative nature of the explanation that were proposed for some of the ionospheric phenomena, before the advent of rockets and satellites. The experimental techniques for ionospheric studies which are in use today can be classified in two catagories.

- i) Ground based techniques.
- ii) Rocket and satellite borne techniques.

The ground based techniques are limited to indirect probings, while rockets and satellites made in situ measurements possible. In addition, they are also capable of making indirect probing as employed by some of the ground based technique like ionosonde. The satellites are capable of making local measurements as a function of the time and geographic location, while the rockets measure the vertical structure of the ionosphere.

The basic limitation of rocket experiments are, that a rocket borne probe can sample only a small part of the ionosphere for a short period of time. The rockets and satellites provide direct measurements of charged particle fluxes. Recent measurements have provided a large amount of information on the solar radiation particularly X-rays and ultraviolet radiation. These measurements have greatly helped in understanding ionospheric physics and a number of other related areas like solar physics, planetary atmosphere and meteorology.

3.1 Ground based techniques: The ground based techniques for studying upper atmosphere can be classified as (a) radio wave technique and (b) optical technique.

The radio wave technique involves the study of reflection and scattering of a transmitted radio wave. There are also the other techniques involving the study of naturally occurring transmission of radio wave signals. One of the well known technique is the ionosonde technique where the frequency of the transmitted electromagnetic wave is swept over a certain range and the resulting echo pattern known as ionogram is used to investigate the E and F region electron densities. The time delay of the echo is a measure of the height of the layer. The technique is not useful below 85 km. The region between 50 km to 85 km has been studied with partial reflection technique and cross modulation technique.

The motion of large scale irregularities of the order of a few hundred meters have been studied with the three spaced antenna technique at a frequency below the critical frequency of the reflection layer. The backscatter radar technique employs a spot frequency transmitter, the frequency of which is kept much above the critical frequency of the layer. The scattered signal is processed for the determination of various ionospheric parameters. The technique has many advantages over other techniques but needs a transmitter of very high power of the order of few megawatts high gain antennas and very sophisticated signal receiving and processing system (Bowles, 1964). Frequencies ranging from 50 MHz to 400 MHz have been used for this purpose. The coherent backscatter radar technique at a frequency of 50 MHz has been employed at Jicamarca for studying the irregularities of the order of a few meters, (Bowles and Cohen 1962). The radio star scintillation studies and the cosmic radio noise studies at frequencies much above the critical frequency of the F layer fall in the category of study of naturally occurring transmission of electromagnetic wave and have provided lot of useful information about the motions of large scale irregularities.

The only ground based method which can provide informations about the composition of the upper atmosphere is that of spectrum analysis of light emitted by excitation

of the atmospheric atoms and molecules. There is a weak air glow emitted regularly by night sky at all latitudes, due to the photochemical processes which radiate some of the energy absorbed from the sun during the day. The presence of sodium and hydroxyl radical was detected from the air glow spectrum.

3.2 Rocket and satellite borne technique: Rocket studies of the upper atmosphere began in 1945 with the use of V₂ rockets by the Michigan University Group. The satellite studies started in 1957. While the ground based studies were mostly limited to indirect measurements involving radio wave propagation, the advent of rockets and satellites has made in situ measurements possible. Many types of studies which were not possible before are now being carried out and our knowledge of the upper atmosphere has grown beyond expectations.

The rocket and satellite borne technique can be classified as direct and indirect probing techniques. The propagation technique is an indirect technique involving the measurement of the amplitude, phase and polarisation of the radio wave propagated between rocket and ground station. The electron density is deduced from these measurements using magnetoionic theory. Langmuir probes have been used for direct measurements of electron density and electron temperature in the ionosphere. Boyd(1968) has given a good review of different type of Langmuir probes used for ionospheric studies. Various types of R.F. probes have been used for direct probing of the ionosphere. Some of the R.F. Probes

are plasma frequency resonance probe, resonance rectification probe, impedance probe and capacitance probe. A comparative study of the above R.F. probes have been carried out by Heikkela et al (1965).

3.3 Various versions of Langmuir probes used for ionospheric studies:- Hok et.al (1953) at the University of Michigan U.S.A employed rocket borne Langmuir probe for ionospheric studies. Though the results obtained by them were admittedly very crude yet they gave the first indication for the suitability of the Langmuir probe technique for the study of the ionospheric plasma. Spencer et.al(1962) have used bipolar probes, which consist of a symmetric system of two guard spherical probes, between which a d.c. voltage, a ramp was applied. The modified version used a cylindrical electrode as a sensor by [Spencer et al (1965)]. Other geometries like planar and spherical geometries have been successfully used by McNamara (1965) and many other workers. Aono, et.al(1963) have used meshed spherical probe of 2 cm diameter to reduce the effect of photoelectrons. Probes with grids like ion traps, Gerdien condensers and electrostatic analysers have been used by various workers. The addition of a grid between the probe (collector) and the ambient plasma allows the electron and positive ion currents to be measured separately. This technique is superior to the simple probe technique for determination of the electron energy distri-

bution since the problem of subtracting the positive ion current is avoided.

Smith (1967, 1969) of G.C.A., U.S.A. has made extensive use of Langmuir probes using the tip of the rocket nose cone, ogive in shape. Bettinger(1965) has employed a new version of Langmuir probe known as pulse probe. The appealing feature of the system is that with proper design the results can be made independent of electron temperature. Satya Prakash and Subbaraya (1967) have developed a Smith type probe with many additional advantages. Many improvements were made by the author in the system and it has been extended to measure microscale irregularities in electron density. The additional device used to study the probe current fluctuations is termed as plasma noise probe in the thesis, (Satya Prakash et al 1968, 1969 a, 1969 b). Langmuir probe and plasma noise probe theory is discussed briefly in forthcoming paragraphs.

3.4 Theory: One of the fundamental technique, and also the first to be used, for measurement of plasma parameters, is the Langmuir probe. The technique was first employed by Langmuir and his coworkers for the measurement of the electron density and the electron temperature in an ionised gas. It consists in measuring the flux of charged particles to a metallic sensor either spherical, planar or cylindrical in shape. A potential is applied between probe and another electrode called return electrode which generally has a

surface area much larger than that of the probe. The current flowing to the probe is measured as a function of applied voltage, by varying the probe voltage from some convenient negative value to convenient positive value. The resulting relation between the probe current and probe voltage is known as the probe characteristics. The Langmuir probe characteristics are analysed to obtain information about electron temperature and electron density, Mott Smith and Langmuir (1926).

The basic assumptions made for electron temperature and density measurement are that 1) electrons have Maxwellian energy distribution, 2) the Debye shielding distance is very small compared to mean free path of charged particles and the electron depletion is negligible in the immediate neighbourhood of the probe. Also Langmuir's theory does not take account of ambient electric and magnetic fields and the presence of negative ions.

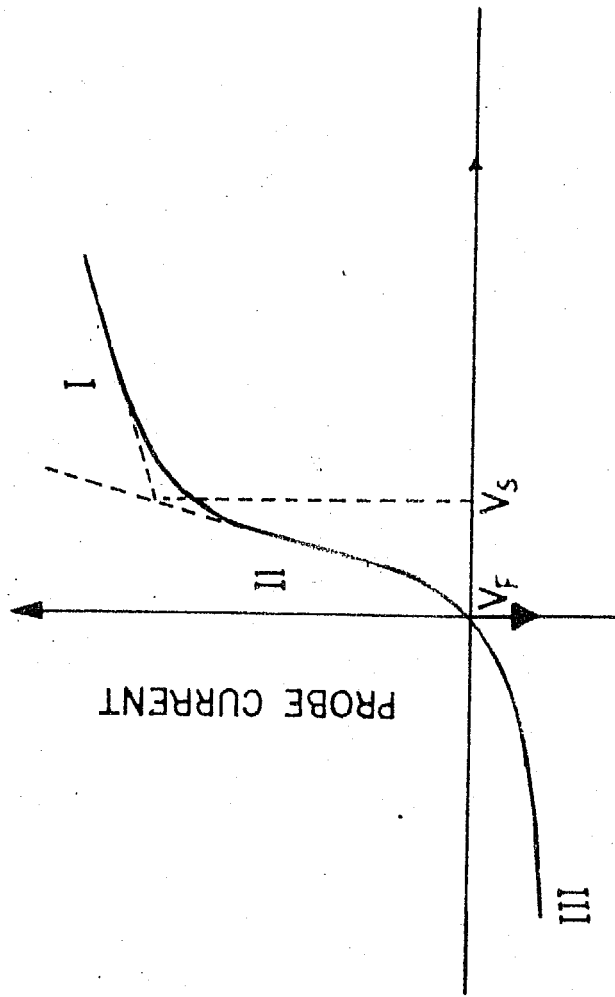
3.4.1 Classical concept: Though the electrostatic probes are simple devices and are ^{capable} of making local measurements the mathematical treatment of the probe theory is extremely complicated. The difficulty stems from the fact that probes are boundaries to a plasma and near the boundary the equations governing the motion of the plasma change their character. In particular the condition of quasineutrality is not valid

near the boundary and a layer called a sheath is formed around the probe in which ion and electron densities differ from each other. The thickness of the sheath depends on the state of plasma as well as the potential and geometry of the probe. The literature on Langmuir probe theory is quite extensive and only a few points will be discussed. A typical characteristic curve is given in fig. 2. The qualitative behaviour of this curve is different in different region and the characteristic can be divided into following sections.

i) Probe at space potential At this potential known as space potential, the plasma would not experience ^{just} any [^] due to probe and hence both +ve ions and electrons will move freely in the vicinity of probe. Due to their random motions both positive ions and electrons will be hitting the sensor and give rise to a net current. The point Vs in the fig.2 represents the behaviour of the probe at space potential. According to kinetic theory the number of particles striking normal to the surface of area A per unit time is given by $\frac{A n_e \bar{v}_e}{4}$. Since the thermal velocity of the electron is much larger than the ion velocity, the probe current will be mainly due to electrons. Therefore, the probe current is given by

$$J_e = \frac{A n_e e \bar{v}_e}{4}$$

7



PROBE VOLTAGE →
TYPICAL LANGMUIR CHARACTERISTIC
ELECTRON CURRENT TAKEN POSITIVE
FIG.2

$$\bar{v}_e = \left(\frac{8 K T_e}{\pi m_e} \right)^{\frac{1}{2}} = 6.21 \times 10^5 \sqrt{T_e} \text{ cm/sec}$$

\bar{v}_e is average thermal velocity of electrons. m_e is electron mass, T_e electron temperature and K Boltzman's constant and e electronic charge.

ii) Probe at slightly negative potential: The typical behaviour of the probe in this region is represented in fig.2 by region II of the characteristic. For small negative voltages of the probe, the probe current consists of two parts, (i) A space charge limited positive ion current and (ii) a current due to the electrons which overcome the repelling field of the probe. In this region the electron current collected by the probe is given by:

$$J = J_e e^{\frac{-eV}{K T_e}} + J_{ion} \quad 8$$

where $V = (V_S - V_P)$ and V_P is probe voltage. The formula assumes that the electrons have Maxwellian energy distribution. Taking the logarithm of this equation, it is evident that a plot of $\ln J_e$ versus probe voltage will yield a straight line with the slope, $e/K T_e$. This slope can be used to determine electron temperature. If the electrons do not have a Maxwellian distribution, then J versus V_P plot will of course not yield a straight line. If the electron temperature is known the electron density value can be determined from the expression of probe current at space potential.

Non-Maxwellian energy distribution: The current voltage curve may be analysed to test for Maxwellian energy distribution. Druyvesteyn showed that j is the current drawn from a plasma by a probe at potential V with respect to space potential, then

$$\frac{d^2 j}{dV^2} \propto \frac{f(V)}{V^2} \quad 9$$

where $f(V)$ is the ordinate of the energy distribution of collected particles. Druvesteyn's method is far more sensitive than semilog plot of $J - V$ characteristic to departure of the energy distribution function from a Maxwellian form. Moreover it offers an important advantage for measurements made from a spacecraft (Bowen et al 1964). From equation 8 it can be easily shown that

$$\frac{d^2 j}{dV^2} / \frac{dj}{dV} = -e/K T_e = m \quad 10$$

Thus the constancy of m can easily be used as a test for Maxwellian energy distribution, and if the distribution is Maxwellian the temperature can be readily be derived from it.

iii) Probe at highly negative voltage: When the probe voltage is made highly negative only +ve ions are collected as the electrons do not have sufficient energy to overcome the applied negative voltage. Region III of the curve fig.2 illustrates the behaviour of $J.V$ curve for large negative potential. The probe current at large negative potentials is

entirely due to positive ions and is proportional to the positive ion density.

At a potential V_F floating potential between region II and III the net current to the probe is zero. At floating potential the electron and ion fluxes become equal. An isolated electrode inserted in plasma will ~~acquire~~ this potential.

(iv) Probe at positive potential: The probe current for accelerating potentials is shown in fig.2 in the region I. When the probe is at sufficiently positive potential the probe current is entirely due to electrons as the ions are not able to reach the probe due to repelling potential. The current collected by the probe when it is sufficiently +ve depends upon the electrode geometry. Current expressions for various sensor shapes is given in the following equations. Exact expressions are available when the dimensions of the electrode are very large or very small compared with the Debye shielding distance.

$$(a) \text{ for large plane : } J = J_e \quad 11$$

(b) long cylinder whose radius is much smaller compared to its length:

$$J = J_e \left(\frac{2}{\pi^{1/2}} \right) \left(\frac{e v}{K T_e} \right)^{1/2} \quad 12$$

$$(c) \text{ Small sphere : } J = J_e \left(1 + \frac{e v}{K T_e} \right) \quad 13$$

3.5 Electron temperature determination by differentiating the Langmuir probe characteristic curve:

The required information in the J - V characteristic may often be more accurately and more conveniently expressed in terms of the derivative of the curve. The maxima of $\frac{dJ}{dV}$ of probe current can determine the point of space potential on Langmuir characteristic. Thus the difference between floating potential and space potential can be determined which in turn is related to electron temperature.

The probe potential U_F at which the net probe current is zero and space potential is related by the following equation:

$$V_F = (U_F - V_s) = - \frac{K T_e}{e} \ln \left(\frac{J_e}{J_i} \right) \quad 14$$

$$V_F = \frac{-5.11 K T_e}{e} \quad \text{for atomic oxygen ions.}$$

$$= \frac{-5.8 K T_e}{e} \quad \text{for molecular oxygen ions.}$$

There is no difficulty in locating the potential at which net probe current is zero. But location of the space potential point on J - V characteristic is difficult due to gradual curvature of the curve. This can be inferred from fig. 2. The method is based on the fact that the first derivative of electron current has a maximum when the probe potential passes from negative to positive values near the upper 'Knee' of the characteristic, the point V_s in fig. 2. The upper Knee of the characteristic is not very well defined

particularly in case of spherical probes which exhibit no saturation of probe current for positive potentials. In most cases this maximum of first derivature of electron current occurs at probe voltages slightly negative with respect to V_s . Because the equation -

$J_{eo} = J_e e^{-\frac{ev}{KTe}}$ is valid for electron current, J_{eo} which are small compared to random current J_e .

3.5.1 Procedure for differentiation:- For differentiating the J - V curve by electronic method both d.c. and a.c. voltages are applied to the probe immersed in plasma. The d.c. voltage is swept between say -1.0 volt to +4.0 volt. The a.c. voltage is a fixed frequency of 800 Hz with small amplitude of the order of a few millivolts. The component of probe current at 800 Hz frequency is picked up and amplified and detected. The detected signal will have maximum amplitude at space potential. This method is considerably easy and very reliable to find the space potential in plasma.

3.6 Langmuir probe for ionospheric studies:- The ionosphere in the E region provides an almost ideal plasma for application of the Langmuir probe technique. The value of some of the relevant parameter is shown in table 1. The theory of the probe is not applicable at heights below about 90 km. because of the following reasons. Firstly the mean free path of charges is small compared to Debye length and secondly the negative ions are present in significant numbers

and have densities comparable to electron density. The use of probe in the region above 1000 km is limited by photo-emission. The photo electric current from a tungsten surface exposed to unattenuated solar radiation is about 4×10^{-9} amp/cm². This becomes equal to the random electron current corresponding to a density of 10^3 ele/cc. Such a density is reached around 1000 kms. Hence the Langmuir probe is most suitable between 90 km to 1000 km for electron density measurements.

3.6.1 Proportionality between probe current and electron

density :- Smith (1969) observed that proportionality between current and electron density remained constant over considerable ranges in altitude allowing a scaling factor, to be established by comparison with ionosonde. Smith also found that this proportionality can be applied to D region. This extension into D region is not justified on theoretical grounds due to short mean free path of electrons and ions. Thus one would expect that the current to the probe in the D region has to be determined by mobility as well as number density of charged particles. A further complication is introduced due to supersonic velocity of the rocket in the D region.

Aikin and Blumle (1968) have reported the results of six flights and find a change in the ratio about a factor of two in altitude region 100 to 200 km. This variation with altitude is attributed to the dependence of probe current on electron temperature. From equation 13 chapter III

it is easily seen that for large accelerating potential for spherical electrode is proportional to $T_e^{-\frac{1}{2}}$. While corresponding equation for cylindrical electrode in the accelerating region is such that the current is proportional to the density and independent of electron temperature.

Thus it can be inferred that between 90 to 180 km region the proportionality between probe current and electron density can be taken as constant. While in D region only structure can be studied.

3.6.2 The effect of earth's magnetic field:- The geomagnetic field influences the collection of charged particle to a moving probe in two ways.

- i) By altering the charged particle trajectory and;
- ii) By altering the equilibrium potential of the spacecraft because of the induction of an e.m.f. by virtue of vehicle motion.

The charged particles are constrained to follow spiral paths in presence of magnetic field. In earth's magnetic field the radius of gyration of electrons is about 2 cms while for atomic oxygen ion is of the order of 5 meters. The ratio of the electron current to positive ion current in the absence of magnetic field is given by the ratio of their random thermal velocities that is equal to the ratio of square roots of ion mass to electron mass. This ratio is of the order of 200 in the lower ionosphere.

The electron current to the probe is therefore, affected to much greater extent than the ion current. In the presence of a magnetic field the ratio of electron saturation current to ion saturation current can get reduced by an order of magnitude.

The current to a rocket borne probe shows two effects which are attributed to vehicle motion in presence of earth's magnetic field. The first is a slow variation having a periodicity equal to that of the rocket precession and second is a much more rapid variation having the same frequency as the vehicle spin. The conical shaped electrodes used in rocket borne probes by Smith(1967) have shown both precession and spin effects. The variation in probe current shows a clearly marked dependence on magnetic aspect angle, the maxima and minima of probe current coinciding with maxima and minima of aspect angle. For 'ogive' shaped electrode this effect is not seen so markedly.

The second effect concerns the potential induced due to rocket motion. It can be shown that for a rocket velocity of about 1 km/sec the potential induced over a distance of 1 meter is of the order of a 40 millivolts. Since the probe normally operates at about four volts with respect to the plasma, the induced potential is considered negligible. However when the probe is operating around zero voltage this effect may be important. The net effect of induced e.m.f. is to shift the characteristic on voltage axis.

3.7

Measurement of microscale electron density irregularities and the theory of plasma noise probe:-

An important aspect of electrostatic probe carried by rockets and satellite is their ability to resolve the fine structure in charge density (Smith, 1969; Satya Prakash et.al 1969a). The smallest scale size of the irregularity that can be resolved by a rocket borne probe is limited by the rocket velocity, the frequency response of the probe electronics and the probe potential which in turn is related to the 'sheath' thickness. For example to resolve a size of one meter by a rocket moving with velocity of 1 km/sec, the frequency response of the associated electronics should be upto 1 KHz. The sheath thickness i.e. the field penetration distance for a sphere of radius 1 cm kept at +4.0 volt with respect to ambient medium for various ambient electron densities shown in the table 2.

The thickness of the sheath for a probe of size more than Debye length at a potential, potential V is given by

$$d = 1.3 \lambda_D \left(\frac{eV}{K T_e} \right)^{\frac{3}{4}} \quad 15$$

where λ_D is Debye length. The value of Debye length for various electron densities is shown in table taking electron temperature of 500°K. For a probe potential +4 volt the above equation can be written as

$$d \approx 8 \lambda_D$$

This will give the thickness of electron sheath for a probe kept at positive potential. The value of ion plasma frequency listed in the table is calculated from the equation

$$f_i \simeq 5.5 \times 10^{-2} \sqrt{n_e} \quad \text{KHz} \quad 16$$

where n_e is electron density per cc. The scale sizes of the irregularities have been calculated by $\frac{V_a}{f_i}$ where V_a is acoustic velocity which is about 360 meter/sec.

Table -2

n_e/cc	f_i KHz	Debye length cm	d - Sheath thickness for a sensor kept at +4 volt cm.	$\frac{V_a}{f_i}$ cm	Scale size which can be seen by the probe. Ten times of sheath thickness cm
10^2	0.55	15	120	750	1.2×10^3
10^3	1.76	4.8	38	240	3.8×10^2
10^4	5.5	1.5	12	70	1.2×10^2
10^5	17.6	0.48	3.8	20	38

3.8 Theory of plasma noise probe:- The rocket borne plasma noise probe has been used by Satya Prakash et.al(1969,a,b) to study ionospheric irregularities. The plasma noise probe measured the fluctuations in Langmuir probe current in desired frequency range. The a.c. component from the Langmuir probe current is selected in the desired frequency range using a band pass filter. The fluctuations are amplified and telemetered to a ground based receiving station.

The composite plasma noise after spectrum analysis gives the amplitudes in different frequency ranges. The filter with $\pm 20\%$ bandwidth were chosen for spectrum analysis as discussed in Chapter IV.

3.8.1 Analysis of plasma noise:- Assuming that irregularities follow a power spectrum like $E(k) \propto K^n$ where $E(K)$ is energy contained in wave number K . The value of spectral index n is determined from the outputs of spectrum analyser. If A_s is the spectrum analyser output in frequency band $f \pm 20\%$ i.e. $f \pm f/5$.

$$\frac{A_s}{2/5 f} = A(f) \text{ is the amplitude of frequency } f.$$

$$A(f) \propto f^{n/2}$$

17

The long-log plot of above equation will yield a straight line whose slope will be a measure of spectral index. The observed scale size of the irregularity can be calculated by dividing rocket velocity V_R by filter frequency f , i.e. $\frac{V_R}{f}$

3.9 Observation of irregularity from a moving body when the irregularities are moving with respect to it:-

The observed scale sizes of the irregularities may be different from the actual sizes depending on the velocity of irregularity as well as the velocity of the rocket.

If the irregularities are stationary with orientation of their wave fronts in vertical plane and the rocket is moving vertically upward or downward it will not see any

fluctuations or irregularities. However, if rocket moves horizontally which happens near apogee it will observe the same. This can be illustrated in the fig.3. The arrow indicating the direction of rocket motion while straight line indicate the orientation of wave fronts.

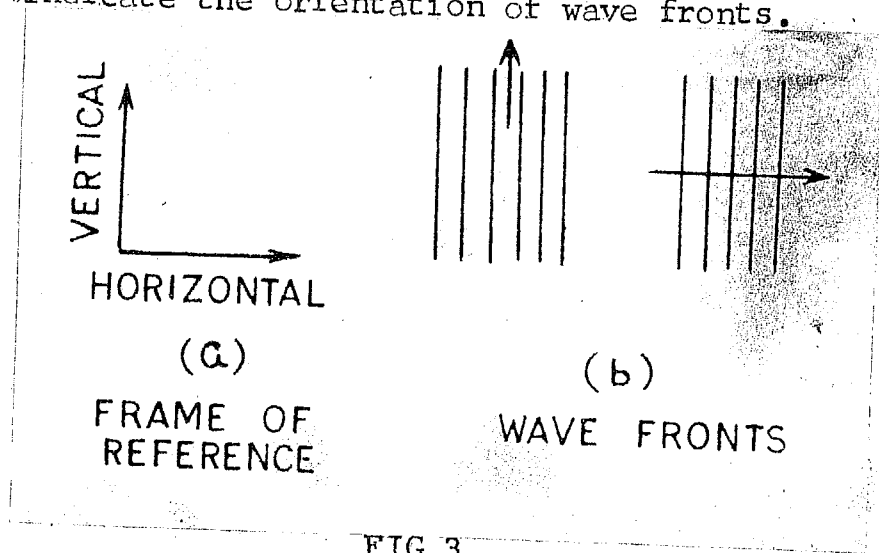


FIG.3.

From the following table it can be seen how the moving rocket samples the irregularities. S is actual irregularity size.

(a) Rocket Velocity	Irregularity orientation	Velocity of Irregularity	Scale size of irregularity sampled by rocket
1. Vertical V_R	Vertical	Zero	Rocket does not sample any scale size.
2. "	Vertical	V'_H (Horizontal)	$\frac{V_R \cdot S}{V'_{Horiz}}$
3. "	Horizontal	Zero	S
4. "	Horizontal	V'_v (vertical downward)	$\frac{V_R \cdot S}{ V_R + V'_{vert} }$
5. "	Horizontal	V'_v (vertical upward)	$\frac{V_R \cdot S}{ V_R - V'_v }$

(b) Now we shall consider the general case i.e. horizontal as well as the vertical motion of rocket. V_H is the horizontal and V_V is the vertical velocity of the rocket while the resultant velocity is V_R .

	Irregularity orientation	Velocity of irregularity	Scale size of irregularity sampled by rocket
1	Vertical	zero	$\frac{V_R \cdot S}{V_H}$
2	Vertical	V'_H (Horizontal)	$\frac{V_R \cdot S}{ V_H - V'_H }$
3	Horizontal	Zero	$\frac{V_R \cdot S}{V_V}$
4	Horizontal	V'_V (downward)	$\frac{V_R \cdot S}{ V_V + V'_V }$
5	Horizontal	V'_V (upward)	$\frac{V_R \cdot S}{ V_V - V'_V }$

Similar calculations can be done for a rocket moving in downward direction. We shall make use of above table in calculating the actual sizes of the irregularities from the observed sizes. The Nike-Apache rocket velocity at 100 km and 170 km (near apogee) are 1.6 km/sec 250 km/sec respectively. For illustration purposes we shall consider only these two altitudes. At 100 km the resultant rocket velocity is in vertical direction while around apogee its motion is entirely in horizontal direction. Let the irregularity velocities in vertical and horizontal direction are 30 meters/sec and 300 meter/sec respectively. We shall assume that these values are same, at both the altitudes under considerations i.e. 100 km and 170 km.

(a) Rocket at 100 km (Rocket supersonic):- Referring section (a) of the above table and considering all the cases one by one.

In case (I) the rocket does not see any irregularity. In case (II) observed scale size

$$l = \frac{V_R \cdot S}{V'} = \frac{1.6 \times S}{0.30} = 5.35 S$$

The observed scale sizes are about 5 times the actual size. In case (III) the observed scale sizes are same as actual size. In case (IV) & (V) the observed sizes are nearly same as actual sizes in both the cases because the irregularity velocity is negligible compared to rocket velocity.

(b) Rocket at 170 km:(Rocket subsonic):- Considering the section (b) of the table and taking each case one by one.

Case(I) The observed scale size $l = \frac{V_R \cdot S}{V_H} = S$

Case(II) If the irregularity moving horizontal in the same direction as that of rocket then l

$$= \frac{V_R \cdot S}{V' - V_H} = \frac{250}{300 - 250} = 5.5 S$$

If both are moving in opposite direction then l

$$= \frac{V_R \cdot S}{V' + V_H} = \frac{250 S}{550} = \frac{S}{2.2}$$

Case (III). In this case rocket will not sample any irregularity. Case (IV)& (V) the observed scale sizes is given by

$$l = \frac{V_H \cdot S}{V} = \frac{250 \text{ S}}{30} = 8.3 \text{ S}$$

From above calculations it is clear that the scale sizes observed by moving rocket can differ from their actual sizes. The observed sizes may be 0.5 to 8 times of actual size.

3.10 The environmental conditions around the moving rocket: The measurements with rocket or satellite borne Langmuir probe is greatly affected by the environmental condition. The major factors are (a) earth's magnetic field (b) photo electron emission from the sensor (c) contact potential (d) excitation by R.F. voltage by telemetry antenna (e) outgassing from the rocket making the plasma contaminated and (f) change in spatial electron density due to rocket motion.

The effect due to magnetic field and photo electrons has been already discussed.

(c) Contact potential: It is observed that when the probe voltage is zero, the probe current does not become zero. The effect is believed to be produced due to the contact potential between two different metals i.e sensor and rocket body, (Smith 1967, Boyd 1968). Fig. 5 shows the value of contact potential for day and night time flights. The actual value of the contact potential does not affect the retarding voltage analysis, while during fixed mode operation a correction can be obtained from individual current voltage plots, (Bourdeau 1963).

(d) The excitation by radio frequency voltage:- The presence of R.F. fields can not be avoided as the transmitting antenna is required to telemeter the data in rocket borne probes. In the presence of R.F. fields the electrons can absorb energy and thus the electron temperature is increased. The effect can be minimised by keeping the antenna far away from the sensor.

(e) The outgassing from the rocket:- The outgassing from the rocket contaminating the environment is a severe problem. The outgassing is much more when an aluminium nose cone is replaced by a fibreglass nose cone. The use of fibreglass nose cone becomes necessary when the Langmuir probe is flown with proton magnetometer.

The effect of outgassing on probe measurement is to decrease the probe efficiency for current collection due to the large no. of collisions with the gas molecules. The effect of outgassing has been observed in the probe current when the probe was flown with Trimethyl aluminium. The probe current values were lower by a factor of about three after the ejection, of the T.M.A. The effect of T.M.A. is shown in the density profile of flight 10.13 fig.34. The thin line and the dotted lines show maximum and minimum values of probe current during a spin cycle showing the extent of spin modulation.

(f) Effects due to vehicle motion in collection of current:- When measurements are carried out by rocket and satellite borne probes it is necessary to consider

effect of the vehicle potential and its motion. The rocket body acquires a negative potential known as floating potential which is about to half volt for $\frac{J_e}{J_i} = 200$ and electron temperature 1000°K . The effect of negative potential will be clear in forth coming paragraphs.

The moving rocket perturbs the plasma in its vicinity and creates the compression region in front and a wake region behind it. Fig.4 shows the schematic representation of disturbed region in the vicinity of the moving body. The shape of the body is considered as spherical and ellipsoidal to simplify the geometry of the disturbed region. In practice the rocket body, a cone cylinder configuration should be considered to represent such a geometry.

In the wake region of the rocket the charged particle density is considerably reduced compared to undisturbed region. The ions are not able to fill the wake region due to their smaller velocities compared to rocket velocity and electrons due to negative potential of the vehicle. If the probe is situated in the wake region it will measure electron density which is considerably less than the density of undisturbed medium. Such wake effects have been observed by Oya (1968).

3.11 Production of disturbances in plasma by moving

rocket:- The study of disturbances created by the moving rocket is of great interest in its own right and has greater importance in the analysis of in situ direct measurements.

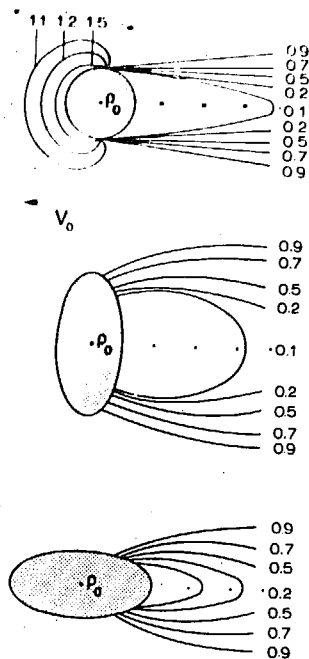


Fig. 4 Lines of equal ratio of the particle concentration $N_1(r, \theta)$ to the undisturbed concentration N_0 (with $H_0 = 0$) in the close zone of a sphere and an ellipsoid.

Figure-4 : Schematic representation of the disturbed regions in the vicinity of the moving bodies of various shapes (From Alpert 1965).

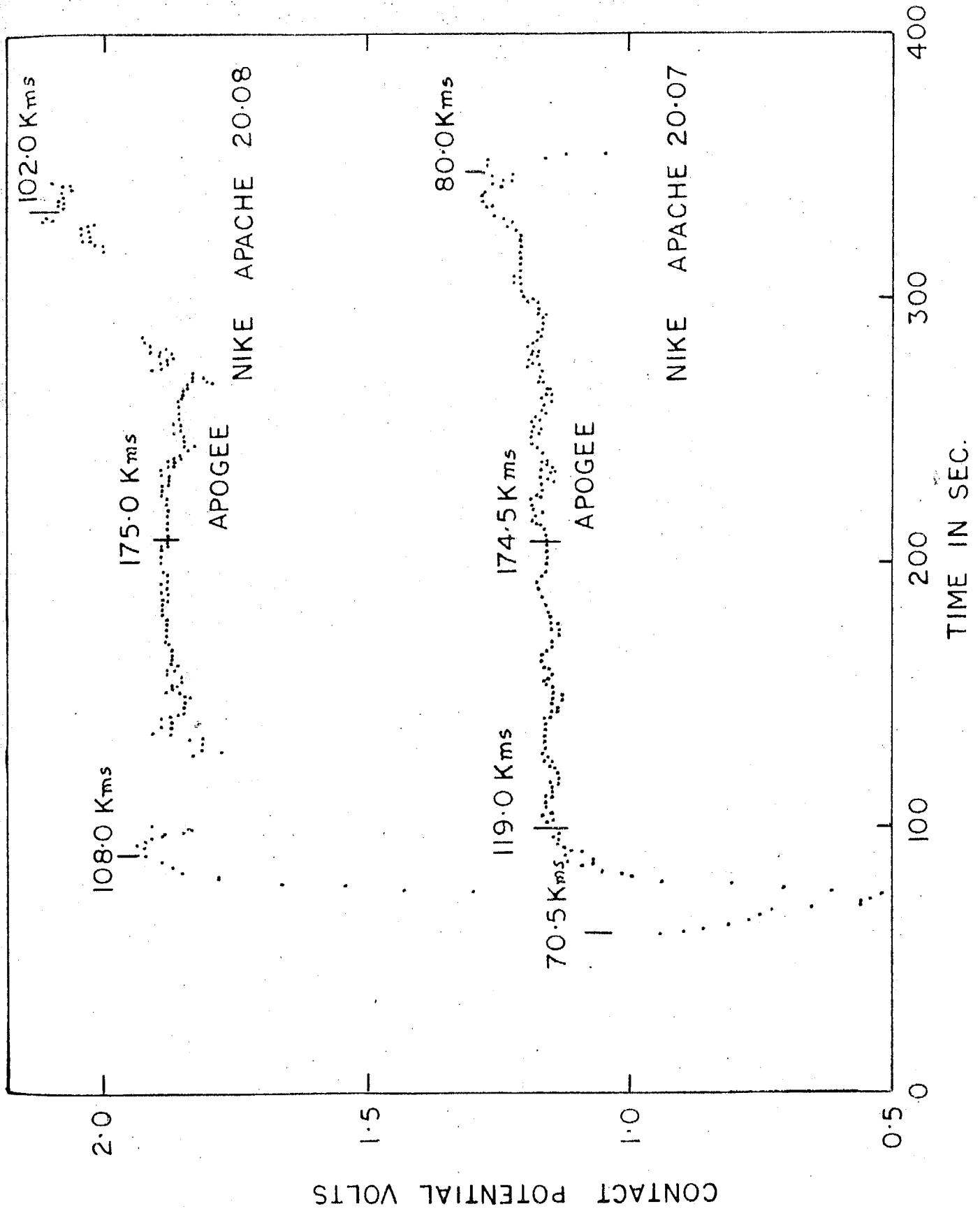


FIG.5

An instrument for example a probe situated at tip of the rocket nose cone collects the particles from its neighbourhood. If some kind of disturbance is present in its vicinity it will record the state of the disturbed region (Alpert et.al 1965). Disturbances created by a moving rocket in the ionosphere can be detected by the probe on vehicle under certain special circumstances. When rocket motion is supersonic the disturbance can't reach the rocket body or sensor. The disturbance thus created spreads uniformly in all the directions, it can move with ion thermal velocity or even less which is much less than rocket velocity. If the rocket is subsonic the probe can record these disturbances.

Alpert et.al(1965) have studied the effects produced by moving body as it advances through the ionosphere. It is believed that in the wake region of the rocket or satellite some kind of instability is developed which results in generation of ion acoustic waves. Gurvich and Pitavsky (1965) have developed a dispersion relation for the ion waves generated in the wake region of moving vehicle. The frequency of these wave ranges from $0.1 W_i$ to $1.0 W_i$ where W_i is the ion plasma frequency of the medium.

The ion plasma frequency around 175 km is around 5 KHz in the evening and in night while at mid noon its value is 18 KHz. In order to study the lower end of the spectrum of ion waves the measuring instrument should have frequency response at about 0.5 KHz for evening and night time conditions while around 1.8 KHz for day time conditions.

CHAPTER - IV

INSTRUMENTATION

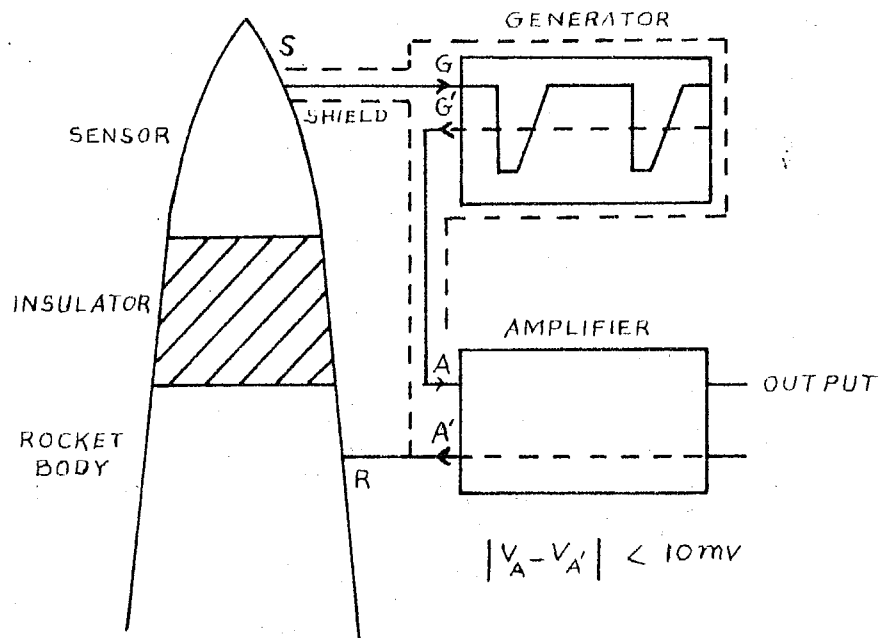
Rocket borne Langmuir probe and plasma noise probe systems were developed to study some of the ionospheric plasma parameters. The Langmuir probe was developed to measure electron density in the range 10^4 electrons to 10^6 electrons/cc and electron temperature greater than 200°K . The plasma noise probe measures the electron density fluctuations in the frequency range 70 Hz to 1 KHz (of scale sizes ranging from one meter to 15 meters) and with amplitudes as low as 0.05% of the ambient level. The systems are described in forth coming paragraphs.

4.1 The conventional Langmuir probe system: In the Langmuir probe experiment the sensor is a small section of the nose tip or a separate electrode projecting out from a suitable portion of the nose cone, which is well insulated from the rocket body. A voltage, varying around the floating potential, is applied to the sensor and the current drawn by it from the surrounding plasma is measured by a suitable electrometer amplifier. In the Smith's version the sensor stays at a potential well above the floating potential for a major portion of the cycle and the saturation electron current is measured for the electron density determination. During a part of the cycle the sensor potential varies linearly from a few volts negative to a few volts positive with respect to the floating

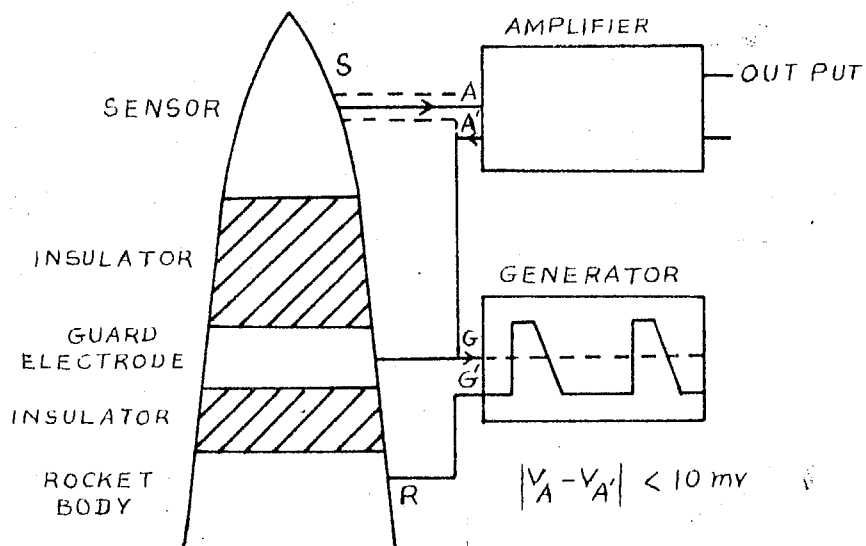
potential and electron temperature is determined in this portion of the cycle by retarding potential analysis of the probe current versus probe voltage curve.

The working of the above system is illustrated in fig.6a. The sweep generator generates the voltage applied to the sensor and the electrometer amplifier measures the sensor current. It is necessary that the input impedance of the electrometer amplifier must be small so as to keep points A and A' very nearly at the same potential, the potential difference between the two points being less than 0.01 volt. The potential at A is not affected to any considerable extent by changes in the input current. It is customary to use amplifiers with 100% negative feed back for this purpose.

While the above system is straightforward, in practice, it involves many precautions. The sweep generating system requires ^{floating} a power supply, ^{while electrometer requires a power supply} which has one terminal in common with the rocket ground. The two batteries are therefore, independent and must be well insulated from one another. In fact, it is essential that the entire sweep generating system from the point S to the point A, be well insulated, and shielded from the rest of the payload with only two points G and G' having any connection with the rest of the system. The electrical shielding is connected to the rocket body at A'. Leakage currents between this section and the rest of the system must be much smaller than the sensor currents that are to be measured. The nature of the difficulty will be



CONVENTIONAL SYSTEM



PRESENT SYSTEM

FIG.6

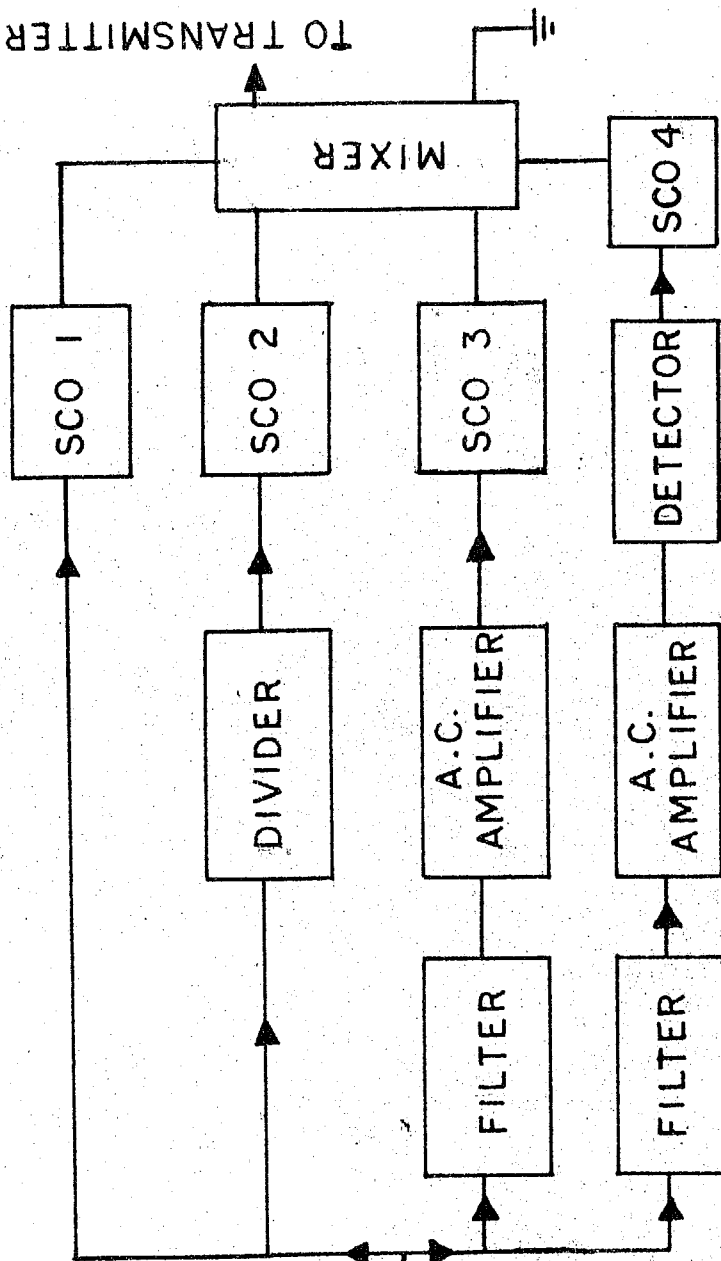
appreciated when one remembers that in a rocket payload any battery that supplies power to the circuitry must have associated relay systems and external batteries for pre-launch check-out procedure. Also if proper care is not taken even capacitive leakage between the systems can give rise to currents of the same order as the currents are to be measured. The distributed capacity of the sweep circuits further adds to the complication by modifying the probe current in that portion of the sweep cycle where the potential of the probe is varying. The probe current is modified most, after the voltage of the sensor is made to change suddenly from positive to negative. The charge collected in the distributed capacity disturbs measurements in a substantial portion of the sweep during which positive ion current is recorded.

4.2 The present system: An alternate system which is functionally similar to the conventional system, was used for the experiment, (Satya Prakash and Subbaraya 1967). This system is illustrated in fig.6 b. A wave form reverse to that which is to be applied to the sensor is generated and grounded to the rocket body. If the potential drop introduced by the electrometer is small (the difference is as before less than 0.01 volt), the sensor voltage varies with respect to the rocket body in a manner determined by the generator. In this system the leakage is reduced to a minimum as the input to the amplifier is directly connected to the sensor. If the payload is so situated inside the rocket nose cone that the sensor and the amplifier are separated by a large

distance, the leakage and distributed capacitances can be minimised by feeding the sensor through a cable and shield of which is kept at V_A since V_A' differs from V_A by 0.01 volts only. (V_A and V_A' represent the potentials at A and A' respectively).

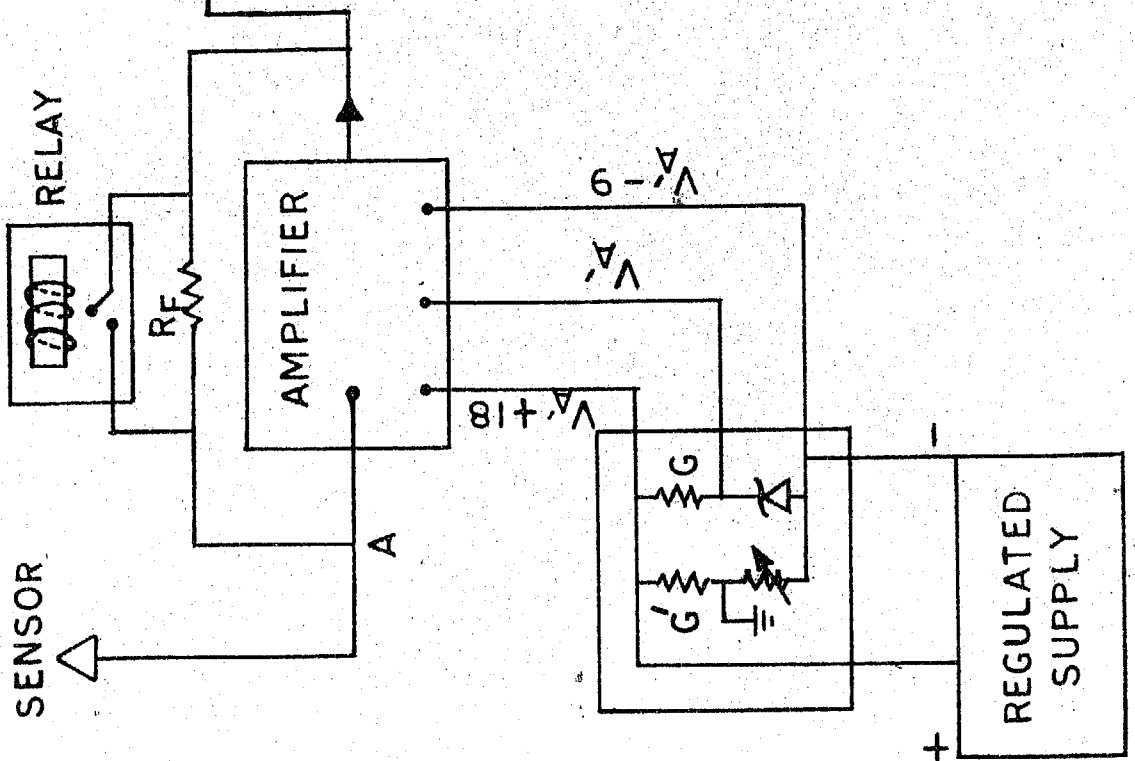
The block diagram fig.7 describes the working of the system. Using a single floating power supply the voltages $V_A' \div 18$, V_A' and $V_A' - 9$ are produced with respect to the rocket body, V_A' varying in a manner shown in fig.6. The electrometer amplifier works on these voltages and converts the sensor current into an analog voltage which can be telemetered by FM/FM telemetry system. The present system is much simpler. The frequency response of the system is high and depends primarily on the feedback element in the electrometer amplifier. Since electrometer amplifiers can be built with frequency response upto 20 KHz. Thus the system is ideal for studying the probe current fluctuations. Also the system works on single floating power supply. It facilitates the use of guard electrode without any additional electronics.

Plasma noise probe selects and amplifies the fluctuations in the probe current in the frequency range 70 Hz to 1 KHz. It can cover a dynamical range from 0.05% to 4% of total probe current. The fluctuations with frequencies smaller than 70 Hz can directly be seen on Langmuir probe current record.



BLOCK DIAGRAM OF
LANGMUIR PROBE AND
PLASMA NOISE PROBE

FIG. 7



4.3

Description of the Langmuir probe and Plasma noise probe instruments:

The mechanical system and electronic circuitry of L.P and Plasma noise probe were designed to withstand a wide range of temperature variation and high vibration levels. Temperature and vibration are the main considerations to be taken into account for rocket borne instrumentation. The mechanical layout of the system is such that after assembling the complete unit there is an easy accessibility for electronic components. Such that in case it becomes necessary, any component can be replaced without much difficulty.

The mechanical system was designed to withstand a thrust of about 50 g (g = acceleration due to gravity) with a vibration rate 3000/sec. Such conditions are likely to be encountered during Nike-Apache launch. The payload was subject to a linear acceleration of 50 g and at a frequency only 140 vibrations/sec. Shake table facility at Thumba was available for low vibration frequency i.e. maximum to 140 revolutions/sec.

The maximum temperature in the payload housing is expected to be around 60°C. Each electronic circuit was designed to withstand this temperature. Only those component i.e. transistors, diodes, capacitors and resistances which can stand high temperatures were used. The electronic circuits were kept at a temperature of 60°C for half an hour in an oven and tested for reliability and proper functioning.

Finally the assembled payload was kept at 60°C for half an hour and checked thoroughly for proper functioning. The operation of the assembled payload is continually evaluated during vibration and temperature test.

4.4 Electrode geometry: Electrodes of various geometries like planar, spherical and cylindrical have been used in rocket borne probes. But for the rocket borne probe, one of the most convenient shape of the sensor is the tip of the rocket nose cone. The sensor replaces the standard nose tip and does not require any modification in the geometry of the rocket and avoids use of any opening device. The conical shaped electrodes however, show marked aspect sensitivity of the sensor in probe current (Smith 1967). The aspect sensitivity of the sensor creates difficulties in the analysis of data and hence should be minimised. The conical nose tip was later replaced to an ogive shaped sensor by Smith and was found to be relatively insensitive to the aspect. This sensor was adopted for the present study. The electrode used had an ogive shape and included angle of 11° .

4.4.1 Guard electrode: The use of guard electrode greatly improves the performance of the sensor by rendering the electric field near the sensor normal to its surface and avoiding the edge effect. Since the guard electrode is kept nearly at the same potential as that of sensor hence the direct leakage current between the return electrode for the sensor is very much reduced. Thus it enhances the

function of the insulator which insulates the sensor from rest of the system. Any leakage between the guard and rest of the body does not affect the measurement.

Stainless steel was used for tip sensors because of its high work function (to reduce photo electric effect), high melting point and low magnetic permability as some of the probes were also flown along with proton precession magnetometers.

4.4.2 The insulator: The insulator material should be such that in addition to its ability to withstand high temperatures it should have high insulating property and good mechanical strength. Some of them which satisfy above requirements are boron nitride, teflon and ceramic (alumina). These materials were used in different flights for the insulator.

The guard electrode was insulated from the rocket body by teflon insulator. The photograph ~~and drawing~~ of the sensor is shown in fig.8. To keep the probe sensor free from moisture the sensor is fitted at the tip of the rocket nose cone just before launching.

4.5 Probe Electronics: Fig.7 illustrates the block diagram of probe electronics. The probe electronics consists of a sweep generator. An electrometer amplifier, plasma noise probe amplifier in frequency range 70 Hz to 1 KHz subcarrier oscillators and band pass filters according to I.R.I.G. standards. The subcarrier oscillators and associated filters form the part of the probe electronics. The probe

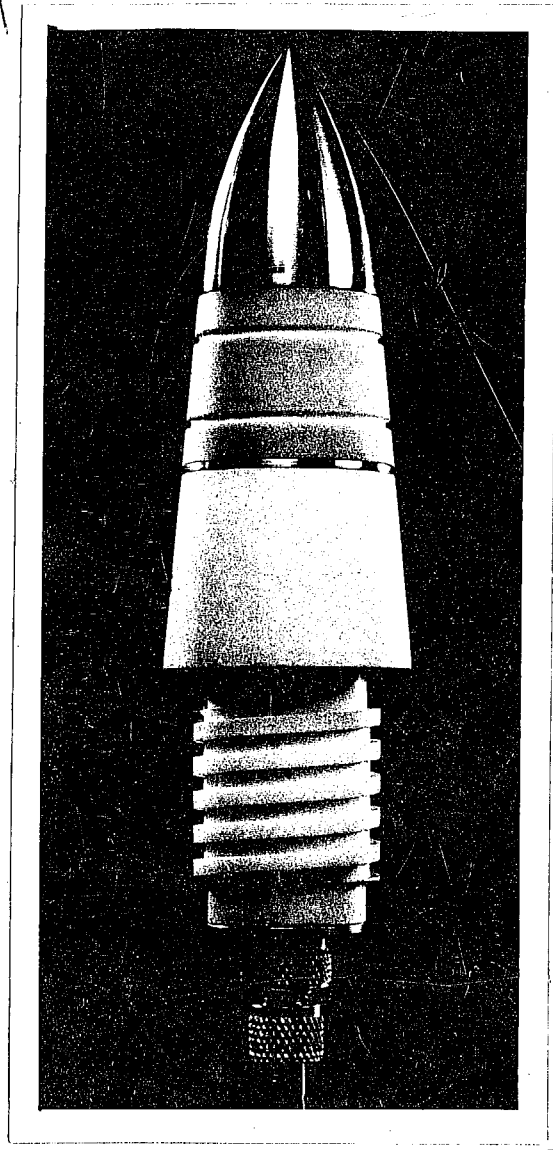


Figure-8 : Nose tip electrode photograph.

electronics operates on floating power supply of voltages $V_A' + 18$, $V_A' - 9$ volt. A battery and voltage regulator provides the required voltages. The a.c. output of the subcarrier oscillators is mixed by a resistance network and mixed output is fed to the transmitter. The transmitter operated on separate power supply. The electronic circuit of each unit will be described briefly in the following paragraphs.

4.6 Sweep circuit: A linear waveform was obtained by charging a condenser with a constant current. The waveform of the sweep voltage and the circuit diagram of the sweep generator is shown in figs. 11 & 10 respectively. The block diagram of sweep circuit is shown in fig.9.

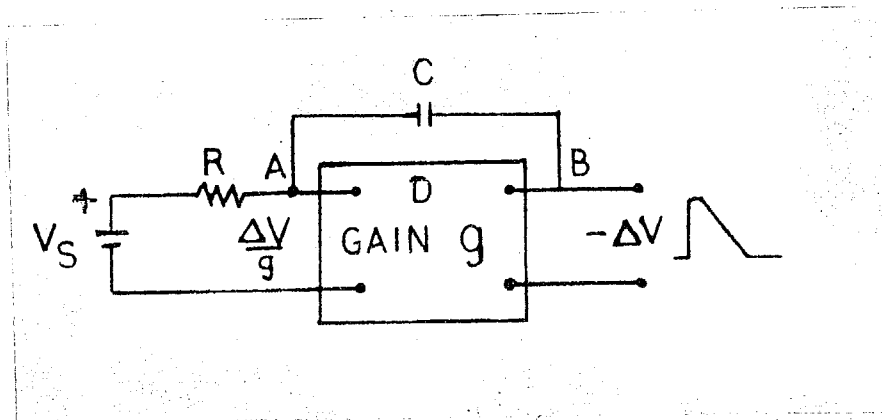


Fig.9 Block diagram of sweep generator

As illustrated in block diagram fig.9 R and C form a charging network and D is a high gain amplifier. V_S is the supply voltage. With the increase of voltage at the condenser terminal A , the output voltage of the diff-

erence amplifier will fall rapidly i.e. a negative going sweep will appear at the output. Let the decrease of voltage in time Δt be $-\Delta V$ at the final output. If g is the gain of the difference amplifier then $-\frac{\Delta V}{g}$ is the input to difference amplifier. Thus the voltage across the condenser C is $\Delta V(1 + \frac{1}{g})$ and charging current is $C \frac{\Delta V}{\Delta t} (1 + \frac{1}{g})$. The charging current through the resistance R is $(V_s - \frac{\Delta V}{g})/R$ equating the two currents we get

$$C \frac{\Delta V}{\Delta t} = \frac{(V_s - \frac{\Delta V}{g})}{R(1 + \frac{1}{g})} = \frac{V_s}{R} (1 - \frac{1}{g} - \frac{\Delta V}{g V_s}) \quad 18$$

On examining the above equation we can see that ΔV will vary linearly with time as long as $\frac{1}{g} + \frac{\Delta V}{g V_s} \ll 1$. For the sweep used following were the values.

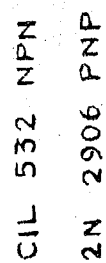
$$\Delta V_{\max} = 5.0 \text{ volt}$$

$$V_s = 18.0 \text{ volt}$$

$$g = 100, \text{ so } (\frac{1}{g} + \frac{\Delta V}{g V_s}) \approx 1.3 \times 10^{-2}$$

obviously $\frac{1}{g} + \frac{\Delta V}{g V_s} \ll 1$. The linearity of the sweep will be within 1.3%.

4.6.1 Working of sweep circuit: Referring to fig.10 the condenser C is charged through a high resistance R , which form a charging network with a fairly large time constant. The other end of the condenser is returned to the final sweep output. The voltage at A is fed to emitter follower T_2 and T_3 which in turn is fed to a difference amplifier T_4 , through diode D_1 . The negative end of the difference amplifier



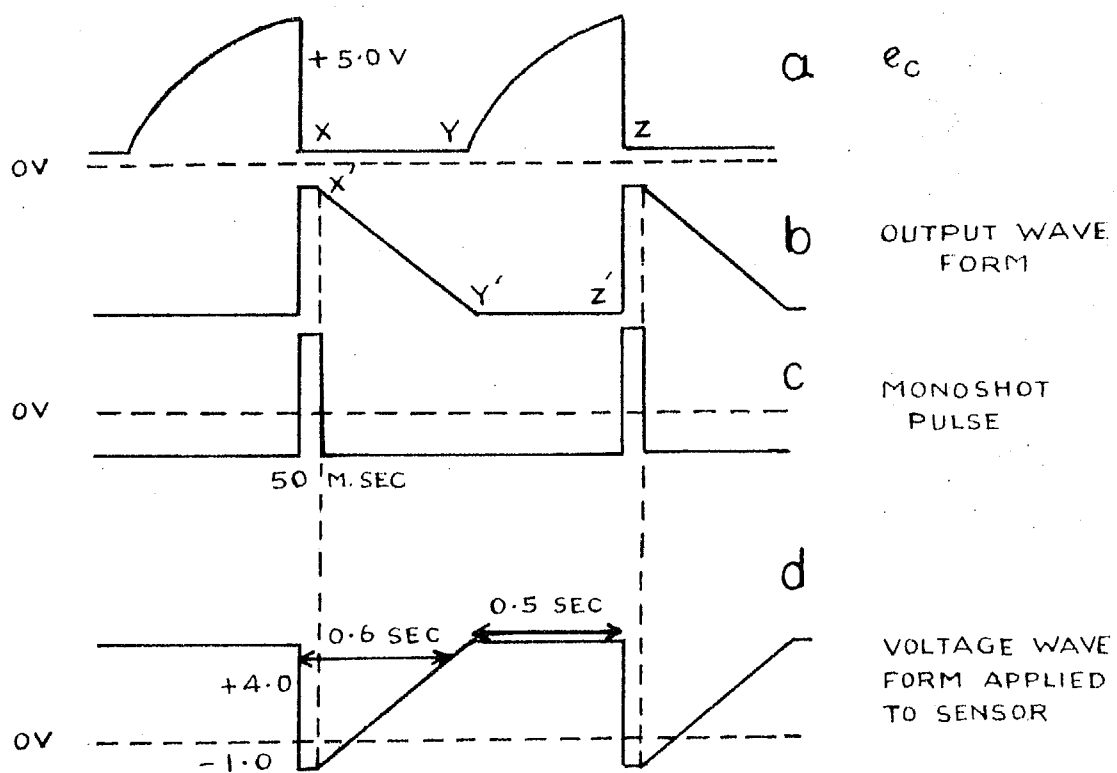
SWEEP CIRCUIT

FIG. 10

is biased at +2.0V. The difference amplifier output is fed to emitter follower T_6 . The diode D_1 and D_2 form a selective network. As long as the voltage at E' is less than the voltage at terminal E the diode D_1 conducts and the output of the difference amplifier goes on decreasing and subsequently the voltage at E' also goes on decreasing. As the voltage at the base of T_4 becomes more than the voltage at E, the diode D_2 becomes conducting and the difference amplifier no longer follows the voltage at the emitter of T_3 with the result the output voltage remains constant while the voltage e_c rises. The voltage e_c is fed to a difference amplifier T_{11} and T_{12} whose negative end is biased at +5.0 volt.

Divided signal from emitter follower T_6 is applied to T_7 and T_8 . The final sweep output is returned to condenser terminal B.

4.6.2 Termination of sweep: The sweep is terminated when the voltage at e_c becomes greater than 5 volts. The voltage e_c is fed to a difference amplifier circuit T_{11} & T_{12} . As soon as e_c becomes more than +5.0 volt, the difference amplifier gives a positive pulse which triggers a monoshot. The monoshot T_9 and T_{10} gives a +12 volt pulse for 50 m.sec. duration. The monoshot pulse makes the transistor T_9 fully conducting resulting in a shorting of the condenser C. The e_c waveform and monoshot pulse wave forms are shown in fig.11. After 50 m.sec the short is removed and the sweep restarts.



VARIOUS WAVE FORMS AT DIFFERENT
TERMINALS OF SWEEP CIRCUIT

FIG. 11

In order that the duration and the linearity of the sweep is not affected by the temperature change, the electronic components were selected carefully. Silicon transistors with $I_{co} \ll 0.1$ micro amp. were used. The charging condenser C was a low leakage current metallized paper capacitor with a leakage resistance more than ten thousand mega ohms.

Following is the specification of one of the sweeps used:-

Sweep voltage levels	-1.0V to 4.0V
Variable voltage duration	0.6 sec.
Fixed voltage duration	0.50 sec.
Zero marker voltage duration (monoshot pulse duration)	50 m. sec.
Total sweep cycle duration	1.15 sec.

4.7 Electrometer amplifier: The probe current (in altitude region 55 to 180 km) that is to be measured ranges from 2×10^{-9} amps to 3×10^{-5} amps. The electrometer amplifier which can measure such currents should meet following requirements.

- 1) Should be able to handle currents of the order of 10^{μ} amp. and respond identically for both the polarities of input currents i.e. positive ion current and electron current.
- 2) Large dynamical range for input current should be about 1.5×10^4 .

- 3) Must be capable of giving output voltage from -5.0V to +10V to handle the positive ion as well as electron current and to satisfy telemetry requirements.
- 4) The frequency response should extend from D.C. to a few KHz and thus must be able to record audio frequency fluctuations present in the probe current. Frequency response should be upto 3 KHz.
- 5) D.C. Voltage drift must not exceed 100 m.volt due to temperature or supply voltage change.

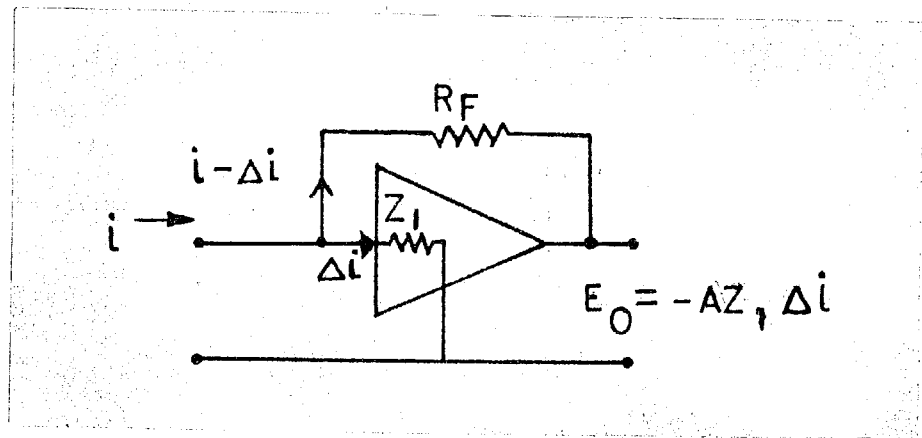


Fig.12 Representation of a feed back amplifier.

The amplifier in Fig.12 has gain A and R_F is the feed back element. i and E_O represent the input current and output voltage respectively. If Z_1 is the input impedance the amplifier and if Δi is the current flows into the

amplifier then,

$$\begin{aligned}
 (i - \Delta i) R_F &= Z_1 \Delta i - (-A Z_1 \Delta i) \\
 &= A Z_1 \Delta i \left(1 + \frac{1}{A} \right) \\
 &= -E_o \left(1 + \frac{1}{A} \right) \text{ where } E_o = -A Z_1 \Delta i \\
 i R_F &= -E_o \left(1 + \frac{1}{A} + \frac{R_F}{A Z_1} \right)
 \end{aligned}$$

For a typical circuit $A = 10^3$

Feedback resistance $R_F = 40 \text{ meg. ohm}$

Grid leak resistance $Z_1 = 10^6 \text{ meg. ohm}$

Hence $\frac{R_F}{A Z_1} \ll 1$

Thus the amplifier output is approximately given by

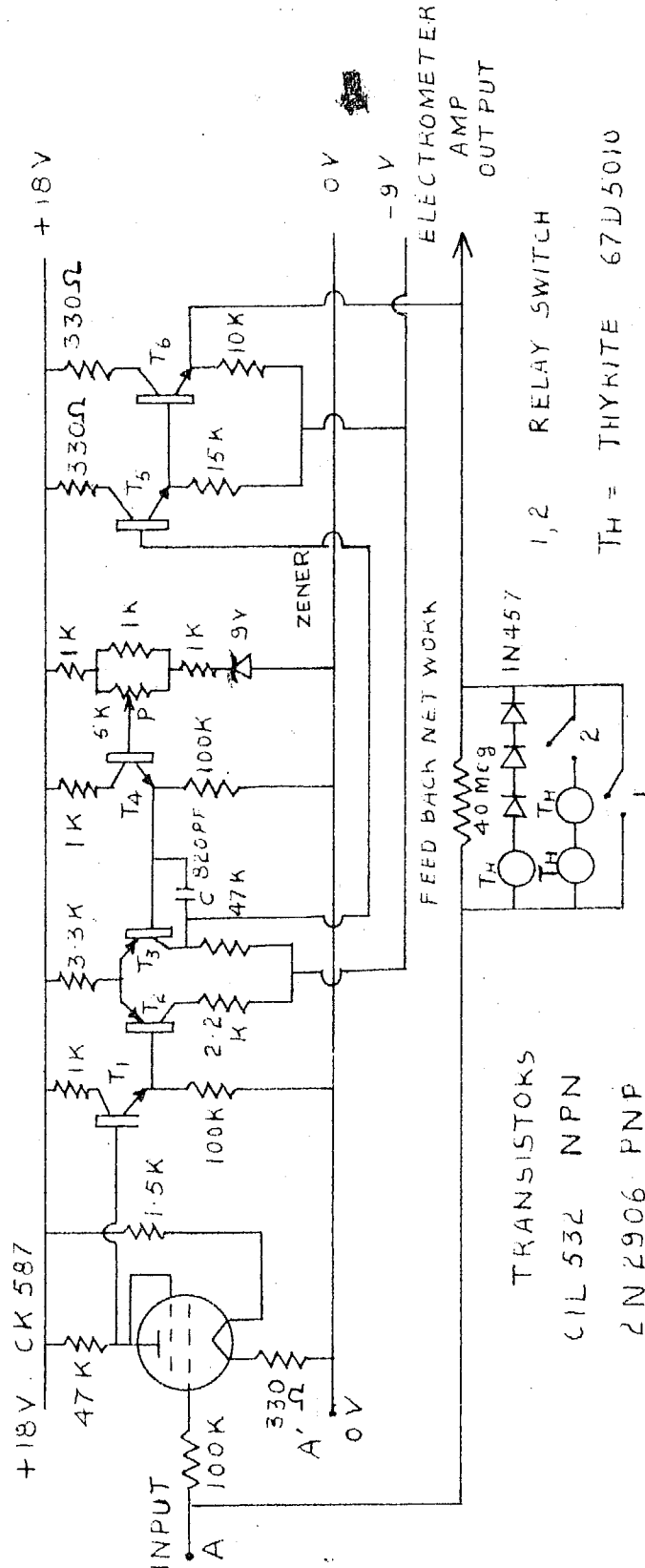
$E_o = -i R_F$ within 0.1% and the input current is given by $i = \frac{-E_o}{R_F}$ 19

Input current is given by output voltage divided by the feedback resistance. Thus it is independent of the amplifier characteristics.

Input impedance of the amplifier = $\frac{R_F}{A} = \frac{40 \times 10^6}{10^3}$
 $= 40 \text{ K ohms.}$ which is much less than the value of Z_1 .

Referring to fig.13 the input stage of the electrometer amplifier is an electrometer tube Raytheon CK 587 which has a maximum leakage current of 10^{-13} amp. The output voltage of the electrometer tube is fed to a difference amplifier T_2 & T_3 through emitter follower T_1 . The difference

:67 (a) :

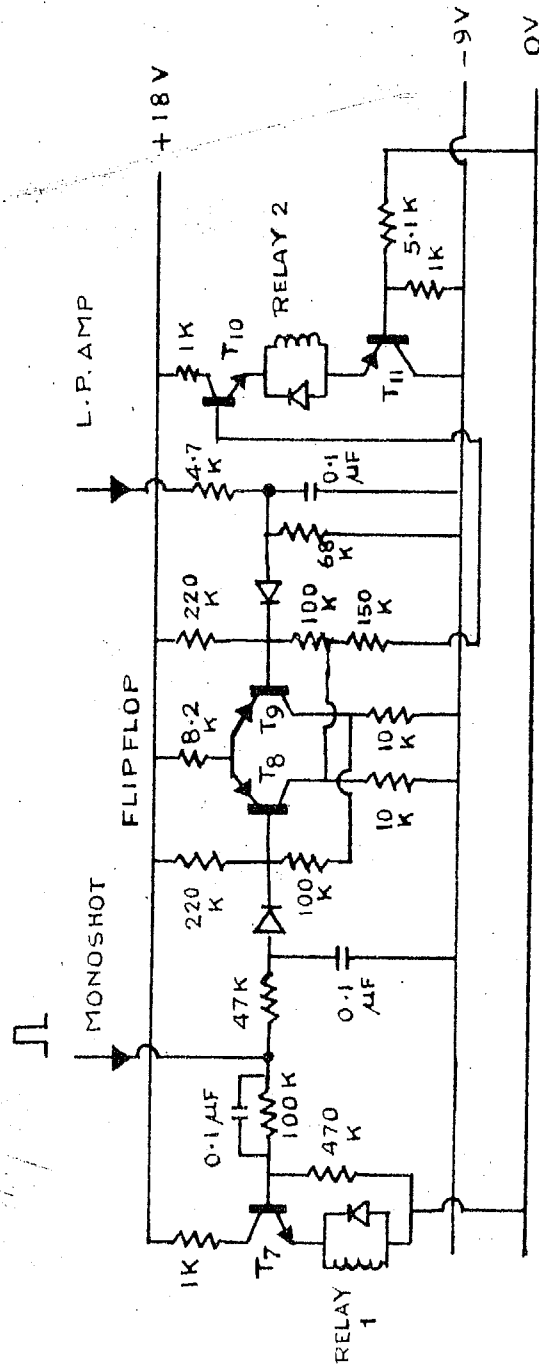


ELECTROMETER AMPLIFIER FIG.

amplifier at its negative input is connected to a potential divider. Potentiometer P is used to adjust the zero level of the amplifier. The difference amplifier output is followed by emitter followers T_5 and T_6 . Output of T_6 is fed back to the input stage through the feed back net work circuit. The condensar C is connected to limit the frequency response of the amplifier and to prevent high frequency oscillations.

4.7.2 Large dynamical range for input current: The large dynamical range of currents is achieved by using a nonlinear resistive element for large currents, a pure resistance for small currents. Thyrites and silicon diodes were used as nonlinear resistance elements. The feedback network used in some of the flights is shown in the amplifier circuit fig.13. The feed back network consists of thyrite, pure resistance and diodes. The resistance and thyrite form the feed back net,work for electron current while diodes for positive ion current. The resistance can cover a dynamical range of 10^2 while the thyrite covers a dynamical range of 1.5×10^2 . Thus the total dynamical range of 1.5×10^4 is achieved for electron current. While diodes cover dynamical range of 10^3 for positive ion currents.

For low electron current from one milli micro amp. to 0.25 μ amp a resistance of 40 meg. ohm is used. The switching from resistance to thyrite is done by the circuit shown in fig.14. The amplifier output is fed to a T_8 and T_9



TRANSISTORS CIL 532 NPN & 2N 2906 PNP
CIRCUIT FOR ZERO MARKER & THYRITE
SWITCH RELAY

FIG.14

which gives a pulse of +15 volt when the amplifier output exceeds 10 volts. The bistable T_8 and T_9 gives a pulse which is fed to T_{10} which puts on the relay No.2 thus the thyrite gets connected parallel to the 40 meg. resistance. After each sweep cycle a monoshot pulse (from the sweep circuit) of 50 m.sec duration resets the bistable. The current range between 10^{-3} μ amp to 0.25 μ amp. is used for electron temperature determination. Any uncertainty caused by using a non-linear element like thyrite as feed back element is avoided.

4.7.3 Zero current marker: The circuit diagram of zero current marker is shown in fig. 14. At the beginning of every sweep cycle a calibration mark is obtained for 50 m.sec. at the amplifier output. This is achieved by shorting the feedback net work for 50 m.sec. during each cycle with relay no.1 which is driven by a monoshot. The shorting of the feed back element gives a more reliable zero mark compared to disconnecting the input to the amplifier. From the expression it can be seen for $i = 0$, $E_o = 0$. Also $E_o = 0$ when $R_f = 0$. Thus a output corresponding to $i = 0$ can be got by shorting R_f . The zero mark can also be obtained by disconnecting the input from tip sensor. Zero mark obtained by shorting the R_f becomes independent of any leakage taking place within amplifier output and the sensor. While in the other method the zero mark will not be free from leakage in the amplifier. Leakages in the amplifier and the sensor are expected during the prelaunch

period due to the moisture. This leakage is reduced very much as the ambient pressure decreases during the flight.

4.7.4 The switching relays: Reed switches of G.E. Co. U.S.A. were used for relay No.1, and relay No.2.

The reed switch coils were wound on a plastic spool of $\frac{1}{2}$ " length and outer diameter $\frac{1}{2}$ ".

The amplifier was tested for temperature variations. The drift at the amplifier output was less than 0.1 volt for supply voltage variation $V_A' + 21$ to $V_A' + 15$ V and temperature variation from 27°C to 60°C.

The standard resistances and standard mercury cadmium cells were used for amplifier calibration.

Typical calibration curves are given in fig.15, curve (A) for electron current with resistance feed back network, curve (B) for thyrite feed back, and curve (C) for positive ion current with diodes as feed back net work.

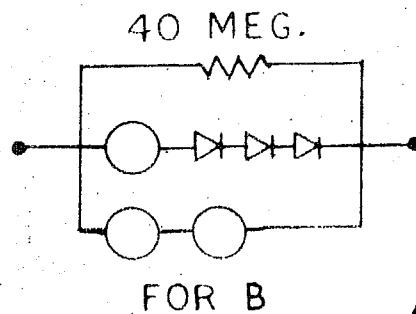
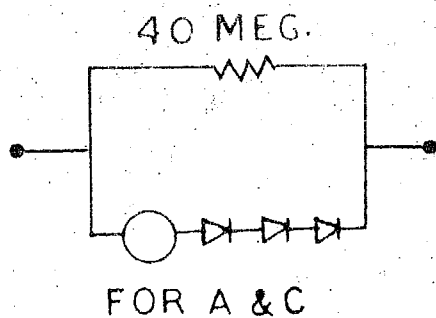
4.8 Plasma noise amplifier: An audio frequency amplifier shown in fig.16 was designed to study fluctuations in the probe current from 0.05% to 4.0% of total probe current. It consists of a band pass filter, a signal divider circuit and an amplifier.

The band pass filter has a band width from 70 Hz to 1 KHz, and is a combination of high pass and low pass filter, tuned at 100 Hz and 800 Hz respectively. The toroidal cores manufactured by Arnold Eng.Co. were used for inductance coils.

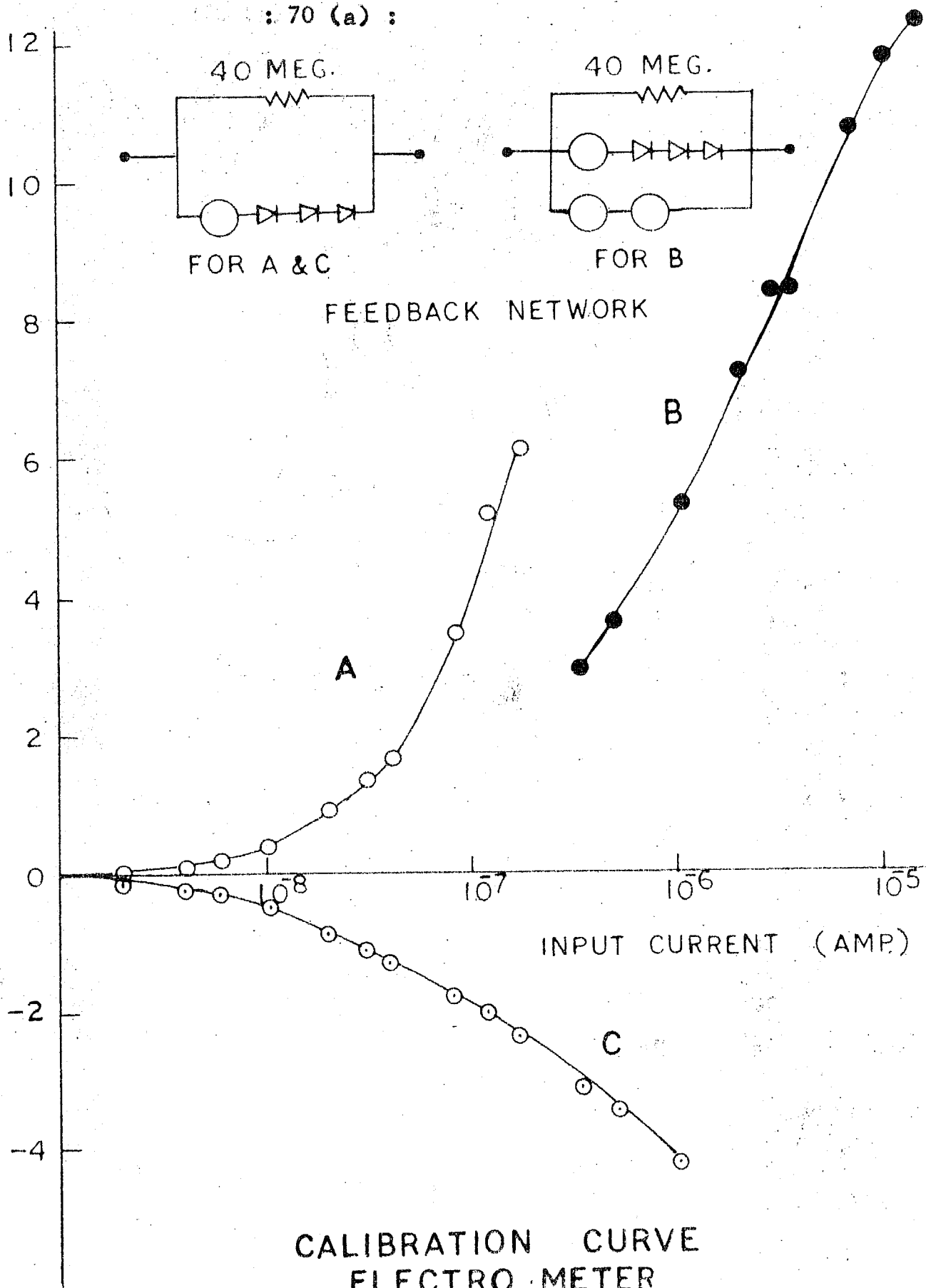
AMPLIFIER OUTPUT VOLTS
(ELECTRON CURRENT)

(POSITIVE ION CURRENT)

: 70 (a) :

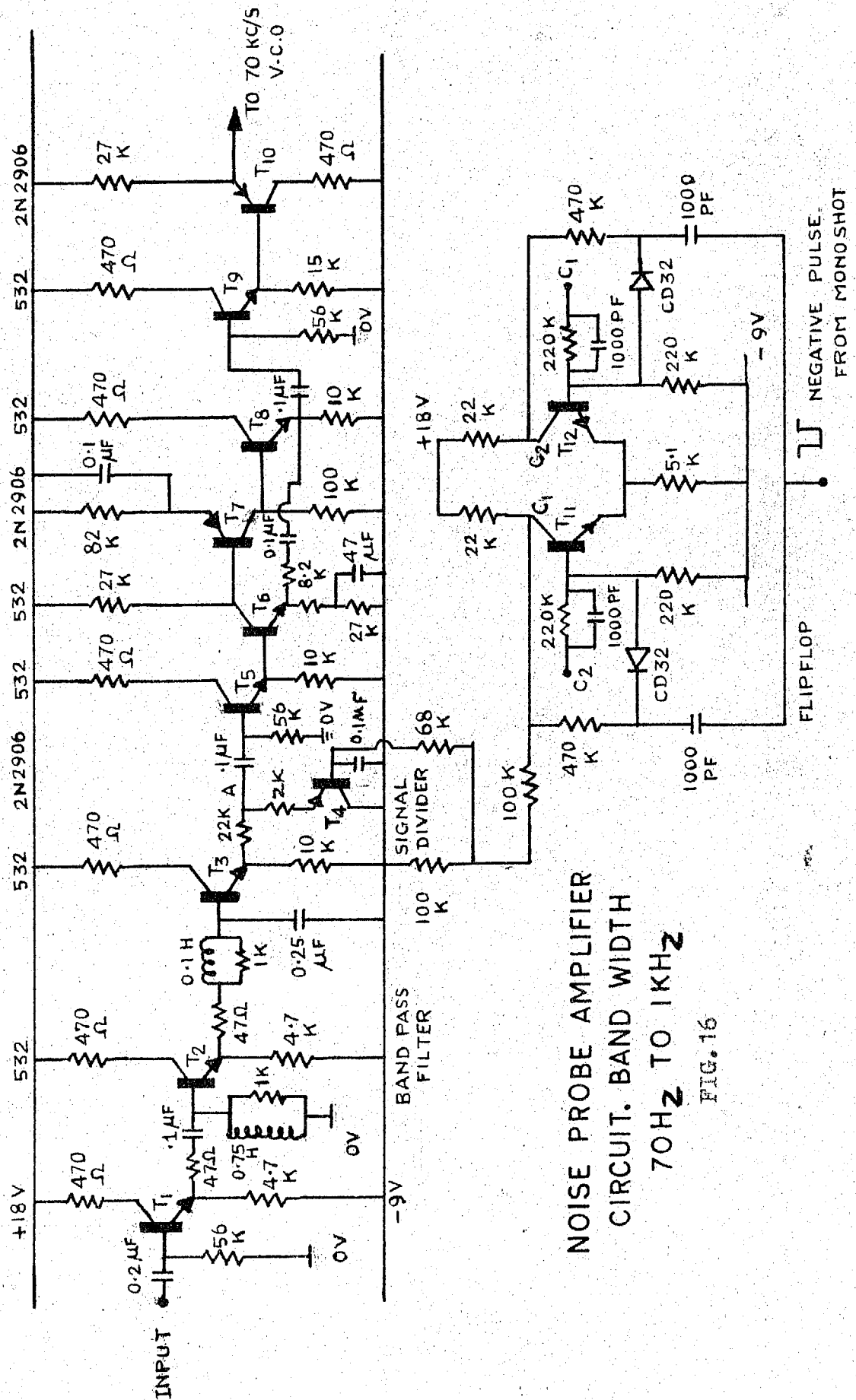


FEEDBACK NETWORK



CALIBRATION CURVE
ELECTRO-METER
AMPLIFIER

FIG. 15

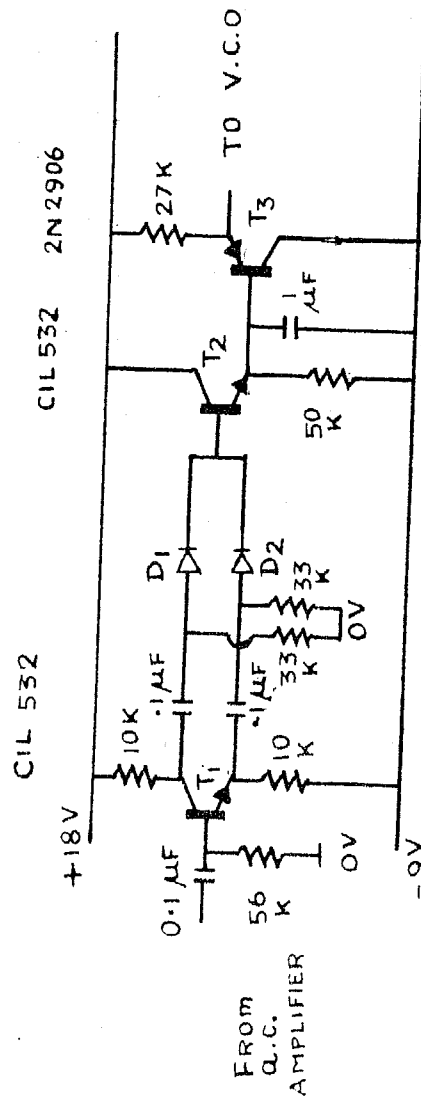


The filter output is divided in the ratio 1:12 every alternate sweep cycle to cover a large dynamical range. The change of gain (division) is obtained by the flip flop shown in the circuit diagram. The flip flop is triggered by a negative pulse fed from sweep circuit. The divider circuit consists of 22 K ohm resistance and 2 K ohm resistance in series with the transistor T_4 . When a positive pulse from flip flop is applied to base of T_4 the transistor remains non conducting and almost full signal appears at terminal A. But for a negative pulse it conducts fully and no voltage appears across the transistor T_4 . The terminal B is shorted to -9V and the signal at A, i.e., across 2.0 K is divided in the above ratio

The filter output is fed to a feedback amplifier. The amplifier can handle a signal of 0.4 volt peak to peak at its input. It has a voltage gain of twenty with feed back and one thousand without feed back.

In two rocket flights plasma noise signals were studied within a narrow band of frequencies. For this purpose narrow band pass filters were employed. In one flight filter frequency was 880 Hz \pm 15%. In another flight filters of 400 Hz and 960 Hz each of band width of \pm 7.5% were employed. The amplifier output used was same as described earlier. The a.c output of the amplifier was detected and telemetered.

The circuit diagram of phase inverter and diode detector is shown in fig.17. The a.c output voltage of the



PHASE INVERTER & DETECTOR
FIG. 17

amplifier is fed to phase inverter T_1 . The voltage at collector and emitter are 180° out of phase. The diode D_1 and D_2 form the diode detector circuit. The rectified output voltage is fed to T_2 . The condenser C is connected across the emitter resistance of T_2 for filtering. The filtered output is fed to an emitter follower and then to subcarrier oscillator.

4.9. Electronic differentiation of J-V Langmuir probe characteristics: In one of the flights electron temperature was determined by differentiating the J-V characteristic curve. The theoretical treatment of this method is given on page The electronic circuit used for this purpose was similar as shown in fig.17. A signal of about 2 m volt of 800 Hz frequency was superimposed on sweep voltage, with the help of a transformer. The signal at 800 Hz was selected at the output of the electrometer amplifier and amplified. The amplifier signal was then detected and telemetered. The a.c amplitude at 800 Hz will be maximum at space potential where the J-V characteristic has maximum curvature.

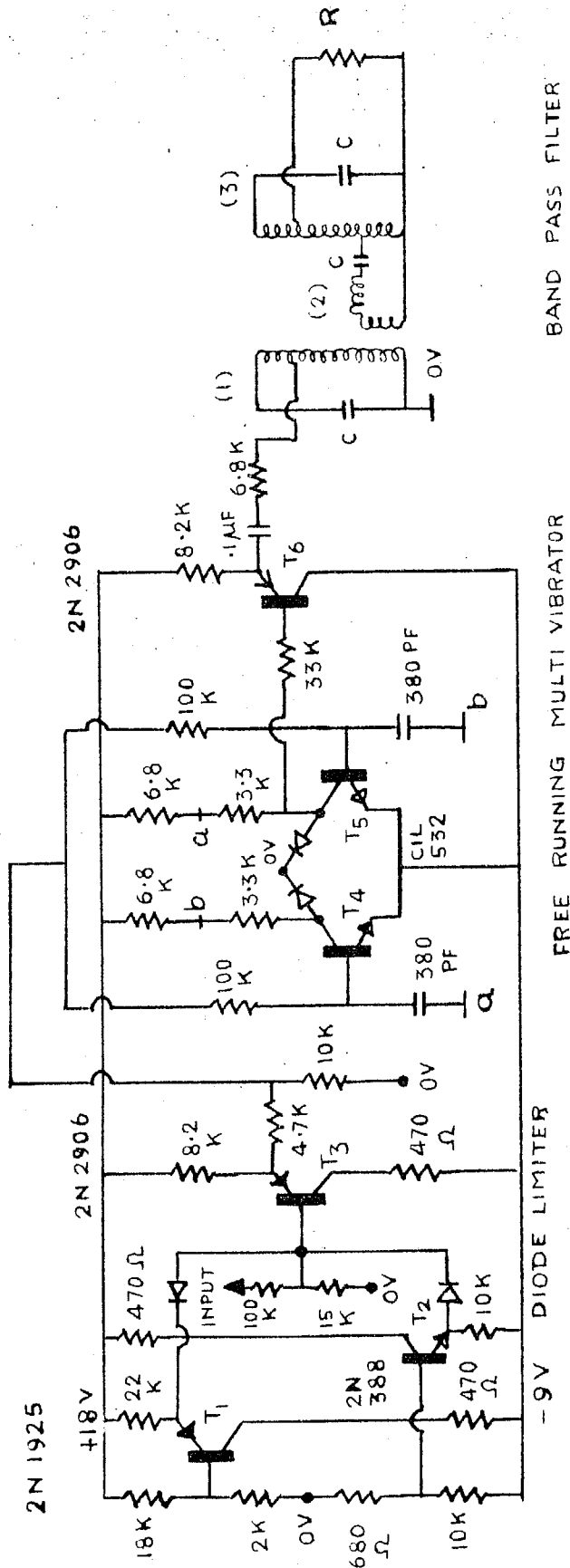
4.10 Subcarrier oscillators: The d.c outputs of the electrometer amplifier and a.c signal output of the plasma noise amplifier are fed to subcarrier oscillators (S.C.O) of FM/FM telemetry system. The oscillators are transistorised multivibrators designed for various IRLG standard subcarrier channels with a band width of $\pm 7.5\%$ of the centre frequency.

The channel selected to telemeter the particular information depends upon the intelligence frequency of the channel. The intelligence frequency is 10% of the channel ^{bandwidth}. The frequency of the signal should not exceed the intelligence frequency. For example, to telemeter plasma noise of 1 KHz frequency 70 KHz \pm 7.5% channel which has intelligence frequency 1.00KHz is needed. In case it becomes necessary to telemeter the signal which has frequency more than a few KHz, then the signal must be spectrum analyzed in the payload itself and the detected signal should be telemetered. Subcarrier oscillators were designed for centre-frequency of 10.5, 22, 40, 70 KHz with \pm 7.5% bandwidth. The circuit diagram of the S.C.O is shown in fig.18. It consists of a voltage controlled oscillator, a limiter circuit and band pass filter.

(a) Voltage controller oscillator: The VCO is a multivibrator whose oscillation frequency varies with input voltage. The frequency of a stable multivibrator is given by

$$\frac{1}{R_b C \ln \left(1 + \frac{V_c}{V_b} \right)} \quad 20$$

Where R_b is base resistance and C is coupling condenser. V_c is collector voltage and V_b is the bias voltage. In present circuit $\frac{V_c}{V_b}$ was about 1, V_b varies from $V_A' - 0.6$ Volt to $V_A' + 2$ Volt. The V.C.O were designed for the frequencies of I.R.I.G channels. The base resistance R_b was taken 100 K ohm and the approximate value of the condenser needed for a given centre frequency was calculated from above equation. In order to



SUB CARRIER OSCILLATOR
FIG. 18

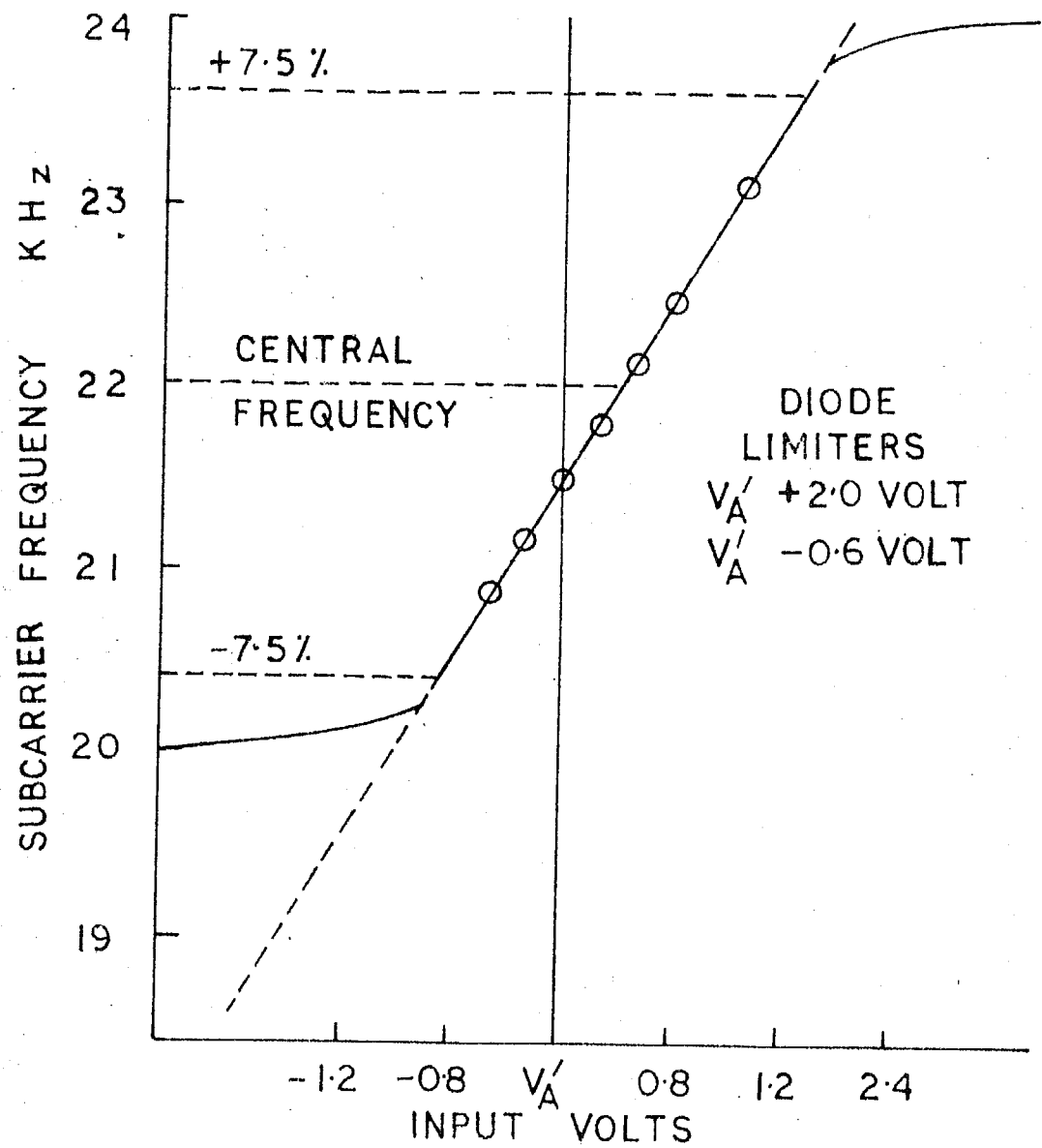
improve the recovery time of the multivibrator pulse the collector resistance used was less than one tenth of the base resistance and the collector voltage was clamped at one third of the total supply voltage. It also makes the frequency of multivibrator less sensitive to supply voltage variations.

The oscillating frequency was found to increase by one percent when the supply voltage is increased from +24 V to +30V. With temperature change from 27°C to 60°C the frequency increase was +1.5% of the central frequency. Typical curve showing the relation between input voltage and oscillation frequency are shown in fig.19.

(b) Limiter circuits: The V.C.O. frequency varies by $\pm 7.5\%$ of its central frequency for input variation of 2.6 Volt. In order that the input voltage variation should not exceed the desired voltage limit, diode limiter circuits (fig.18) were used to limit the input voltage levels.

(c) Band pass filters: The square wave output from V.C.O. is filtered to provide a sine wave input to telemetry transmitter. Band pass filter were designed for bandwidth $\pm 7.5\%$ centered at 10.5, 22, 40 and 70 KHz. The circuit diagram of the band pass filter is shown in fig.18.

It consists of three independent tuned circuits. The two parallel tuned circuits are coupled by a series tuned circuit. All the three networks were tuned at nearly same



FREQUENCY V_s VOLTAGE CHARACTERISTIC

FIG.19

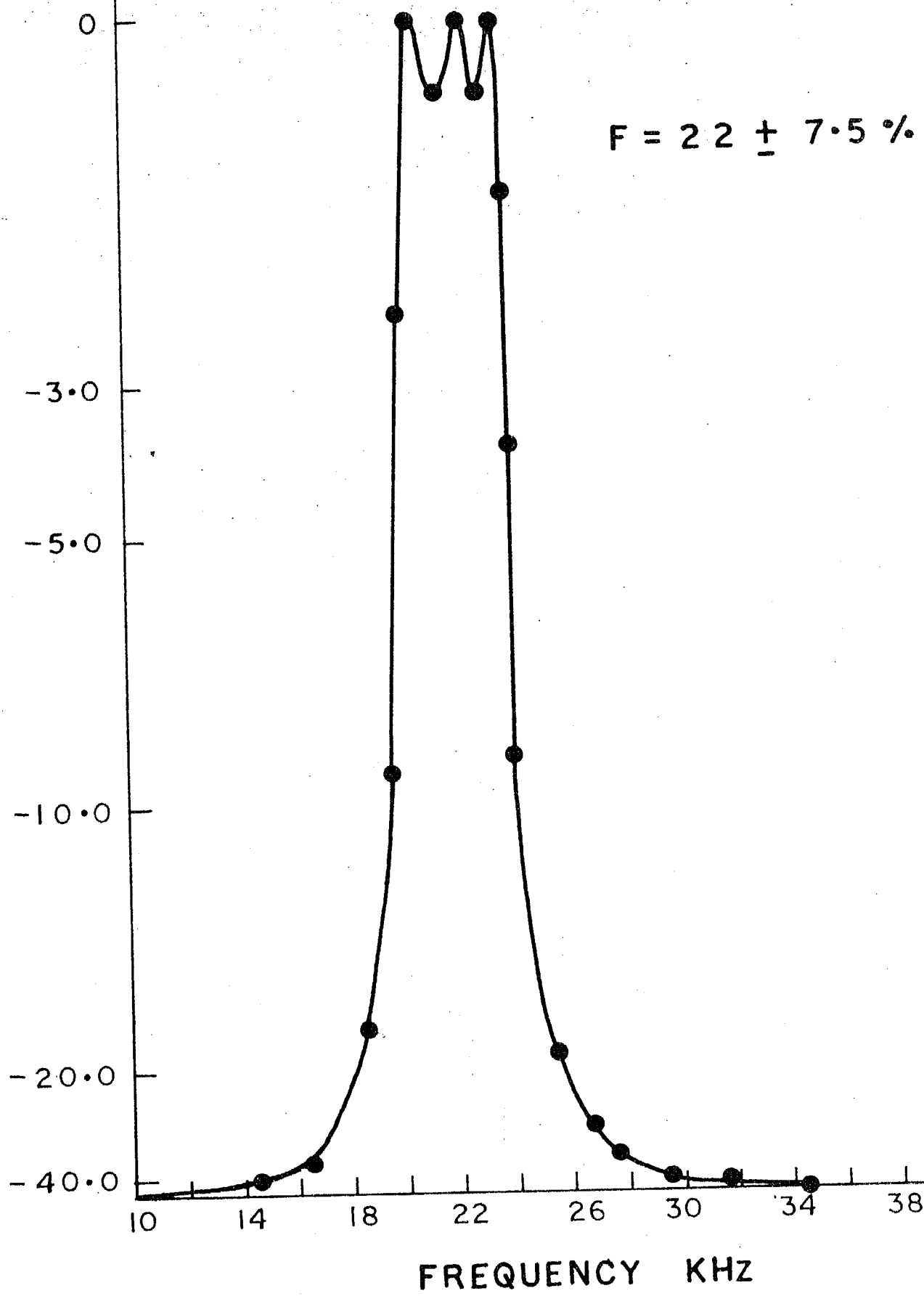
frequency. The inductance were wound on toroidal cores (Arnold Eng.Co.U.S.A.). The inductance values were chosen to get coil about twenty. The bandwidth of the filter is governed by the coefficient of coupling between coils (1) and (2) as well as between coil (2) and coil (3). The filter provides an output voltage with nearly constant amplitude around the resonance frequency and a sharp fall in amplitude at frequencies away from resonance by more than $\pm 7.5\%$. The frequency response of the filter is shown in fig.20. Specifications of the filter, frequency bandwidth $\pm 7.5\%$. Attenuation at 2nd harmonic and subharmonic 40 db.

4.11 Power supply: The power supply consists of a battery and a regulator. A 40.5 volt battery pack was used which can give 100 m.a. current for ten hours. Six burgess 135 R mercury cells each of 6.75 volt were used which have an ampere hour capacity with maximum current drain of 100 m.a. When the batteries are loaded by 100 m.a. the voltage drops to 36.0 volt because of the internal impedance of the cells which is about 45 ohms.

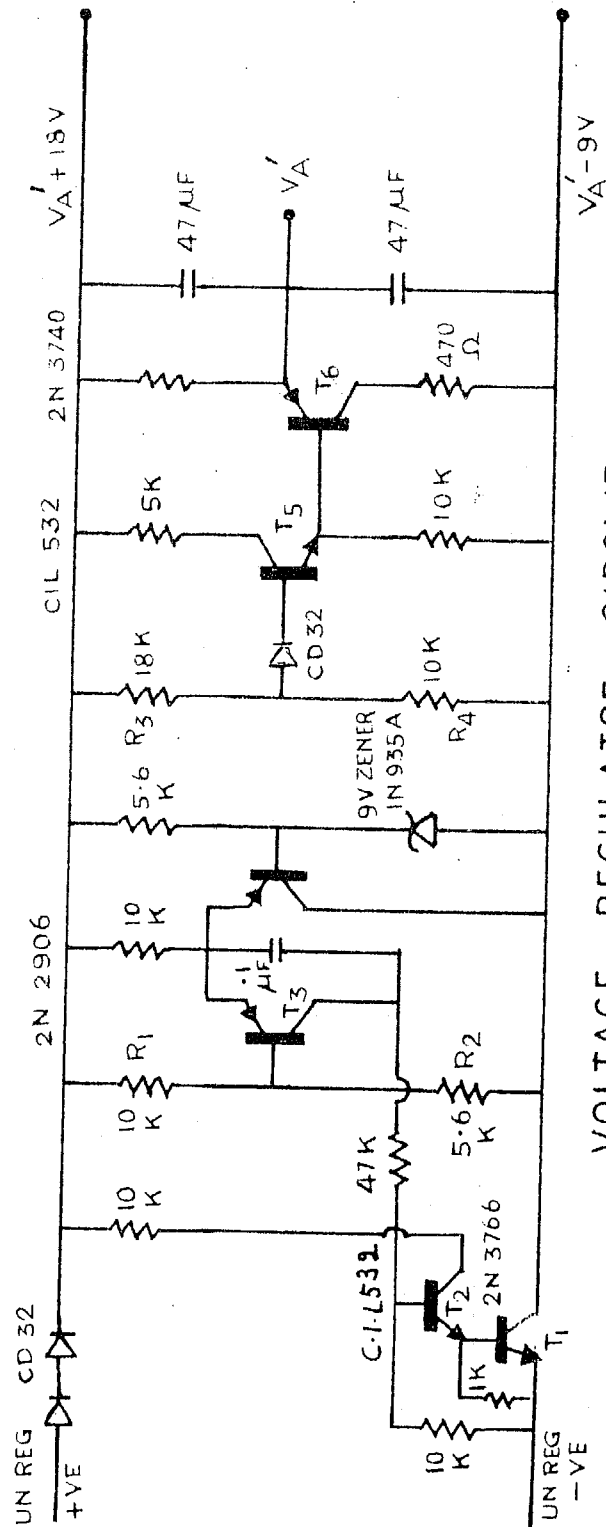
The probe electronics operated on floating power supplies at voltage $V_A^1 + 18$ volt and $V_A^1 - 9$ volt and requires 100 m.a. current. A voltage regulator was designed for these requirements. It had an output impedance of the order of ten milli ohms. The circuit diagram of the voltage regulator is shown in fig.21. The transistor T_1 and the power Transistor T_2 form a series control circuit. Transistor T_3 and T_4 form

FILTER OUTPUT db

$F = 22 \pm 7.5 \% \text{ KHZ}$



RESPONSE CURVE OF PRL MADE FILTER



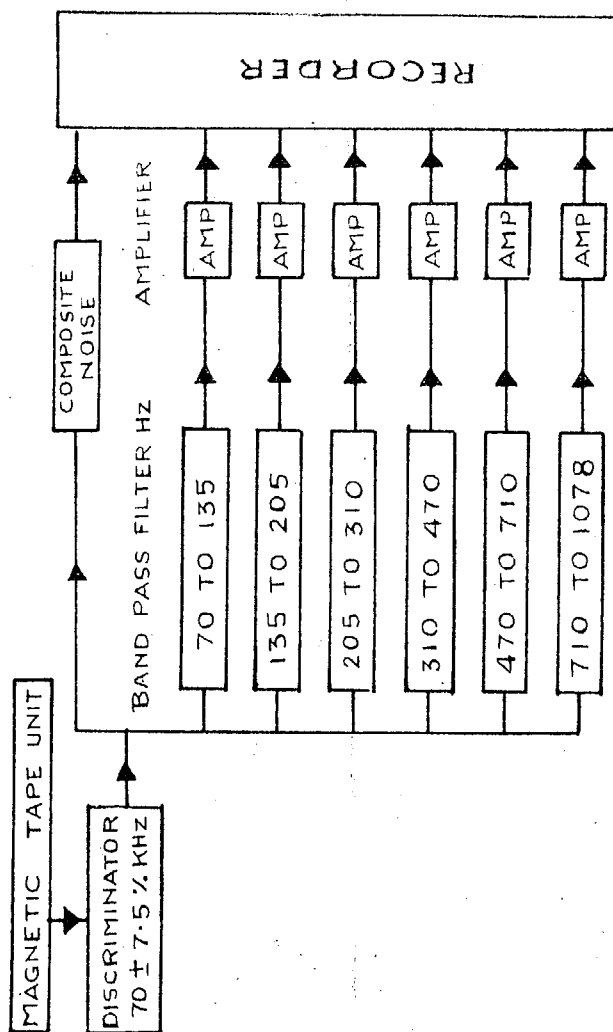
VOLTAGE REGULATOR CIRCUIT
FIG. 21

comparator and amplifier circuit. The zener diode of 9.0 volt is used for reference voltage. The condens^er C is used to suppress oscillations in the power supply.

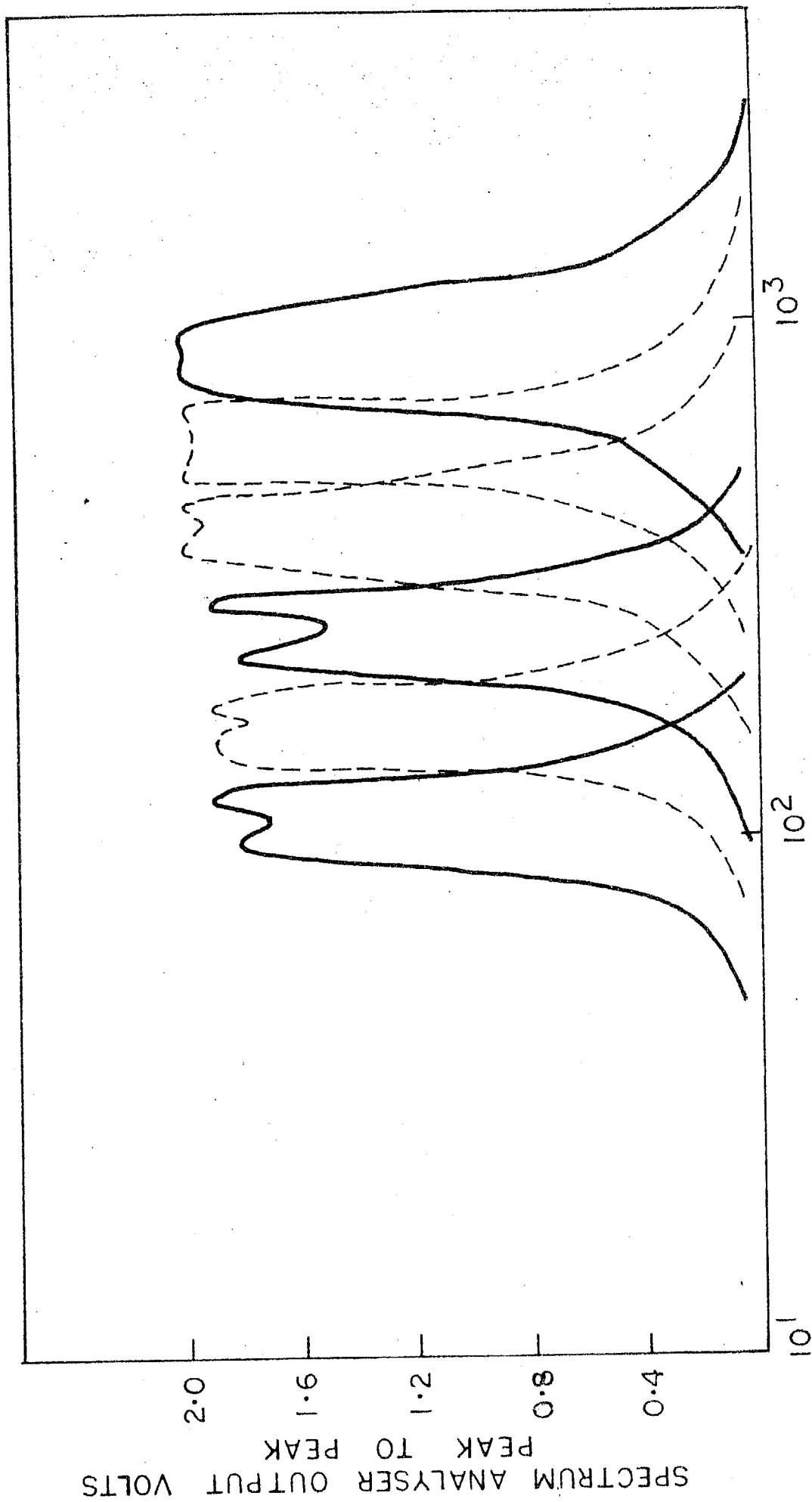
The power regulator provides regulated voltage of 27 volt. It is divided as +18 V and -9V with respect to V_A^1 . The divider circuit is also shown in the same figure. The resistance R_3 and R_4 divide the 27.0 volt in the ratio 2:1. The divider output is taken through emitter followers T_5 and T_6 . T_6 is a power transistor. T_6 output taken as reference voltage V_A^1 . The circuit provides two voltage as $V_A^1 - 9V$ & $V_A^1 + 18V$. High value capacitors are connected across these two voltages to by pass high frequencies or transients.

4.12 Spectrum analyser: For spectrum analysis of the composite plasma noise a spectrum analyser was designed which consists of six band pass filters. The filters are centered at frequencies 110, 170, 260, 400, 600 and 900 Hz each with a bandwidth $\pm 20\%$ of centre frequency. The block diagram of spectrum analyser and recording systems is shown in fig. 22. The composite plasma noise is fed to a driver stage and the driver output is fed to the six filter sections. The filter outputs are amplified and fed to a recorder. Frequency response of spectrum analyser is shown in fig. 23.

4.13 Wiring of the payload circuits: The complete electronic circuitry was wired on six fibreglass cards. A photograph of one of the wired cards is shown in fig. 24. The



PLASMA NOISE PROBE DATA RECORDING
USING SPECTRUM ANALYSER
FIG.22



RESPONSE CURVE OF SIX CHANNEL SPECTRUM ANALYSER

FIG. 23

electronic components were mounted and soldered on one side while interconnections were made on other side. To assemble all the cards of one payload, four brass rods of 3/16" diameter and length $6\frac{1}{2}$ " were used. Spacers of about 1" height were used between the two successive cards. The assembled payload photograph is shown in fig.25. The assembled unit is tested for proper performance. After proper checking and adjustment the unit was given a conformal coating.

4.14 . Potting of the payload: The payload undergoes a certain amounts of acceleration and vibration during rocket launching. Hence it is necessary that each electronic component should be tested upto certain specified condition. Mechanical support is necessary for bigger components. The payload cards were potted to give firm support to the components.

First an araldite layer was put on both the sides of the card. After the araldite is cured the units were potted with eccofoam. For potting an aluminium mould was designed. The material used for potting was the F P H Resin and 12-4H catalyst manufactured by Emerson and Cumming Co.of U.S.A.. The Resin and catalyst were mixed in the ratio 4:3 by weight. The mixed compound is poured on card kept in the mould. The mould is then closed by an aluminium plate. After about ten minutes the potted card is taken out from the mould. The card acquired a solid shape with thickness about 3/4". All the electronic components are completely covered by the

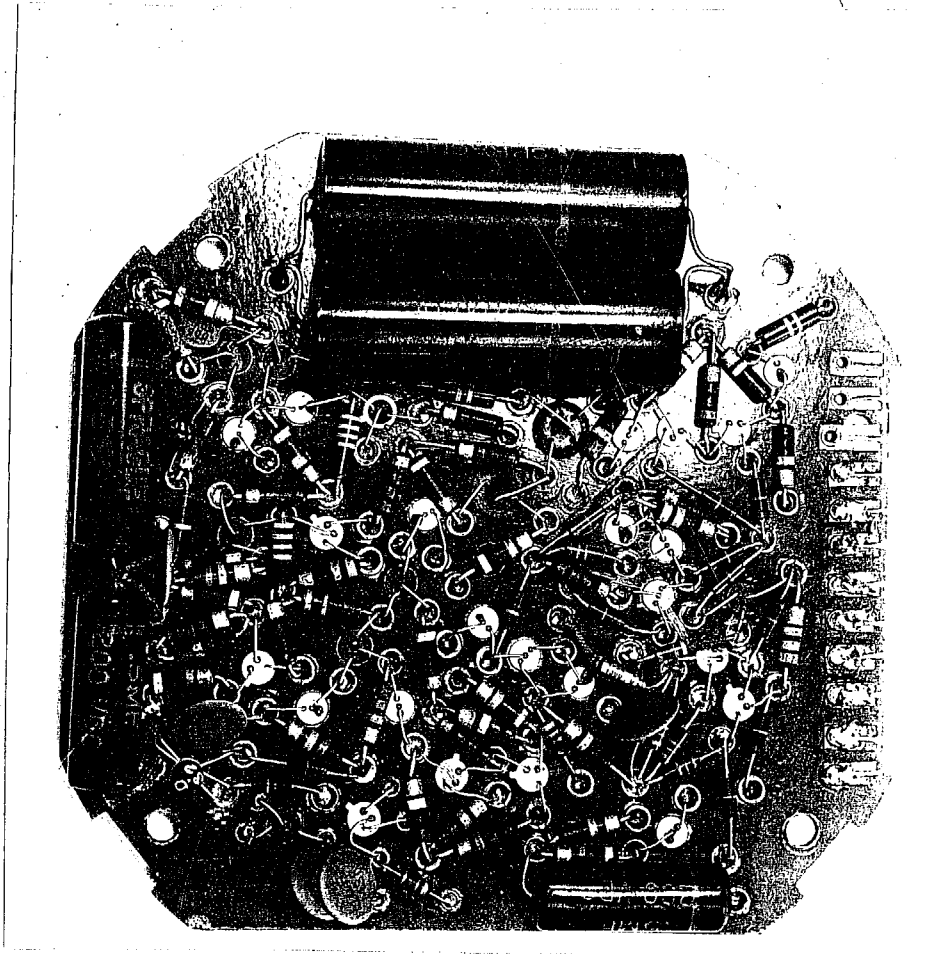


Figure-24 : Photograph of wired circuit.

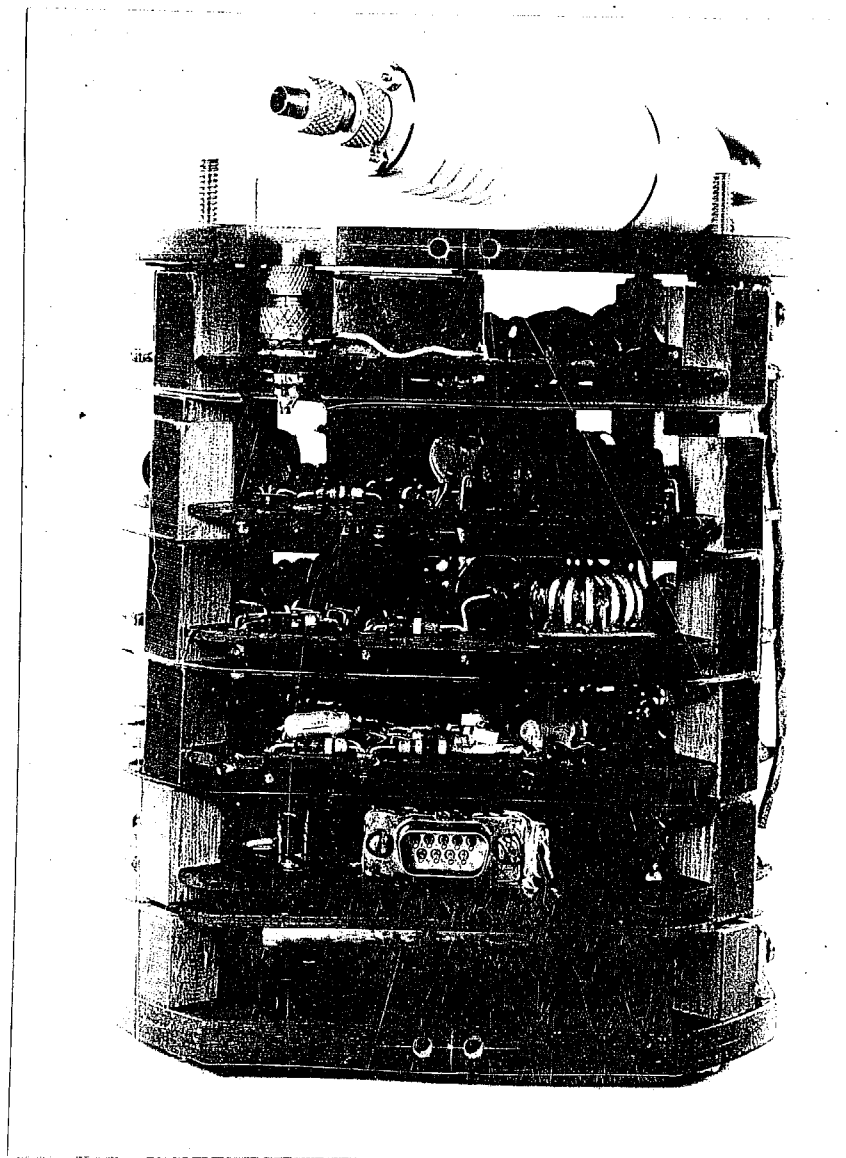


Figure-25 : Photograph of Langmuir probe and Plasma noise probe payload.

potting compound. The silastic R.T.V. rubber was used to cover the intercard connection terminals and other points where potting compound cannot be used. The R.T.V. rubber does not require a mould and hence is quite convenient to use. However, the resistance of the material remains low till it gets completely cured. Hence care should be taken not to use rubber to cover terminals where high resistances are used.

4.15 Telemetry requirements: A FM/FM standard telemetry system was employed. The mixed output from subcarrier channels modulates the transmitter frequency. The transmitters used had a carrier frequency in the vicinity of 240 MHz. Following were the specifications of one of the telemetry system.

Transmitter:

Frequency	244.3 MHz
Power	2 Watt
Sensitivity	100 KHz/volt r.m.s
Bandwidth	500 KHz
Output impedance	50 Ohms

Antennas:

The transmitter output is fed to the pair of circularly polarised turnstile antennas. The characteristics impedance of the antenna was 50 Ohms, and length about $\lambda/4$. Where λ is wavelength of the electromagnetic wave.

4.15.1 Transmitter supply: The transmitter operates on separate power supply whose one terminal is grounded to rocket body. A D.C to D.C converter was used to supply proper volt-

ages to the transmitter. The D.C - D.C converter operates at 6.0 Volts. Yardney silver cells HR-3 were used for converter supply. In one of the flight DC-DC converter operated on 30.0 Volts.

4.15.2 Mixing of subcarrier channels: A linear taper law was adopted for setting the carrier deviation to correspond to different subcarrier channels so that the signal to noise ratio remains equal in all the subcarrier channels.

This presumes that the signal strength at the receiver is more than 100 microvolt and no receiver noise is added to the signal. Foster (1965). However if weaker signal is expected then the channel voltages should be mixed in proportion of $f^{3/2}$ law.

Following table shows R.f deviation required for linear taper and also r.m.s modulation voltage for each channel for a transmitter described above.

Central frequency channel KHz	R.F deviation required KHz	R.M.S voltage	Experimental values	
			Input to mixer r.m.s volts	r.f deviation observed in KHz
10.5	8.40	0.084	0.13	10
22	17.6	0.176	0.26	20
40	32.0	0.32	0.43	35
70	56.0	0.56	0.60	55
	114 KHz	1.14 V R.M.S	1.42 R.M.S	120 KHz

4.16 Mounting & fixing of the payload and probe: The Langmuir probe and plasma noise probe including telemetry are accommodated in the cylindrical portion of the rocket nose-cone. In one rocket flight a part of conical portion of the rocket nosecone was also used. The whole payload is mounted in a rack. Fibreglass racks were used for flights accompanied by magnetometers. While for other flights the aluminium racks were used. Mounting procedure of the payload for one of the flight accompanied by T.M.A payload is described below, and the photograph of integrated payload including telemetry is shown in fig.26.

In the photograph the nosecone A, cylindrical portion B (a part of apoche body) and the integrated payload c is shown with sensor electrode. The sensor electrode is screwed at the tip of the nosecone. The cylinder B encloses the integrated payload C and is ~~screwed~~ at the telemetry housing portion. Above this the nose cone is fitted.

The rack used in one of the flight consists of four aluminium strips ^{each} of length twelve inches. Three strips of width one inch while the 'raceway' strip had a width of two inches. The base and top plates of the rack were also of aluminium.

The rack is mounted on the telemetry housing region which encloses the D.C to D.C converter and extend upto the region where it is screwed with the T.M.A payload housing

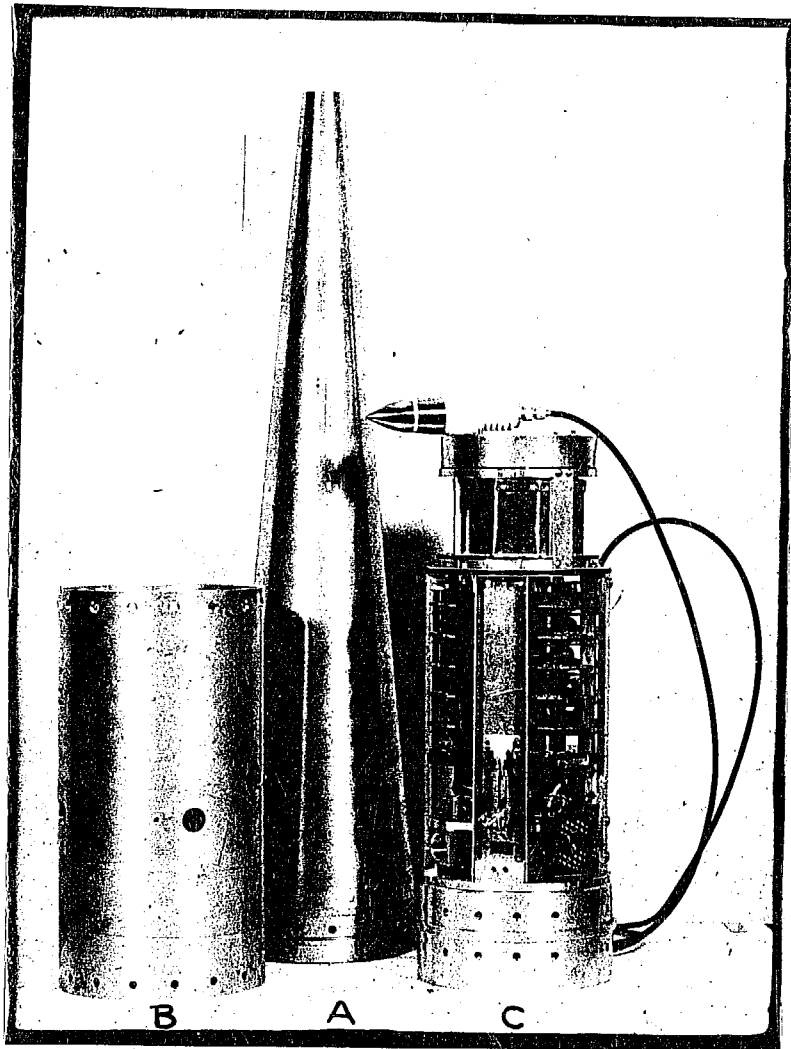


Figure-26 : Installation of Langmuir Probe, Plasma noise probe and Telemetry system in a Nike - Apache rocket.

portion of rocket. The D.C to D.C converter connections are brought through the bottom plate, through a connector. The transmitter, antenna bases and rocket umbilical is mounted on the bottom portion of this rack. In the upper portion the Langmuir probe and plasma noise probe payload is fitted. The battery box, consists of a pack of batteries for D.C to D.C converter and is mounted on the top plate of the rack. The top plate is provided with a hole, so the cable coming from the tip sensor is connected to the electrometer amplifier input.

4.17 Prelaunch testing: Prior to launching extensive tests are carried out while the rocket is on the launch pad. This includes horizontal checks and vertical checks. The block diagram/^{of} payload control and monitoring is shown in fig.27. The payload mounting points are brought from rocket umbilical to block house through cables. All the testing is carried out on external power. The payload performance is checked at ground-based telemetry station while the payload and transmitter voltage supply is monitored from block house. The FM/FM telemetry station at Thumba confirms the IRIG standard (TERIS hand book 1967). The telemetry station, subcarrier discriminator and recording oscillograph levels are properly adjusted before final calibration.

The control box was built to monitor the payload from block house whose circuit diagram is shown in fig. 28.

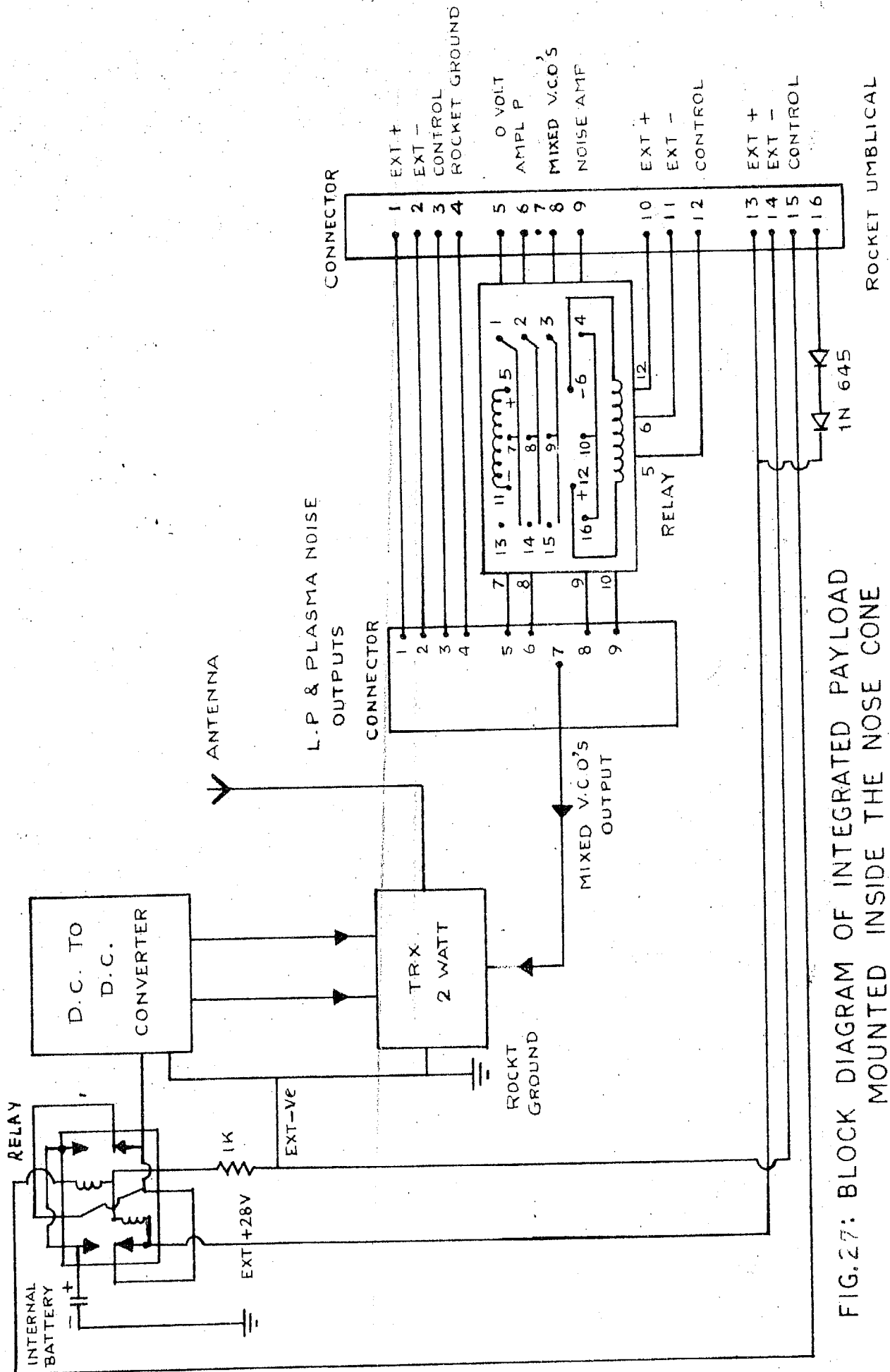
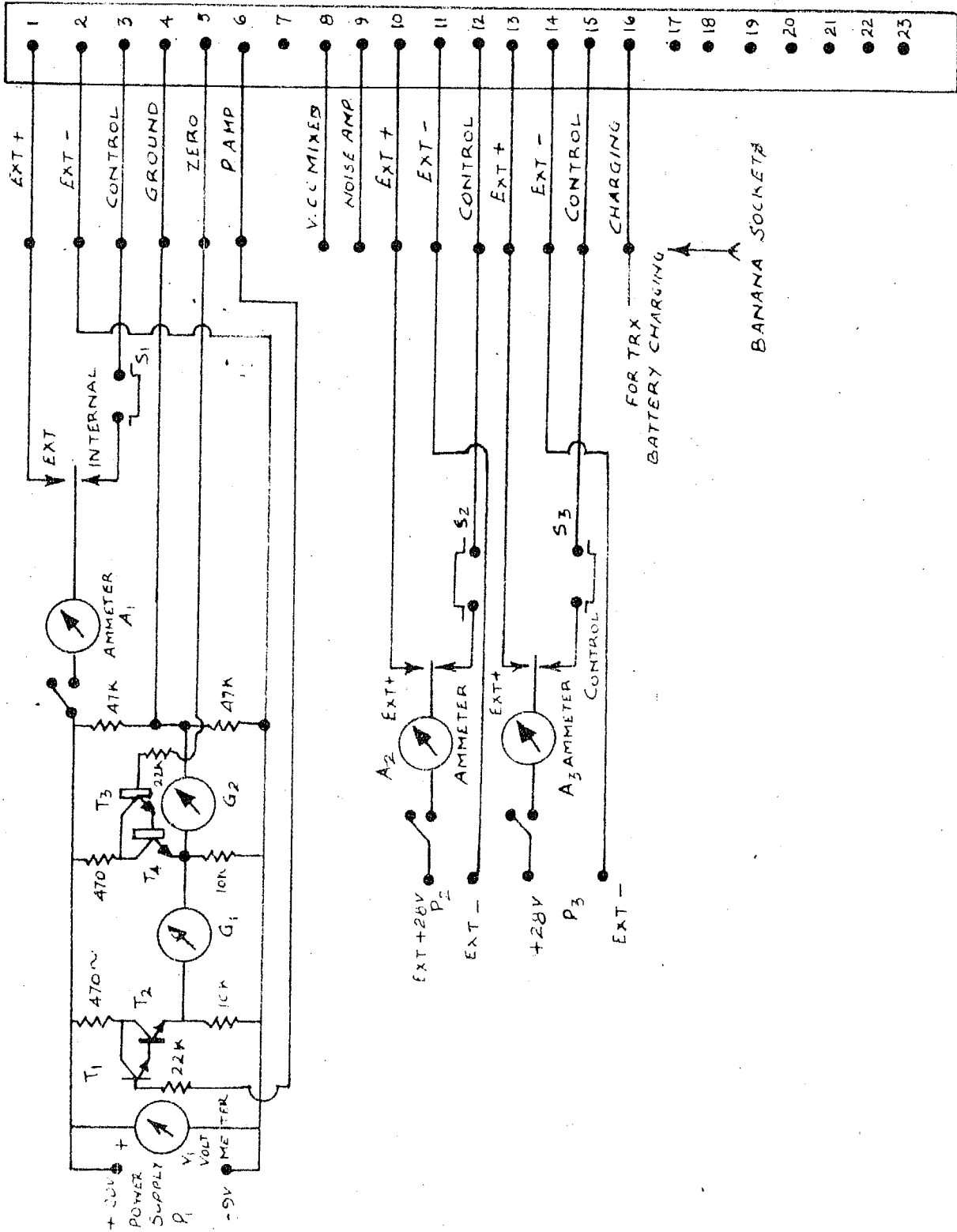


FIG.27: BLOCK DIAGRAM OF INTEGRATED PAYLOAD MOUNTED INSIDE THE NOSE CONE



22 PIN CONNECTOR

FIG. 28
CONTROL BOX DIAGRAM

The control box consists of driver circuits of transistor T_1 , T_2 and T_3 , T_4 . The voltmeter V_1 indicates the external power supply P_1 voltage. G_1 and G_2 galvanometers indicate amplifier output and sweep voltages respectively. Ammeter A_1 indicates the current drawn by the payload, when it operates on external supply. Switches are shown for changing the supply from external to internal.

The transmitter supply P_2 and relay control supply P_3 with ammeter A_2 and A_3 are also shown. The push button switches are shown by S_1 , S_2 and S_3 . The transmitter and the probe electronics can be switched separately. Indicating meters are fixed in the test box to indicate sweep voltage and also Langmuir probe amplifier output. The transfer of payload to internal power is also indicated by the same meters.

Just before launch calibration of the amplifier and sweep is carried out. Known resistances are put between the sensor and rocket body and the discriminator outputs are recorded. Calibration is done while the instrument operates on internal batteries.

The telemetered signal i.e receiver output is tape recorded. At the same time a real time record is obtained at a chart speed of 10"/sec. Slow speed, record is prepared by playing back the tape at a chart speed 1"/sec and 0.16"/sec. The slow speed record is used for quick look of electron density profile.

CHAPTER - V

EXPERIMENTAL RESULTS

Four Nike-Apache rockets carrying Langmuir probe and plasma noise probe were flown from Thumba (India) (8.52°N lat. 76.87°E , long. 0.47°dip) during 12th March 1967 to 29th August 1968. Each rocket was launched at an elevation angle of 84° (effective) and azimuth angle of 270° (effective).

A brief summary of each rocket flight including payload and vehicle performance is as follows:-

1. Flight 10.11, 12th March 1967, 1857 Hrs. I.S.T. Tip sensor with guard electrode was used for Langmuir probe. The insulator between the tip and guard electrode was of boron nitride. The plasma noise probe was flown to study the fluctuations in the Langmuir probe current at frequency $880\text{ Hz} \pm 15\%$. A signal of 2 milli volt at a frequency 800 Hz was superimposed on sweep voltage of differentiating the Langmuir probe characteristic to measure electron temperature by space potential method. The whole system was flown with sodium vapour payload. Sodium failed to eject. Hence both ascent as well as descent data were available for electron density, temperature and plasma noise. The rocket reached an estimated height of 164 km .

The performance of probe and associated electronics was satisfactory. Some leakage due to absorption of moisture by the boron nitride insulator was observed in the initial stages of the flight. The leakage decreased with

time and became negligible at about 100 seconds after launch during ascent, which corresponds to an altitude of 120 km.

This leakage was corrected for during data analysis. In later flights boron nitride insulator was not used.

1856 Hrs

2. Flight 10.13, 2nd February 1968 Hrs. IST: The tip sensor with guard electrode was used. In this flight the insulator was replaced by teflon. The Langmuir probe was accompanied with plasma noise probe which studied the fluctuations in probe current in the frequency range 70 Hz to 1 KHz. An inflight spectrum analysis facilitated the recording of plasma noise at frequencies 400 Hz and 960 Hz each with band width of $\pm 7.5\%$. The rocket also carried a trimethyl aluminium payload. The rocket reached an estimated height of 192 km.

The probe and associated electronics functioned satisfactorily. The T.M.A ejected around 165 km during descent. Near the apogee for a distance of about 20 km the probe data were not useful since the probe amplifier got shorted to the rocket ground at $T + 158$ sec. i.e 173 km during ascent. The short was removed due to the shock from squibs used for releasing T.M.A.

3. Flight 20.07, 29th August 1968, 1415 Hrs. IST: Tip sensor with guard electrode with a ceramic insulator was used. The insulator was replaced by ceramic alumina. The Langmuir probe and plasma noise probe (frequency range 70 Hz to 1 KHz) were accompanied by a proton precession magnetometer. The rocket reached an estimated height of 175 km.

The probe electronics functioned satisfactorily. The electrometer amplifier got saturated above 105 km due to the large resistance of feed back element (thyrite) and also due to high electron densities during day time hours. However the electron density profile was plotted above 105 km also by knowing the probe sensitivity at different probe voltages.

4. Flight 20.08, 29th August 1968, 23.00 Hrs.IST: The sensor assembly and the payloads were identical to those on flight 20.07. The system was flown with proton precession magnetometer. The rocket reached an estimated height of 175 km. The probe and associated electronics functioned satisfactorily.

The data from these four flights were analysed and the results are presented in this and the following chapters.

5.1 Nike Apache 10.11: The tip sensor was insulated from guard electrode by a boron nitride ring $1/8$ " in height. The guard ring was of $1/2$ " thickness insulated from the rocket body by teflon insulator of height $1/2$ ". Tip sensor diagram is shown in fig.29(a).

The sensor electrode is connected by cable to input of the electrometer amplifier. The sensor voltage was varied from -1.0V to +4.0V for 0.5 sec. and kept at +4.0V for 1.0 sec.

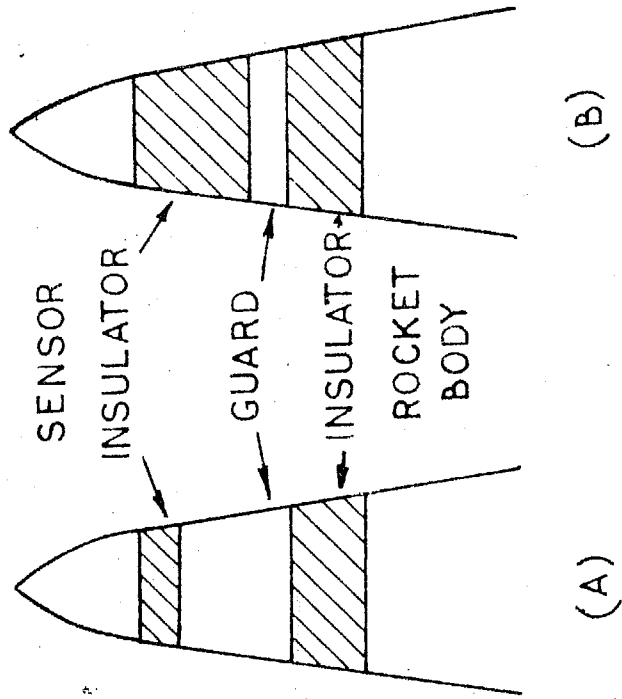


FIG. 29

The probe amplifier employed the electrometer tube CK587 (Raytheon) at the input. The amplifier was similar to that shown in fig.13 with thyrite as the feed back element. The thyrite feed back was employed to cover a dynamical range of about 10^4 . Thyrites (G.E. Co. U.S.A) which responded identically for positive as well as negative currents were used in the amplifier circuit. Thyrites which showed polarity effect were rejected. An inflight zero current marker was obtained by shorting the thyrite by a reed relay at the end of every sweep cycle.

The amplifier output was telemetered on two telemetry channels. The full signal was telemetered on 40 KHz \pm 7.5% channel. The probe amplifier output was fed to the plasma noise probe which consisted of a band pass filter in the frequency range 750 Hz to 1 KHz and an audio frequency amplifier.

The Langmuir probe characteristic was electronically differentiated by super-imposing a sine wave voltage of 2 milli volt of frequency 800 Hz on sweep voltage. The a.c signal at output of electrometer amplifier was amplified and detected. The detected D.C signal was telemetered on 22 KHz channel. The a.c amplitude will be maximum at space potential.

The plasma noise was also telemetered on 22.0 KHz channel. But the plasma noise was studied when sensor was at much more positive potential compared to space potential. At

such potentials the differentiated signal amplitude will be only about 5% compared to its value at space potential.

A calibrated baroswitch with two pairs of contacts set at 50,000 ft and 70,000 ft respectively was used to get information about rocket trajectory. When the pressure reached reference value during ascent the contact closes thereby shifting the d.c level of an electronic circuit. This was telemetered on 10.5 KHz \pm 7.5 channel.

The four subcarrier outputs were mixed by resistive network. The mixer output modulated the carrier frequency 241.6 MHz of Bendix transmitter of power 2 Watt.

During the flight the telemetry signal was received with modulation upto 336 sec. after launch. The R.F. signal continued to be received upto 405 sec. which was taken to be the total flight time. The receiver output was recorded on magnetic tape and simultaneously it was fed to discriminators of corresponding telemetry channels. The discriminator output was recorded on the photographic paper with a chart speed 10"/sec.

The telemetry record showed the presence of leakage between the sensor and the guard electrode when the rocket was still on the launch pad. The leakage gradually decreased during rocket ascent and became negligible around 120 km. It is believed that the leakage was due to absorption of moisture by the boron nitride insulator during

prelaunch period which gradually decreased due to heating during rocket ascent.

Operation of the baroswitch could be recorded only during ascent. This record together with the total flight time was used to get the rocket trajectory.

The correct rocket trajectory was obtained by matching ascent and descent electron density profile at the base of E region.

5.1.1 Determination of electron density: The current collected by the sensor when it is operated in the fixed potential mode i.e at +4.0V is measured from the telemetry chart. The telemetry chart calibration and electrometer calibration are made use in this process. The sensor is kept at +4.0 for 1.0 sec. So on the telemetry chart about 10" length is available (for chart speed 10"/sec). The average of 10 readings taken during the each sweep is tabulated versus time. The above probe current is later tabulated against altitude.

5.1.2 The conversion of probe current into electron density: The probe current could not be normalised to give electron densities since the densities were too low to be detected by the ionosonde at Thumba. The probe sensitivity was extrapolated from the previous day time flight, Satya Prakash et al (1968). It is found that a probe current of 1 μ amp. corresponds to an electron density of $1.5 \times 10^4/\text{cc}$.

The electron density profile for flight 10.11 is shown in fig.30.

5.1.3 The electron temperature: The probe current is plotted against probe voltage for individual sweeps (in the variable portion). The part of the graph representing collection of positive ions is extrapolated to obtain the contribution of positive ions to the probe current and subtracted from the total probe current to give electron current. This is then plotted on a conventional semilog graph. The slope of this semilog plot is used to calculate electron temperature. A typical plot is given in fig.31. The electron temperature values thus determined are plotted in fig.32. Full line represents neutral gas temperature for flight day conditions taken from CIRA (1965).

Because of some leakage observed upto 120 km, no attempt was made to determine electron temperature below 120 km during ascent. As can be seen from the figure, the electron temperature values are much larger compared to neutral gas temperature. The electron temperature show a sharp maxima around 140 km. The region of electron temperature maxima coincides with the regions of maxima in electron density profile.

An attempt was made to determine electron temperature by differentiating the Langmuir probe characteristics. The theory of the method has been discussed in chapter 3. A

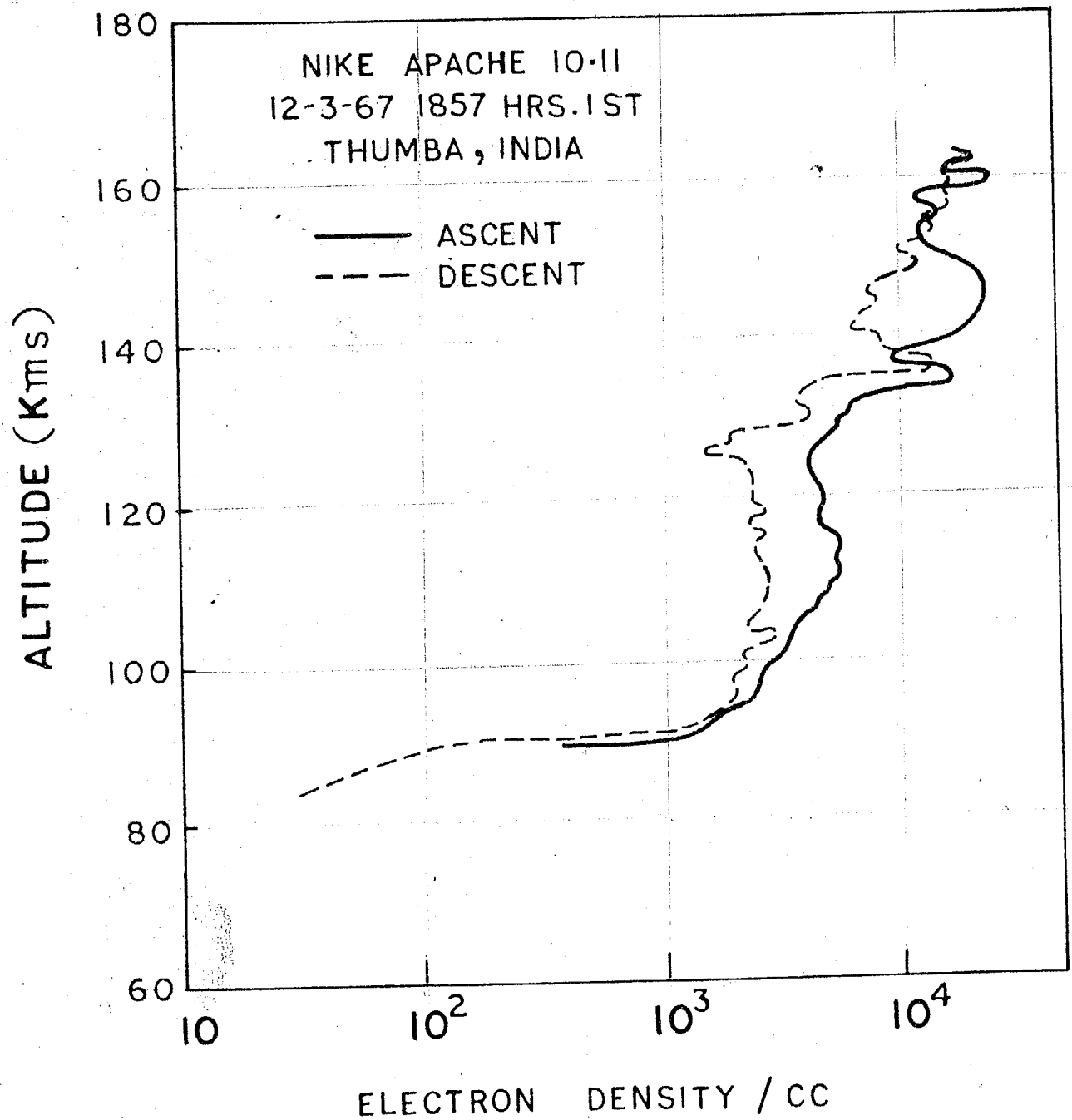


FIG-30

$$\frac{d \ln I}{dv} = \frac{e}{kT}$$

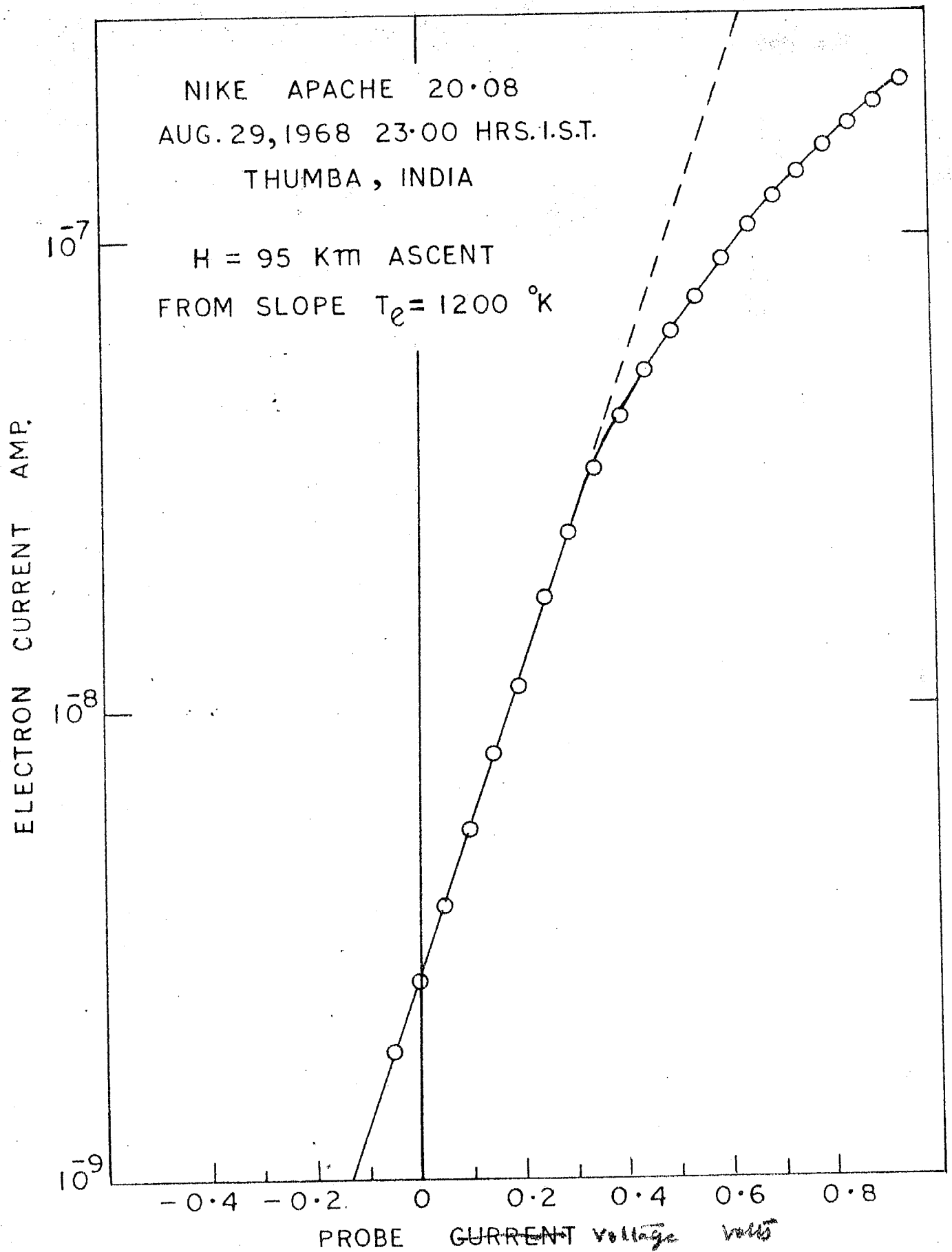
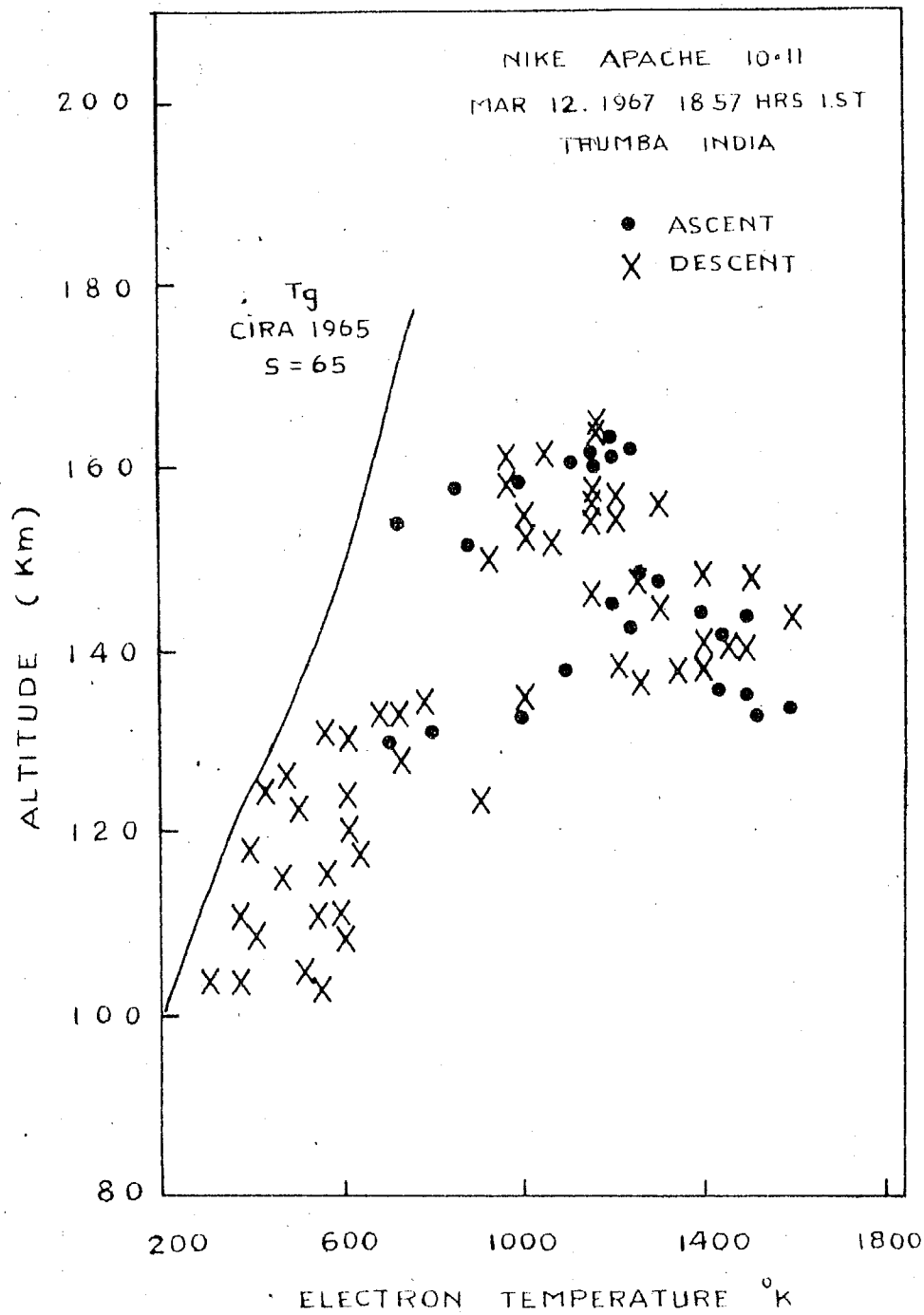


FIG. 31



sine wave of about 2. millivolt at a frequency of 800 Hz was superimposed on the sweep applied to the sensor. The a.c component at the electrometer amplifier output will have maximum amplitude when the sensor voltage is equal to space potential as the curvature, in the probe characteristic is maximum at space potential. This facilitates in locating the space potential point on Langmuir characteristic.

Electron temperatures determined by this method for a few sweep cycles. Only those sweeps were selected in which the point of inflection was clearly shown up in the telemetry record. The actual electron values of T_e were calculated from the equation:

$$V_o - V_s = \frac{5.1 K T_e}{e} \quad 21$$

Where V_o is probe potential at which probe current is zero and V_s is the observed space potential. These values were lower than the electron temperature values obtained from the usual retarding potential voltage method by a factor of about 1.8. But the number of observations available was small hence this factor required further confirmation.

5.1.4 Small scale irregularities: Small scale fluctuations in frequency range $880 \pm 15\%$ in the Langmuir probe current of amplitudes upto 0.5% of the total probe current were observed, in some height regions. In these regions the first differential of J-V characteristic was less than 0.05% of the probe current. Large scale fluctuations of sizes more than 50 meters can be seen directly on Langmuir probe current.

The percentage fluctuation in the probe current is shown in fig.33. The right hand side figure represents the absolute value of electron density fluctuations. This curve when compared with the electron density profile shows that fluctuations in electron density are observed mostly in the regions where the electron density gradient is positive (in upward direction). The fluctuations are seen between 90 to 120 km and between 130 to 145 km region both in ascent as well as in descent. Fluctuations seen between 150 km to 164 km i.e around apogee is due to rocket motion itself (Satya Prakash et al 1969). Fluctuations were not seen between 115 to 125 km region where electron density gradients are negative in upward direction.

5.2 Nike Apache 10.13 The sensor had the same size and shape as that on flight 10.11. The boron nitride insulator was replaced by a teflon insulator of 1/8" thickness. The guard electrode thickness was 1" and it was insulated from rocket body by a teflon insulator of thickness 1". Tip sensor diagram is shown in fig. 29 (a).

The sensor electrode was connected by cable to input of electrometer amplifier. The sensor voltage was varied from -1.0V to +4.0V for 0.5 sec. and stayed at +4.0V for 0.5 sec.

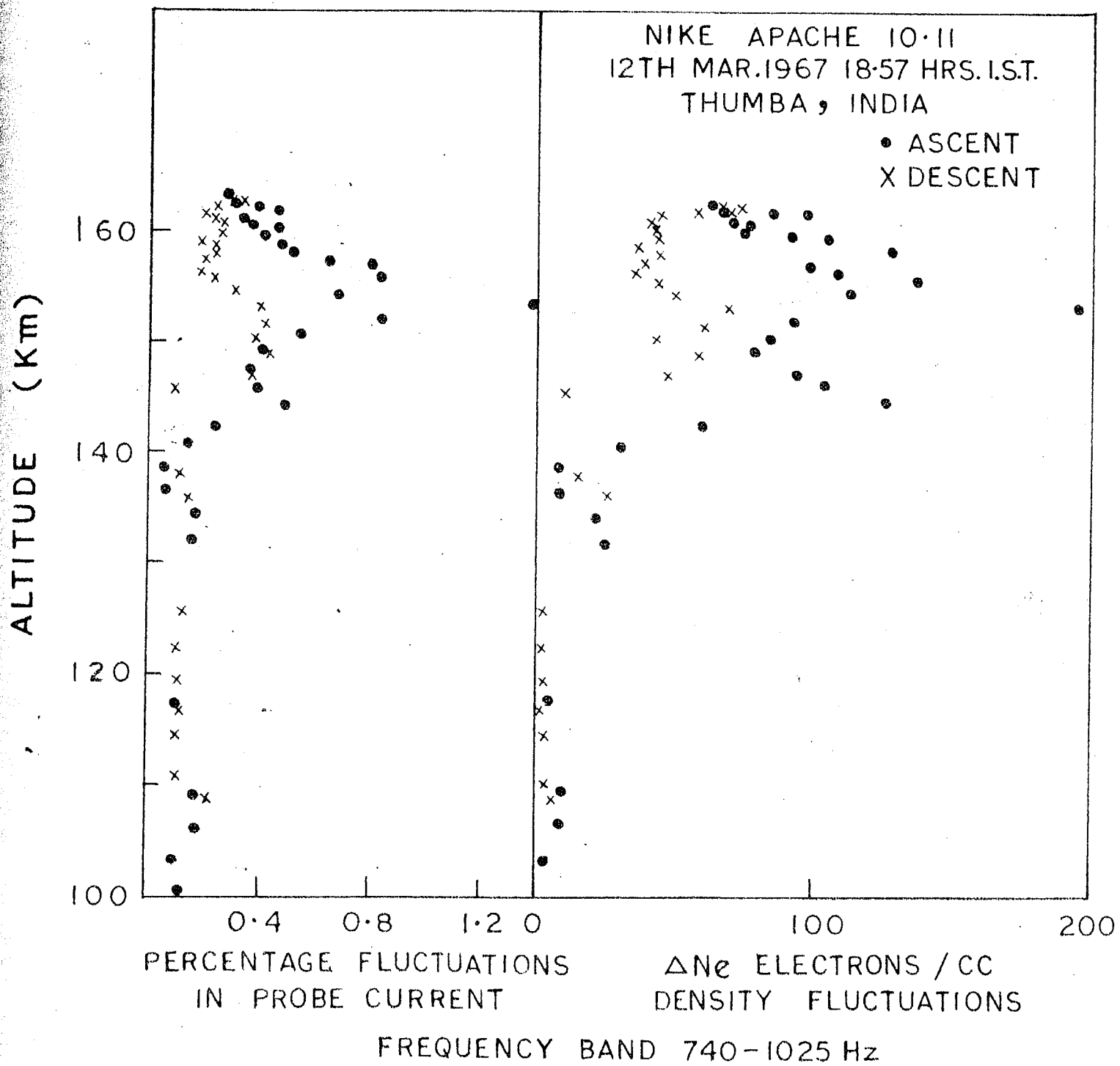


FIG. 33

The probe amplifier consisted of electrometer tube CK587 (Raytheon). The amplifier was similar as shown in fig.13. The resistance feed back of 40 Meg ohm was employed for current range 0.1 μ amp (positive ion current) to +0.25 μ amp. (electron current). While for current larger than 0.25 μ amp. thyrite feedback was employed. The resistance to thyrite feedback switching circuit is shown in fig.14.

The amplifier output was telemetered on two telemetry channels. The full signal was telemetered on 40 KHz \pm 7.5% channel while signal was telemetered on 22 KHz \pm 7.5% channel. Plasma noise measurements were carried out in the frequency 70 Hz to 1 KHz a.c output of the amplifier which represents the total noise in this frequency range was telemetered on 70 KHz \pm 7.5%.

The plasma noise in frequency bands 400 Hz \pm 7.5% and 960 Hz \pm 7.5% were filtered and telemetered after proper amplification and detection on 10.5 KHz \pm 7.5% channel on time sharing basis. This provided an inflight spectrum analysis of plasma noise.

The four subcarrier outputs were mixed by resistive network. The mixer output modulated the carrier frequency 244.3 MHz of transmitter of power 2 watt.

During the flight the telemetry signal was received upto 420 sec. which was taken to be the total flight time. Radar could track the rocket upto 50 km. Radar data

together with total flight time and matching of the ascent & decent^d electron density profiles at the base of E region was used to determine the rocket trajectory as described earlier.

5.2.1 Electron density: The probe current when the sensor is operated at +4.0 volt is determined from telemetry record. The probe current values were converted into electron density from ionogram obtained at Thumba around flight time. The ionogram at 1830 Hrs I.S.T. at Thumba showed a clear E region echo with a critical frequency of 1.7 MHz at a virtual height of 165 km.

At 1850 Hrs I.S.T. a diffuse patch was visible upto 1.3 MHz. With some reservation this can be taken to correspond to peak probe current observed during the flight. This gives a scaling factor of 1 amp. of probe current = 1.15×10^4 electron/cc.

Near the apogee for a distance of about 20 km the probe data was not useful since the probe amplifier input got shorted to rocket body at T + 158 sec., corresponding a height of 173 km. The short was removed due to the shock from squibs used for releasing T.M.A at T + 289 sec. during descent (corresponding to a height of 165 km). The effect of T.M.A. release on the probe performance was to decrease the current collection and also introduce a marked spin modulation in the probe current profile. However, the general

features of the probe current profile could be made out even during this period and the electron density is plotted for this period also.

The electron density profile is shown in fig.34. For descent values the thin line and dotted line show maximum and minimum values of probe current during a spin cycle. The difference between the two shows the effect of spin modulation.

5.2.2 Plasma noise: The fluctuations in frequency range 70 Hz to 1 KHz (scale sizes 1 to 15 meters) were recorded in probe current. The fluctuations in probe current were observed when the sensor voltage was such that it was operating in region II and I of Langmuir probe characteristic see fig.2.

The percentage fluctuations in the probe current in frequency range 70 Hz to 1 KHz corresponding to scale sizes from 1 meter to 15 meters is plotted in fig.35. The right hand side plot shows the absolute value of electron density fluctuations. The values are plotted only for alternate sweep cycles when the plasma noise probe amplifier gain was high. Also only ascent values are plotted. Due to T.M.A. ejection around apogee no attempt was made to determine percentage fluctuations in probe current during descent. This plot when compared with the electron density profile of fig.34 shows that fluctuations in electron density are

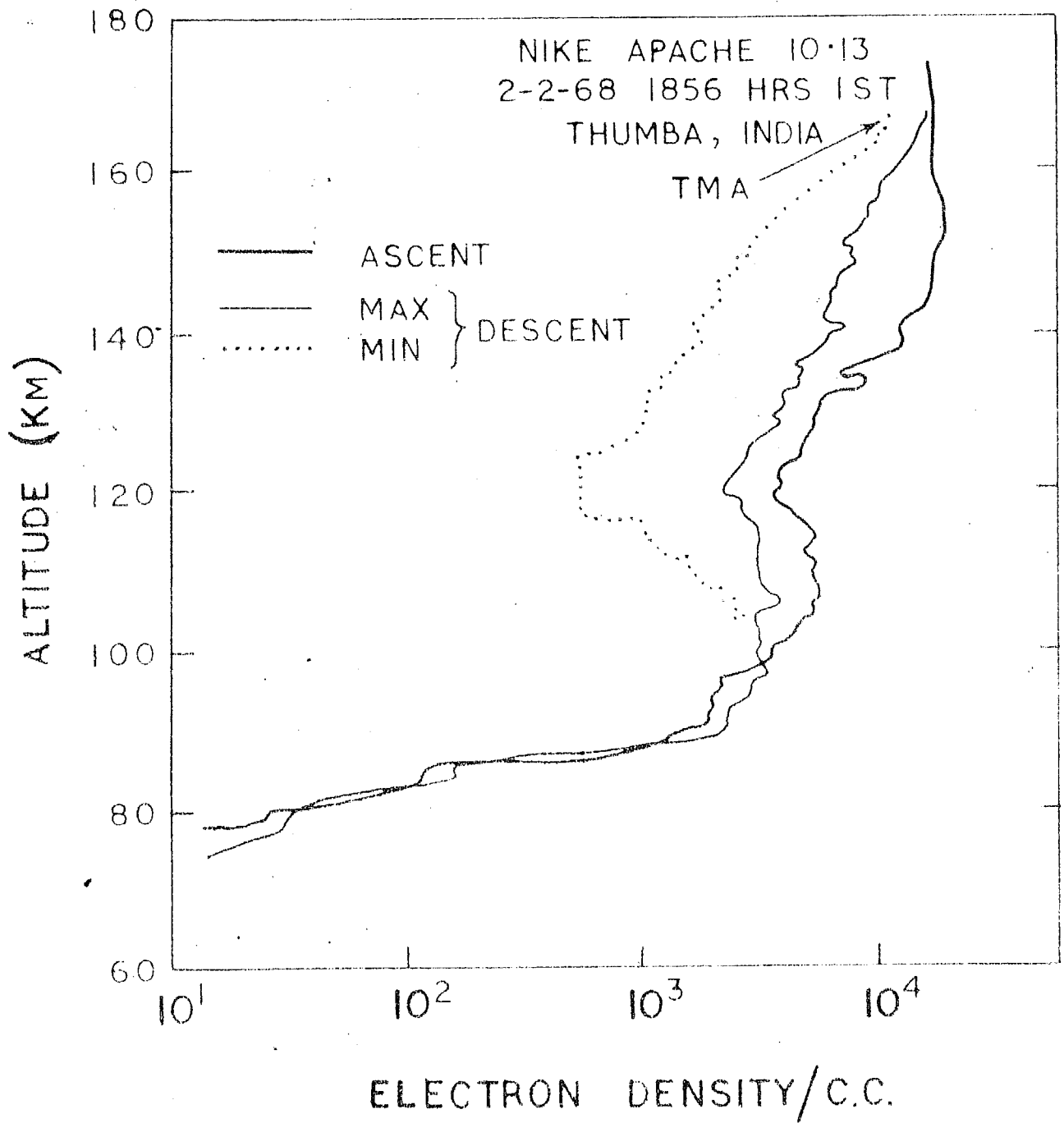


FIG.34

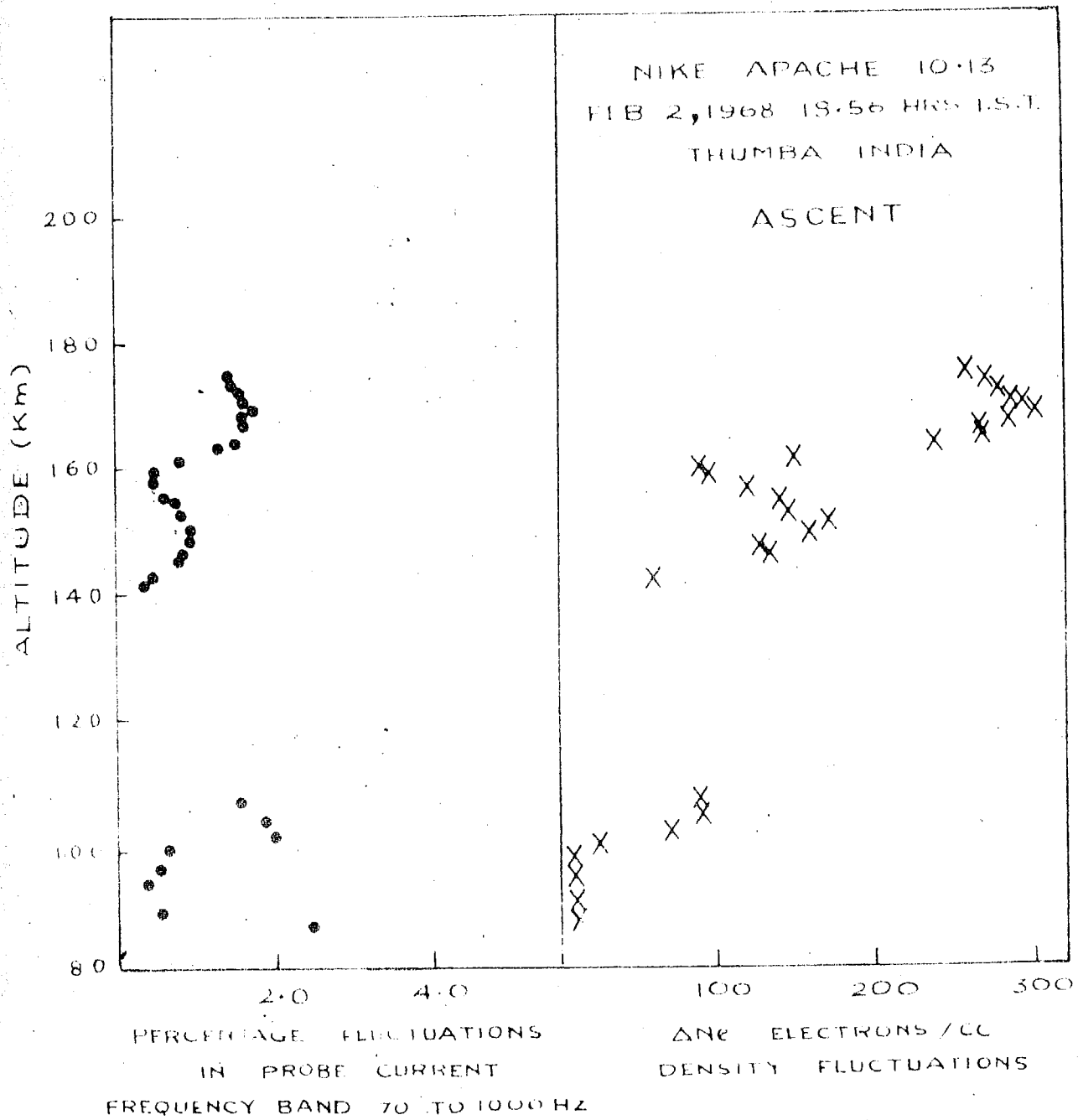
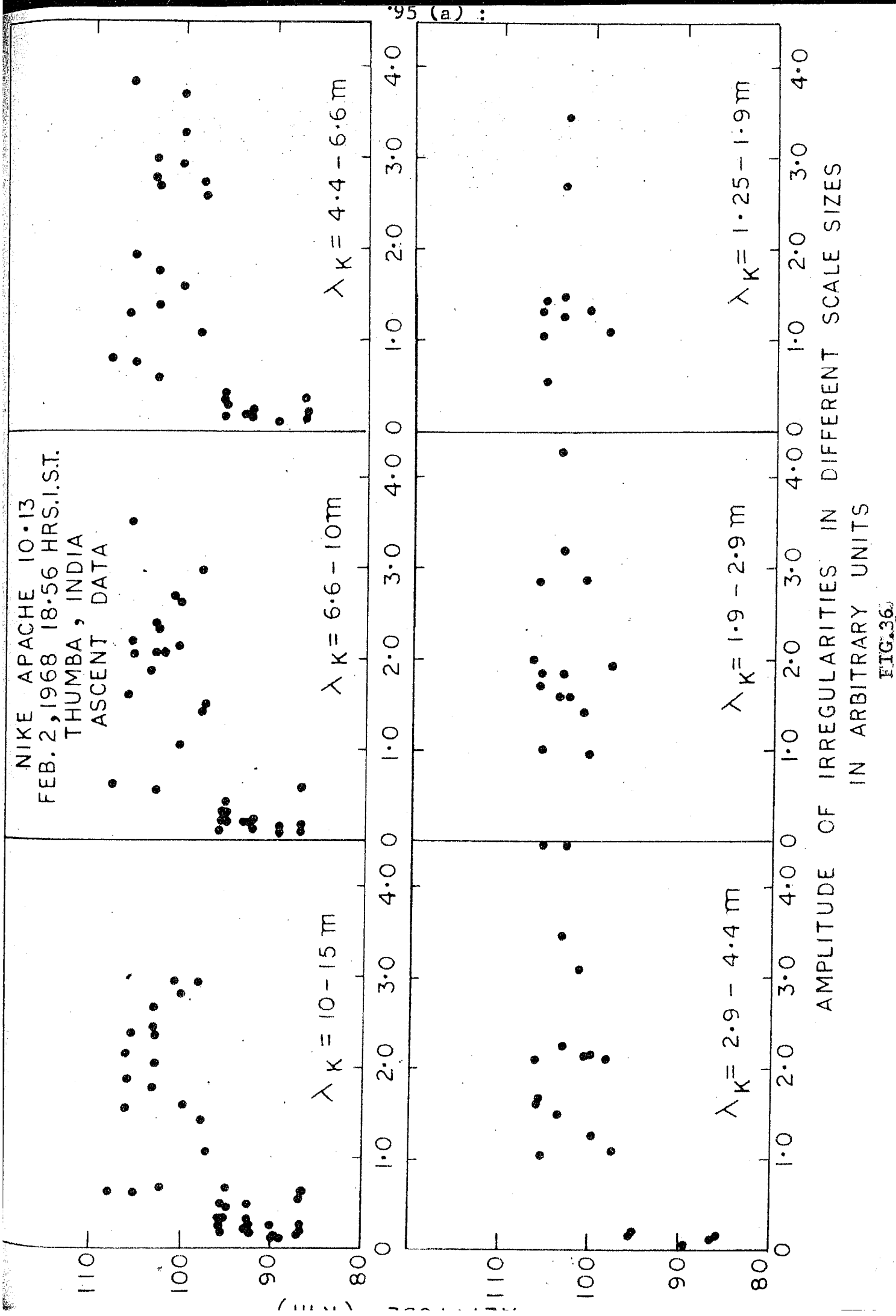


FIG. 35

observed when electron density gradients are positive in upward direction. The noise observed ^{near} apogee i.e around 175 km is due to rocket motion itself.

5.2.3 Spectrum analysis of plasma noise: The composite plasma noise was spectrum analysed by playing back the magnetic tape. The discriminator output was fed to the spectrum analyser. It consists of six band pass filters each of band width $\pm 20\%$, and centered at 110, 170, 260, 400, 600 and 900 Hz. The scale size of the irregularities has been calculated by V_R/f where V_R is rocket velocity at the altitude under consideration and f is the filter frequency. The amplitude of different scale sizes is shown in fig.36. The amplitude scale along the abscissa when multiplied by a certain calibration constant will give directly the absolute value of fluctuations in electron density over the ambient medium. The constant in this case is 7. An examination of fig.36 shows that in the height range 97-106 km the fluctuations amplitudes are large in entire range of scale sizes covered i.e 1 meter to 15 meters.

Below 97 km the amplitude are small. It should be pointed out that in the height range 87 to 97 km fluctuations corresponding to frequencies less than 70 Hz i.e. scale sizes larger than 15 meters can be directly seen on Langmuir probe current.



The fluctuation amplitudes were plotted against their scale size on a log-log plot and spectral index n was calculated for a power law of type $E(k) \propto k^n$ where $E(K)$ is the energy in wave number K . A typical plot is shown in fig. 37. The resulting values of ' n ' are shown in fig. 38. It shows that ' n ' is of the order of -3.5 at lower heights. With increasing height the negative value of n was decreased to a value of -1.6.

5.3 Flight 20.07: The probe assembly in this flight consisted of a stainless steel ogive electrode with a ceramic insulator of height 1". The guard ring was of stainless steel and 1/16" in height Fig.29.b. The guard electrode was insulated from the rocket body by a teflon insulator.

The sensor voltage was varied from -1.0 volt to +4.0 volt in 0.5 sec. and kept at +4.0 Volt for 0.5 sec. The electrometer amplifier was same as the one used on flight 10.13. The full signal of electrometer amplifier was telemetered on 40 KHz channel while divided signal on 22 KHz. The amplifier output was telemetered on two channels. The plasma noise was telemetered on 70 KHz \pm 7.5% channel. The mixed signal of three subcarrier oscillators was fed to the transmitter for frequency 241 MHz and 2 watt power.

During the flight the telemetry signal was received upto 408 sec. This was taken as the total flight time. The rocket trajectory was determined by the matching

NIKE APACHE 20.08
AUG. 29, 1968, 2300 HRS IST
THUMBA, INDIA

ALTITUDE
a 98 Km
b 102 Km
c 105 Km

PERCENTAGE
FLUCTUATIONS

10^{-1}
 10^{-2}
 10^{-3}
 10^{-4}

10

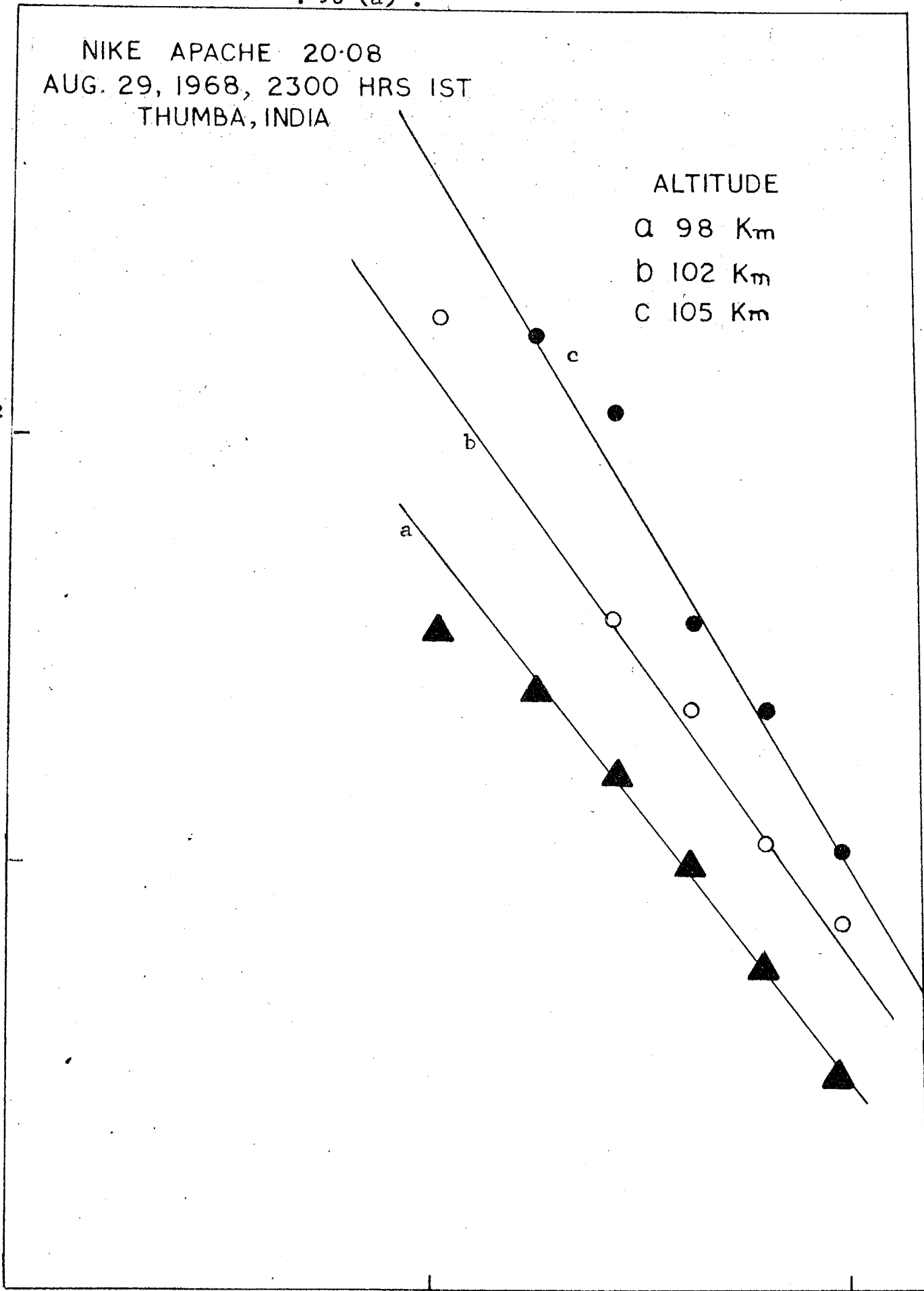
10^2

10^3

FREQUENCY Hz

LOG-LOG PLOT OF PLASMA NOISE SPECTRUM

FIG. 27



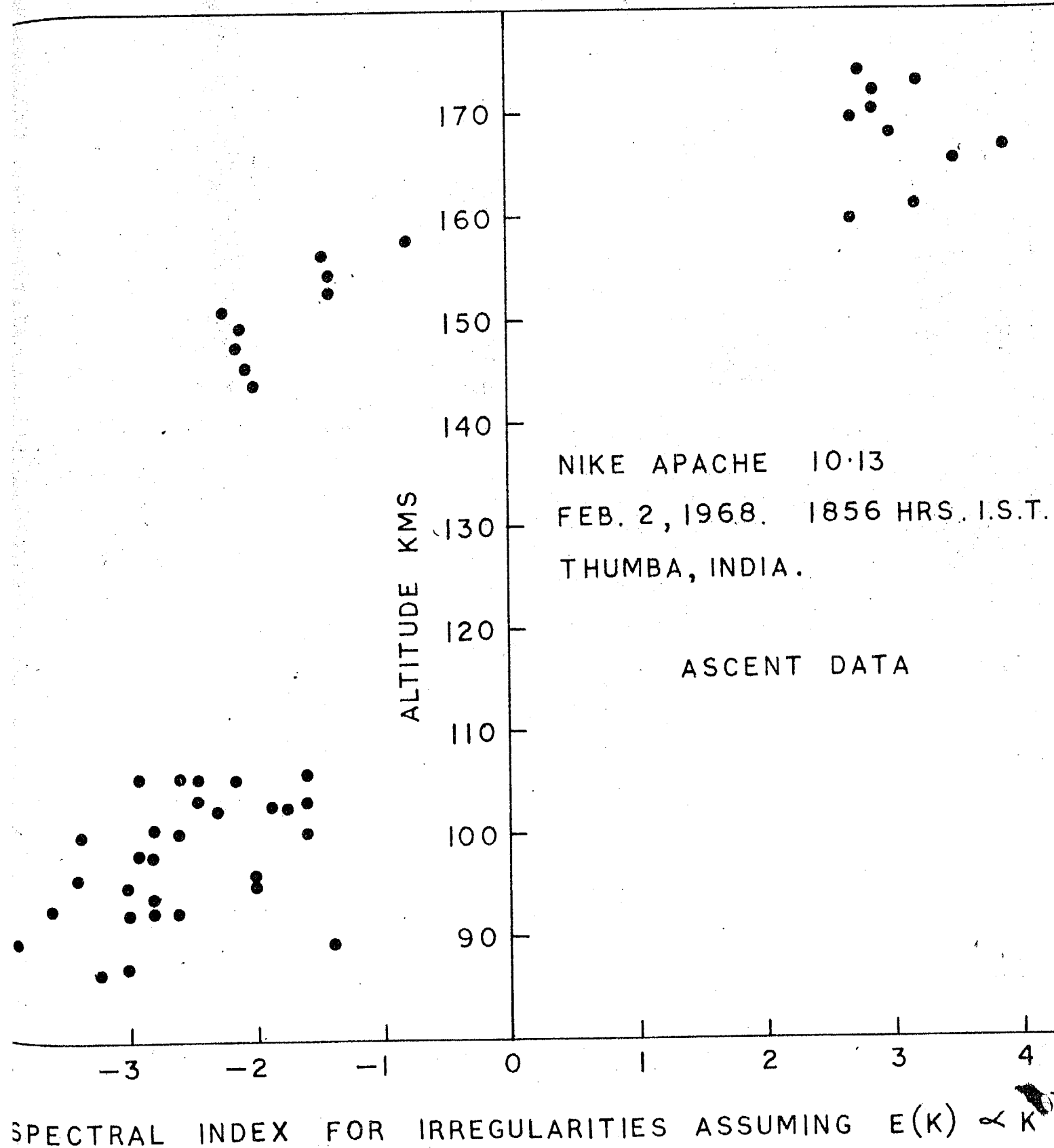


FIG. 38

of electrons density profile for ascent and descent at the base of E region and the total flight time.

5.3.1 Electron density and electron temperature: The probe current profile was first obtained in the usual manner. The flight took place at 1415 hrs. I.S.T. when Thumba ionosonde recorder could not give any marked reflection due to presence of sporadic E. The average value of critical frequency of E layer over Ahmedabad (dip 34°N) for the month of August, 68, was taken for calibration purpose. The average value of critical frequency at 1430 hrs I.S.T. was 3.5 MHz at 100 km altitude over Ahmedabad. This gives a scaling factor one micro amp. equivalent to 7.5×10^3 ele/cc. This scaling factor was used to convert probe current into electron density. The resulting electron density profile for flight 20.07 is shown in fig. 39.

The electron temperature value obtained from semi log plot is shown in fig.40.

5.3.2 Plasma noise: The percentage amplitude of probe current fluctuations in frequency range 70 Hz to 1 KHz is shown in fig.41. In the same figure the absolute value of density fluctuations is also shown.

5.4 Flight 20.08: The probe assembly and probe electronics were identical to that of flight 20.07. During the flight the signal was received upto 405 sec, which was

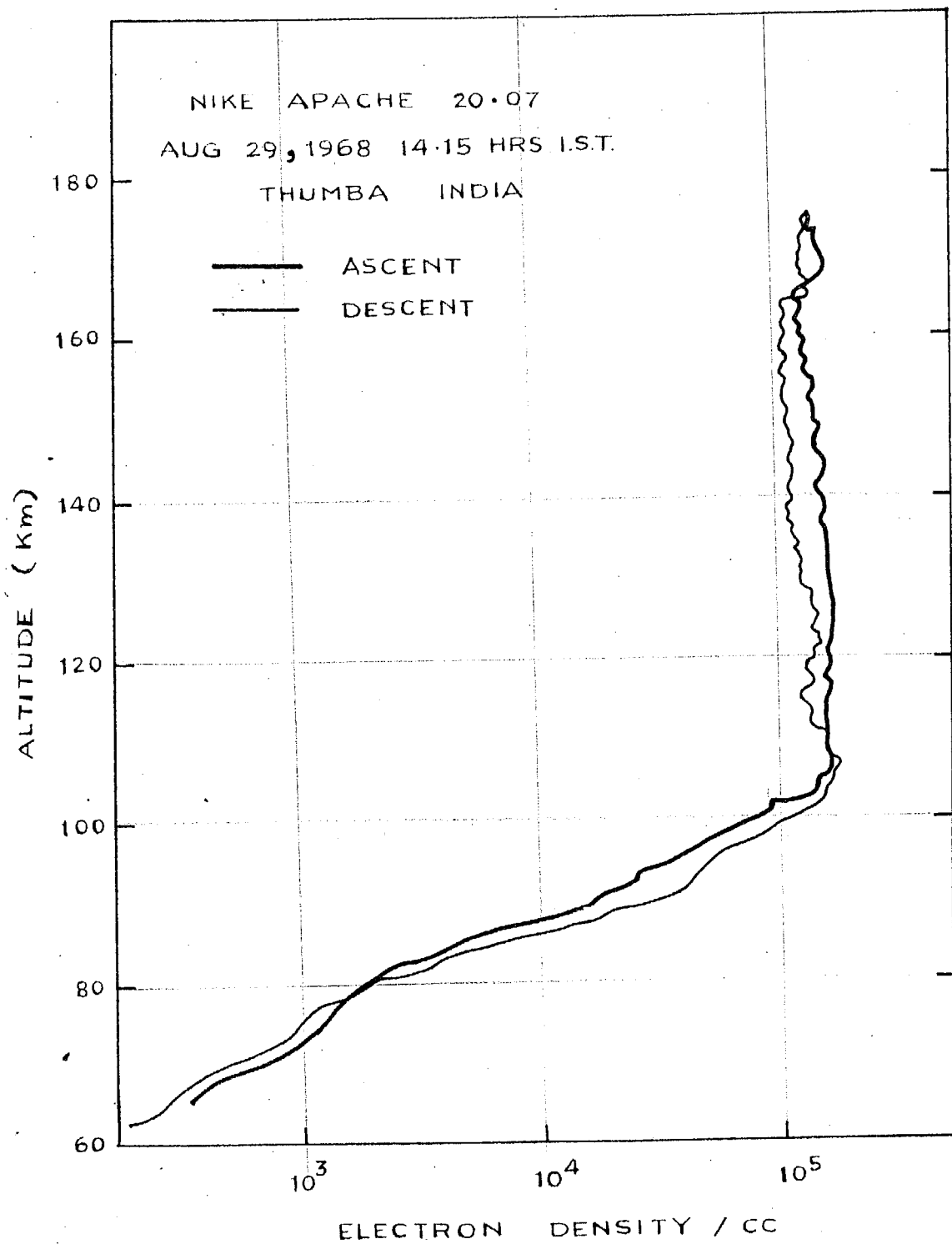


FIG. 39

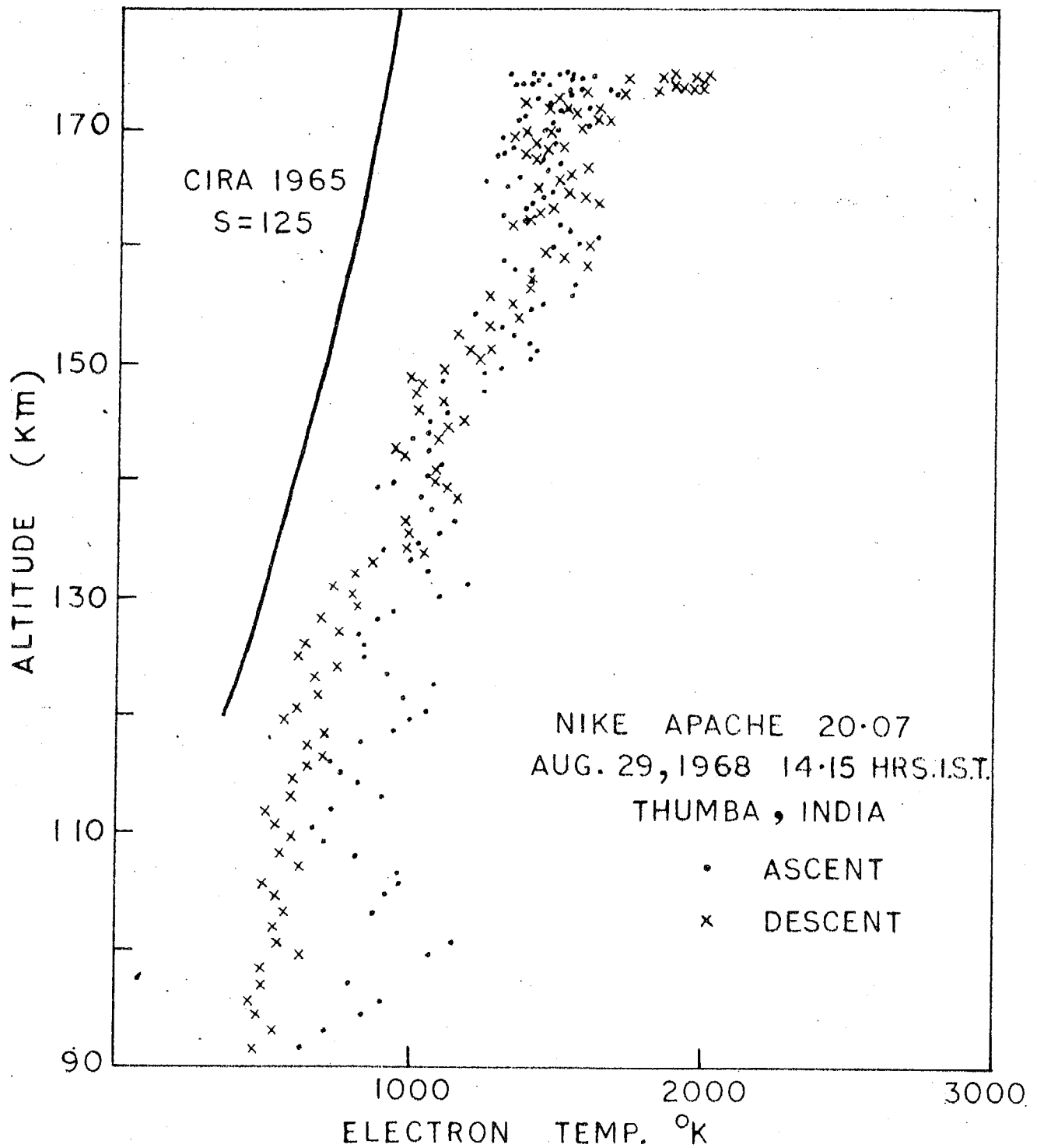


FIG. 40

taken as total flight time. The rocket was tracked by radar upto 50 km. The complete trajectory of the rocket was calculated using radar data, total flight time and by matching the density profile for ascent and descent at the base of E region. Since the probe system was identical to that of flight 20.07, the normalizing factor for conversion of probe current into electron density was taken to be the same as that for flight 20.07. The electron density profile for 20.08 is shown in fig.42. It can be seen that profile has large structures around 110 km which coincide with during ascent and descent. The electron density values change as much as a factor of 20 within a few km.

5.4.1 Electron temperature: The electron temperature values for this flight is shown in fig.43. A gap between 120 to 140 km is due to low electron densities in this region. Even during midnight hours the electron temperature values are seen to be higher than neutral gas temperature.

5.4.2 Plasma noise: The amplitude of plasma noise observed in 70 to 1000 Hz frequency range is shown in fig.45. The fluctuations were spectrum analysed, the amplitude for different scale sizes and tabulated in table 4 as percentage fluctuations. These amplitude are plotted against frequency in a log-log plot and the spectral index 'n' calculated from the slope of this plot. These values are shown in fig.46.

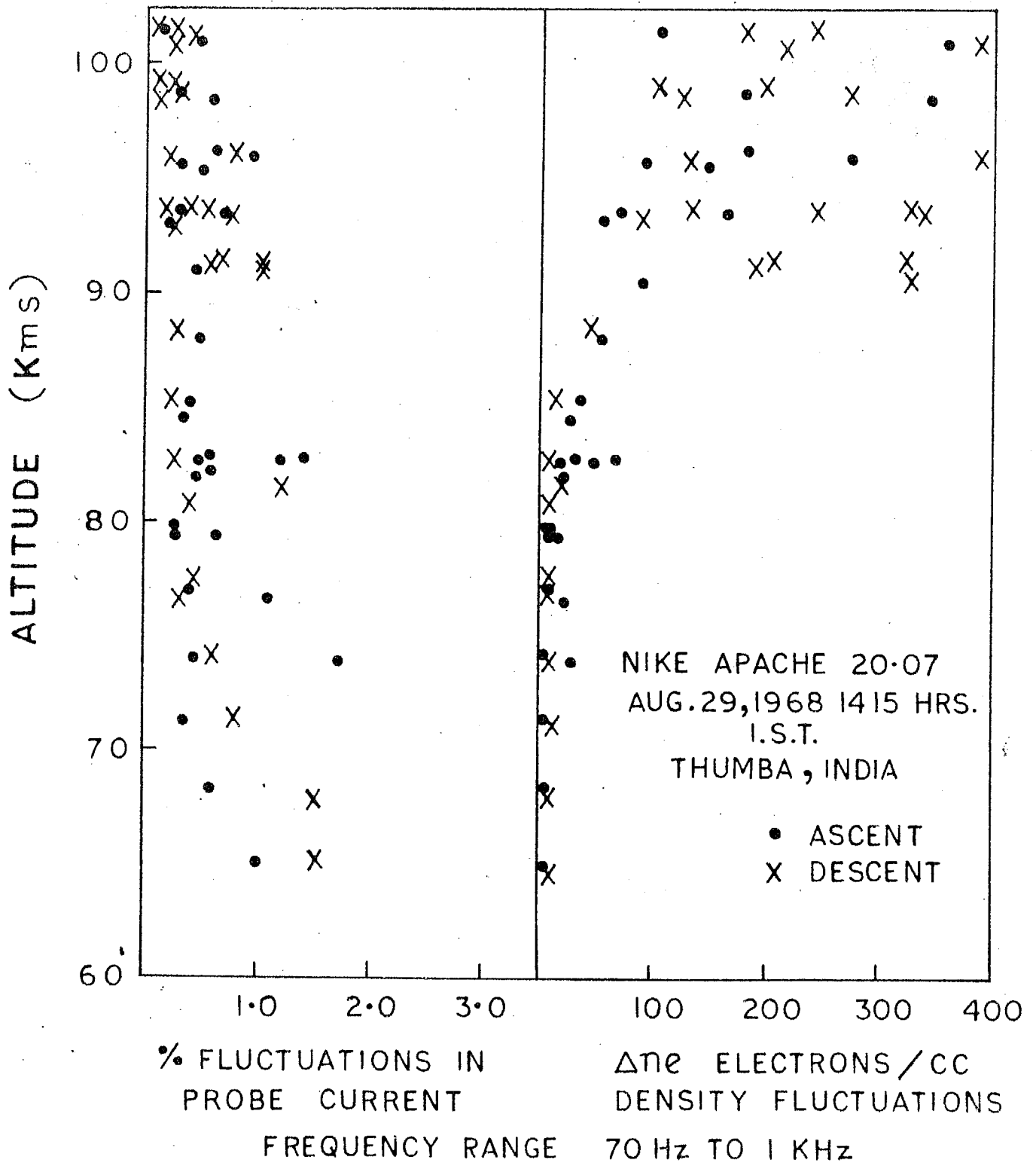


FIG. 41

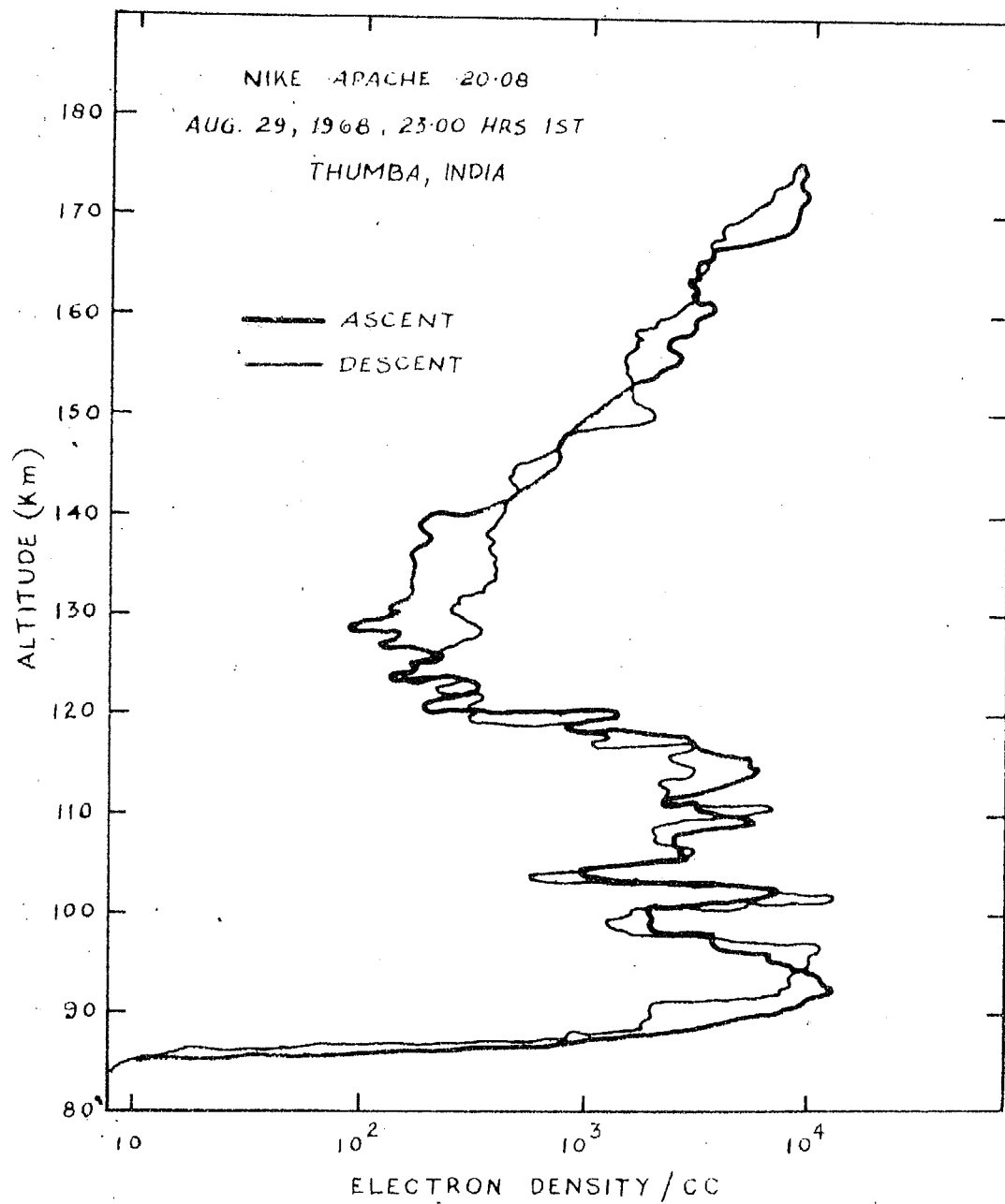


FIG. 42

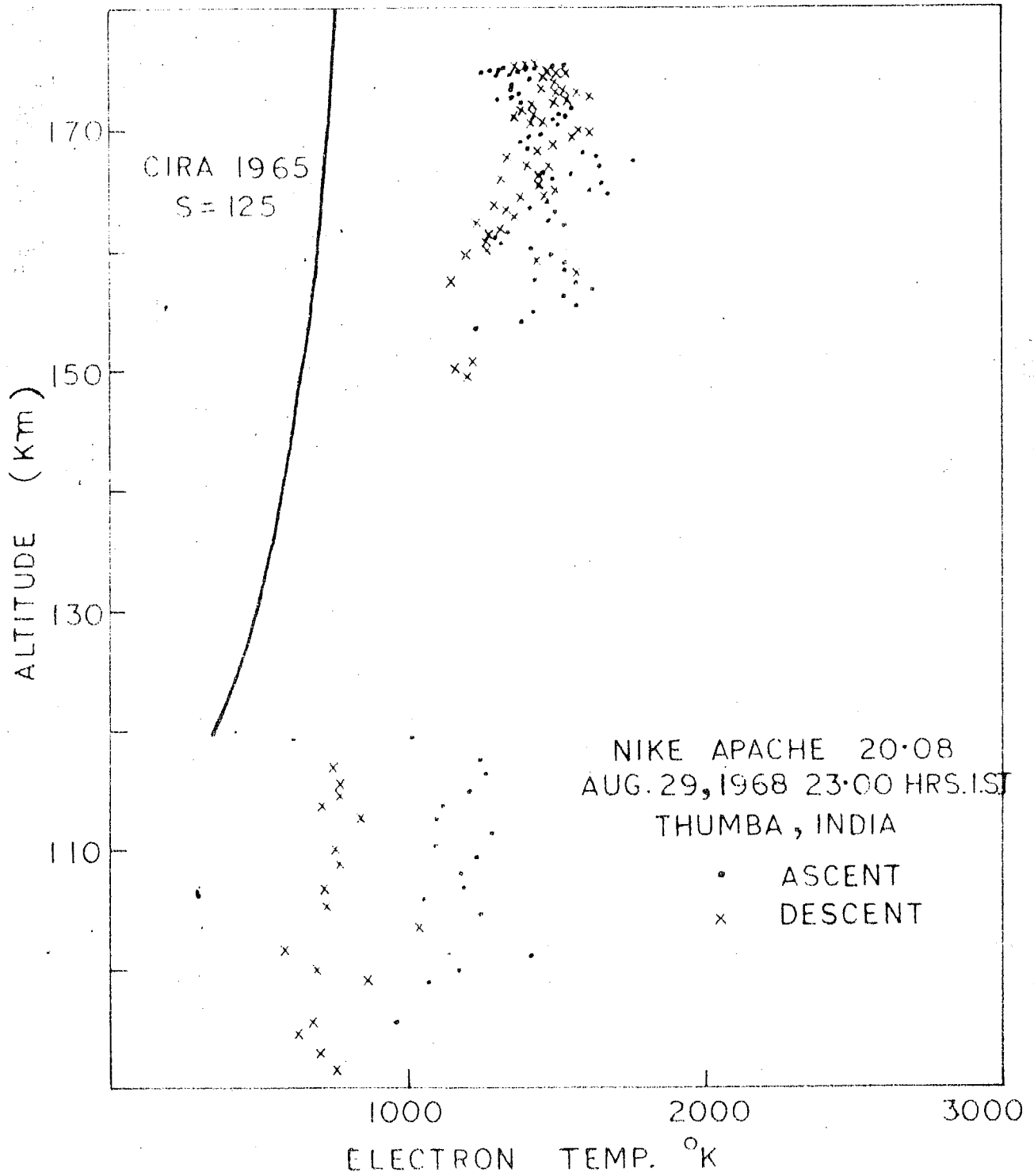


FIG.43

5.4.3 Large scale irregularities: Percentage fluctuations in probe current of scale sizes ranging from 30 meters to 300 meters are tabulated in table No.3. These fluctuations are directly seen on Langmuir probe telemetry record. The percentage fluctuations and electron density profile for ascent and descent are shown in figs. 44, a, b. On examining this figure it is seen that fluctuations occur where the electron density gradients are negative in upward direction.

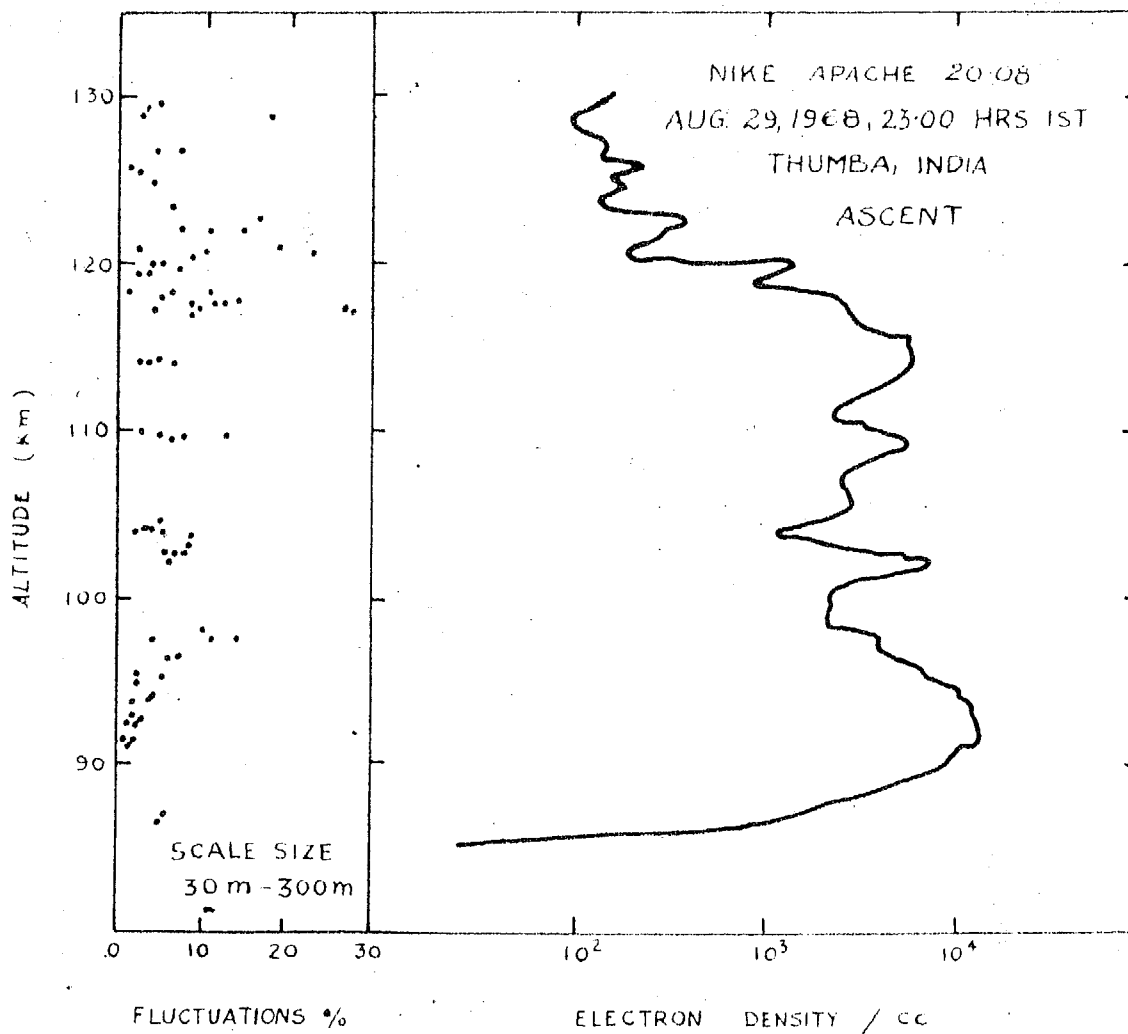


FIG.44 (a)

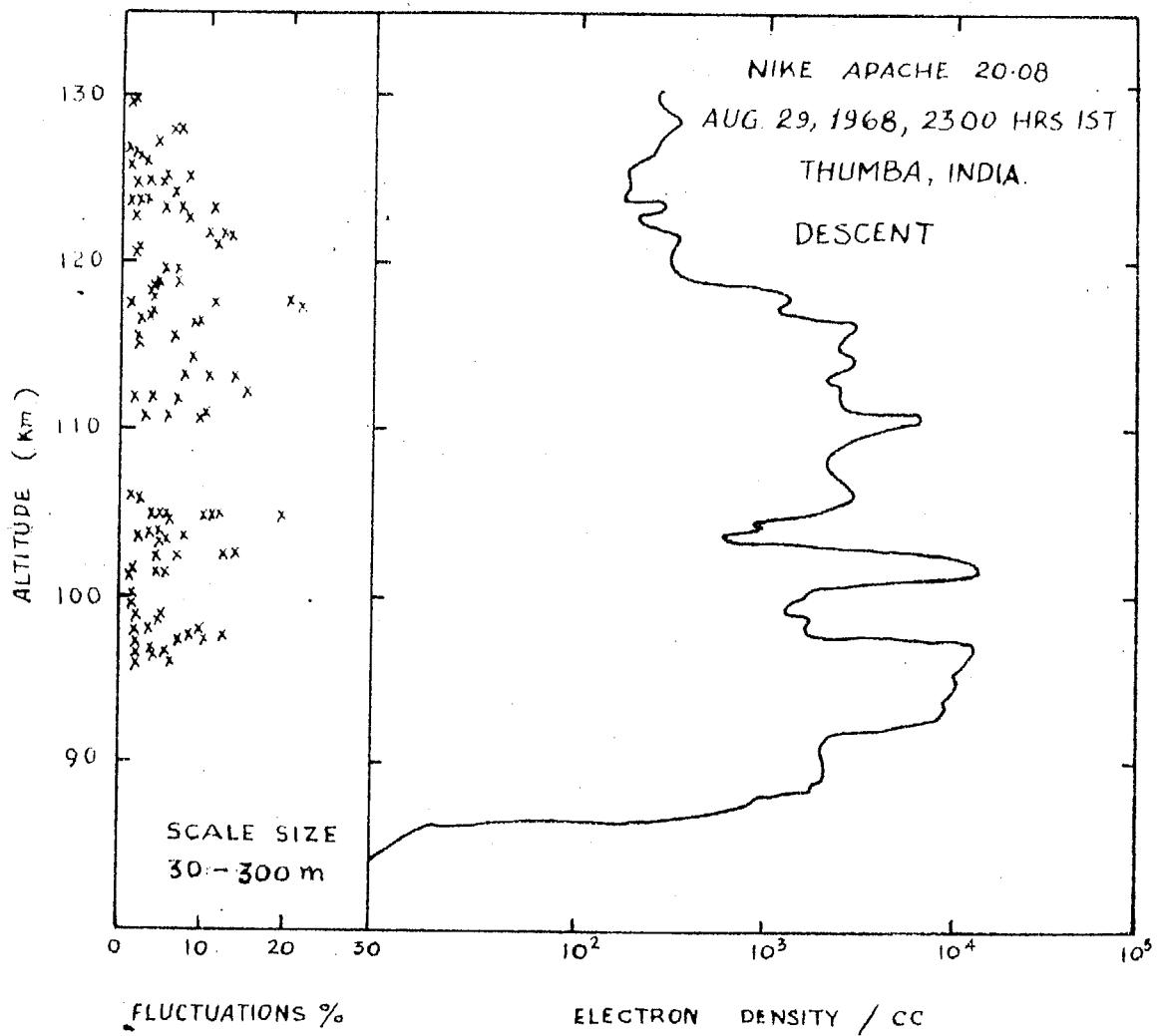


FIG. 44 (b)

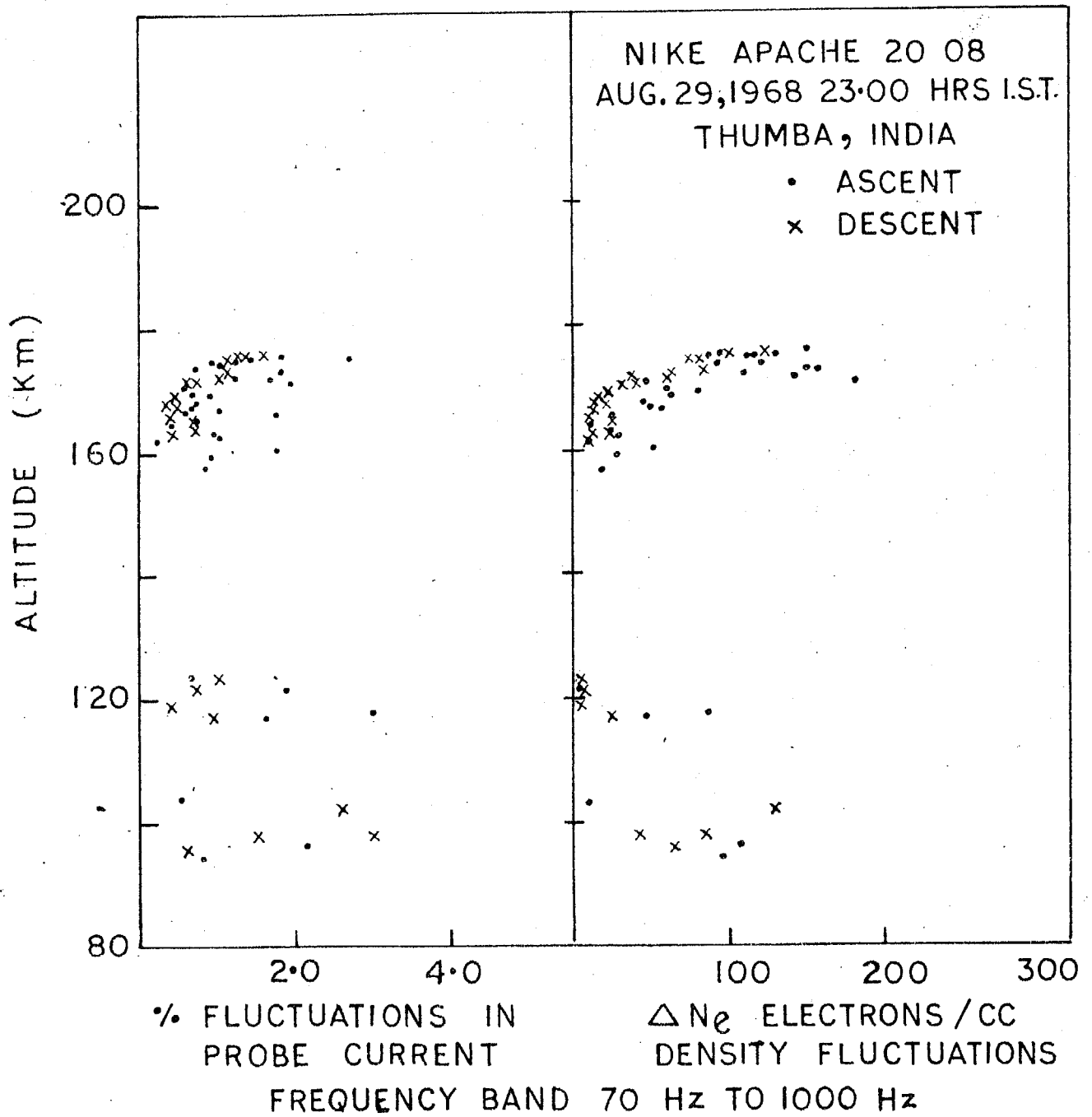
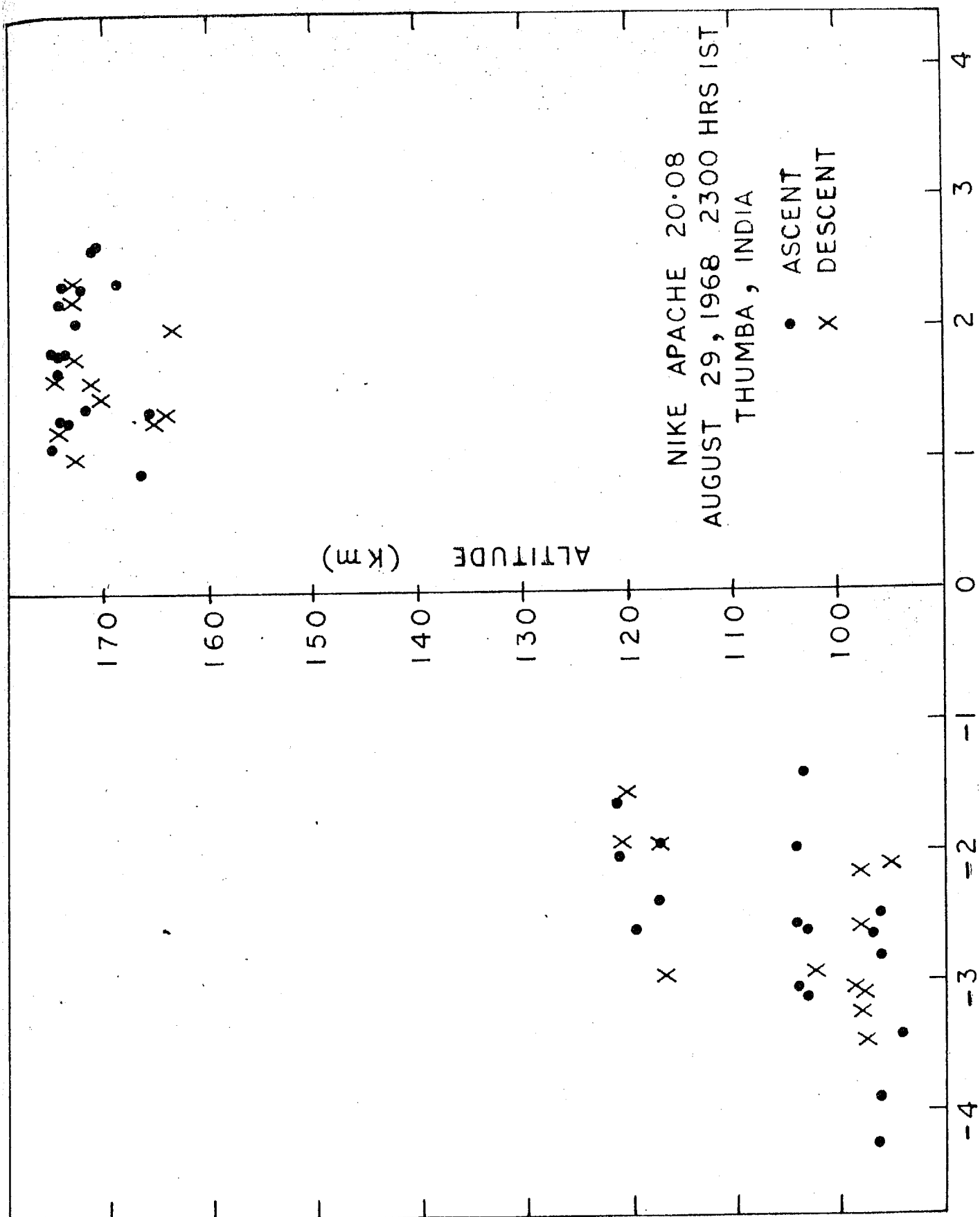


FIG.45



SPECTRAL INDEX FOR IRREGULARITIES ASSUMING $E(K) \propto K^n$

TABLE - III

Percentage fluctuation in the irregularities of scale sizes
30 m to 300 m.

Ascent:

Flight No.20.08

Altitude range km	Scale size of bursts (meters)	Amplitude of fluct- uation (%)	Altitude range km	Scale size of bursts (meters)	Amplitude of fluct- uation (%)
86-87	204	5.2	102-103	72	6.4
	131	6.0		51	5.7
91-92	99	1.1		57	7.7
	90	0.8		114	8.3
	138	1.9	103-104	252	9.2
92-93	135	2.0		90	5.1
	102	1.2		90	2.0
	150	3.1		39	3.5
	81	2.0		78	4.0
93-94	96	2.0		60	5.0
	117	4.1	109-110	99	6.7
	51	4.2		111	8.0
	42	4.3		129	13.3
95-96	132	2.5		75	5.3
	174	6.0		117	3.3
	120	5.0	114-115	39	4.2
	81	2.5		51	5.2
96.97	90	5.8		120	2.7
	186	7.4	117-118	78	8.4
	84	5.1		72	28.2
97.98	54	4.6		66	27.2
	30	4.8		144	11.5
	126	14.2		42	4.3
	282	11.0		42	9.3
	156	10.0		135	14.1
				81	12.8

Table III(Cont....)

Altitude range km	Scale size of bursts (meters)	Amplitude of fluct- uation (%)	Altitude range km	Scale size of bursts (meters)	Amplitude of fluct- uation (%)
118-119	72	5.6	120-121	90	8.6
	54	6.0		135	22.9
	114	10.5		60	10.0
	120	2.9	121-122	96	18.7
	96	1.3		87	18.7
119-120	72	3.6			
	96	2.1			
	135	3.9			
	186	7.1			

TABLE - III

Percentage fluctuation in the irregularities of scale sizes

30 m to 300 m

Descent:

Flight No.20.08

Altitude range km	Scale size of bursts (meters)	Amplitude of fluct- uation (%)	Altitude range km	Scale size of bursts (meters)	Amplitude of fluct- uation (%)
124-123	54	5.0	118-117	54	4.0
	42	7.2		81	20.3
	63	11.2		168	11.1
	36	5.3		51	0.5
	60	1.3		321	21.2
122-121	180	7.6	117-116	60	3.6
	63	10.4		66	2.0
	150	10.0		60	4.0
	156	12.5		141	9.2
	156	12.8		156	8.7
	51	2.2	116-115	78	1.6
121-120	147	10.9		69	1.6
	135	1.5		147	6.1
	201	2.3		60	1.5
	75	1.7		69	1.5
	120	5.0		69	1.4
120-119	81	5.1	115-114	216	8.5
	180	6.6		192	7.1
119-118	144	6.8	113-112	66	7.4
	66	1.2		120	13.8
	159	4.1		135	10.4
	165	3.6		81	15.0
	84	2.8			

Table III (Cont....)

Altitude range km	Scale size of bursts (meters)	Amplitude of fluct- uation (%)	Altitude range km	Scale size of bursts (meters)	Amplitude of fluct- uation (%)
112-111	57	1.7	102-101	51	1.9
	69	4.2		114	5.1
	231	6.4		189	5.4
111-110	159	10.0	101-100	69	1.2
	45	5.9		141	1.8
	60	2.8		153	1.6
	84	9.5		138	1.6
	141	9.5		123	2.1
106-105	126	1.4	99-98	111	1.9
	75	2.4		75	5.1
	57	3.8		304	5.2
	93	6.0			
105-104	51	4.9	98-97	90	3.6
	72	11.0		96	9.6
	51	10.6		30	3.7
	72	19.6		36	1.8
	87	10.0		20	8.2
	114	6.0		192	9.5
	72	5.2		96	12.0
				45	3.8
104-103	48	5.0	97-96	36	2.2
	87	3.7		96	6.8
	81	2.1		51	2.0
	69	1.9		108	4.0
	60	5.4		108	2.0
	39	4.8		159	6.0
	36	7.6		126	4.0
103-102	240	12.1			
	220	14.3			
	60	7.0			
	57	4.6			

TABLE 4

Ascent

Flight No. 20.08

Altitude km	Amplitude fluctuation for different scale size range(%)						Total amplitude of fluctuations for the range 1 to 15 meters(%)
	10 to 15 m	6.6 to 10 m	4.4 to 6.6 m	2.9 to 4.4 m	1.9 to 2.9 m	1.25 to 1.9 m	
94.1	6.5	0.38	0.38	0.19	-	-	1.46
96.1	0.99	0.49	0.44	0.36	-	-	2.28
96.2	0.44	0.33	0.22	-	-	-	0.99
96.4	0.60	0.44	0.35	0.18	-	-	1.57
96.6	0.55	0.49	0.38	0.18	-	-	1.61
96.8	0.49	0.46	0.33	-	-	-	1.28
103.3	0.10	0.12	0.09	-	-	-	0.32
103.4	0.10	0.14	0.10	0.06	0.09	0.13	0.63
103.5	0.10	0.10	-	-	-	-	0.21
103.6	0.10	0.14	0.09	-	-	-	0.33
103.9	0.14	0.10	0.07	-	-	-	0.31
104.0	0.14	0.14	0.09	-	-	-	0.37
104.2	0.52	0.32	0.24	0.19	0.14	0.1	1.51
117.2	0.5	0.87	0.5	0.53	0.54	0.50	3.44
117.5	0.35	0.78	0.78	0.59	0.57	-	3.08
121.3	0.48	0.32	-	-	-	-	0.80
121.4	0.81	0.64	0.56	0.26	-	-	2.28

TABLE 4 (Cont....)

Descent

Flight No. 20.08

Altitude km	Amplitude fluctuation for different scale size range(%)					Total amplitude of fluctuations for the range 1 to 15 meters(%)
	10 to 15 m	6.6 to 10 m	4.4 to 6.6m	2.9 to 4.4 m	1.9 to 2.9 m	
121.3	0.43	0.36	0.29	-	-	1.07
121.1	0.64	0.71	0.43	-	-	1.78
118.5	0.35	0.39	0.23	0.22	-	1.20
117.0	0.38	0.46	0.23	0.22	0.14	1.56
102.2	0.42	0.52	0.42	0.34	0.19	1.88
98.3	0.46	0.36	0.21	0.26	0.13	1.43
98.1	0.28	0.32	0.28	0.26	0.16	1.31
98.0	0.54	0.32	0.39	0.29	0.25	2.09
97.9	0.57	0.78	0.71	0.47	0.47	3.52
97.8	0.71	0.57	0.5	0.35	-	2.13
97.6	0.65	0.71	0.5	-	-	1.86
97.5	0.43	0.43	-	-	-	0.86
97.2	0.33	0.29	0.25	0.14	0.30	1.54

CHAPTER - VI

DISCUSSION OF EXPERIMENTAL RESULTS

The results of four rocket borne Langmuir probe and plasma noise probe experiments described in Chapter-V were critically examined and discussed in this Chapter. The equatorial D and E region ionisation irregularity measurements are interpreted in terms of presently known theories. The results of ion acoustic waves produced in the wake of moving rocket are also discussed. The electron temperature observed in the E region has been also discussed.

6.1 Ionisation irregularities

As pointed out earlier ionisation irregularities have been of great interest as they give rise to many well known effects on radio wave propagation. Some of these effects have been discussed in Chapter II. Most of the information about the nature of these irregularities obtained earlier was from the ground based observations. The rocket borne technique using Langmuir probe and plasma noise probe gives the information about the amplitude and spectrum of these irregularities and their height distribution. The ground based techniques and rocket borne techniques are complimentary in nature and should be used simultaneously to derive best results. No simultaneous ground based observations of the irregularities were available for the present rocket results.

The plasma noise probe was used to determine the amplitude and spectrum of irregularities in the scale size 1-15 meters. The irregularities of scale size 30-300 meters were measured from the Langmuir probe outputs. Hereafter, the irregularities of scale size 30-300 meters are termed as large scale irregularities while the 1-15 meters are termed as small scale. The amplitude and spectrum of these irregularities and their relationship with other ionospheric parameters have been used for the identification of the production mechanisms operating at various altitudes during different times of the day.

It can be said that all the mechanisms mentioned in Chapter II are operative under various conditions in the equatorial ionosphere. A study of the occurrence and spectrum of the ionospheric irregularities will be useful in identifying the mechanisms responsible for the production of these irregularities.

6.1.1 Irregularities in the 60-80 Km region

This region is characterised by negative gradients in the neutral gas temperature with height giving rise to unstable atmospheric conditions. There has been much discussion about the nature of the origin of ionisation irregularities which give rise to weak partial reflections from the D region (Clemesha 1963). Gardner and Pawsey (1953) have pointed out that a change in electron density in a distance

less than the wave-length of the exploring electromagnetic wave of only 2 electrons/cc would cause the typical observed reflection coefficient of 10^{-5} at 70 Km. Since in the 70 Km region, the total electron density is about 10^2 ele./cc, the required changes would be only a few percent of the mean ionisation.

Figure 39 shows the electron density profile in this region obtained on mid-day flight. It can be seen that the electron density increases monotonically from 60 to 100 Km. The values of $\frac{\text{Grad } N_e}{N_e}$ for mid-day flight are given in table 7. This factor which will be represented as Δ is a measure of gradient in electron density. The value of Δ is 0.11 Km^{-1} between 75-80 Km, for the mid-day flight. During the evening and night time flights, the electron densities below 80 Km were less than 10 ele./cc., hence no irregularities were observed in these flights.

The amplitude of composite plasma noise in frequency range 70 Hz to 1 KHz corresponding to scale sizes 1-15 meters that was measured on flight 20.07 is shown in Figure 41. The composite amplitude is about 1.0% between 65 to 82 Km, and between 82 to 90 Km, it is about 0.5%. These amplitudes corresponds to density fluctuations of about 5 electrons/cc. in scale sizes 1-15 meters. The values are comparable to the value of 2 ele./cc. obtained by Gardner and Pawsey for the 70 Km region for 18 meters irregularities.

6.1.2 Irregularities in the 80-90 Km region

This region is characterised by large wind shears and large electron density gradients in the upward direction. Large wind shears can give rise to turbulence which in the presence of a background gradient of ionisation can produce appreciable electron density fluctuations. Gallet (1955) has taken recourse to turbulence in the presence of background density gradients to explain D region scatter propagation.

The nature of the irregularities changes with altitude and period of the day. While both large scale irregularities and small scale irregularities have been observed in this region on two evening flights 10.11 and 10.13 on the mid-night flight 20.08, very few irregularities (small as well as large) have been observed below 90 Kms. On the afternoon flight 20.07, only small scale irregularities have been studied.

The telemetry record for the flight 10.13 illustrates the nature of the irregularities at two different altitudes during evening times. In figure 47a starting from the bottom of the record the first two channels represent the Langmuir probe current outputs. The third channel represents the fluctuations in Langmuir probe current in 70 Hz to 1 KHz which correspond to 1 to 15 meter scale sizes with high and low gains on alternative sweep cycles. The top channel represents the fluctuations in the frequency band $400 \text{ Hz} \pm 7.5\%$ and $960 \text{ Hz} \pm 7.5\%$ telemetered on a time sharing basis.

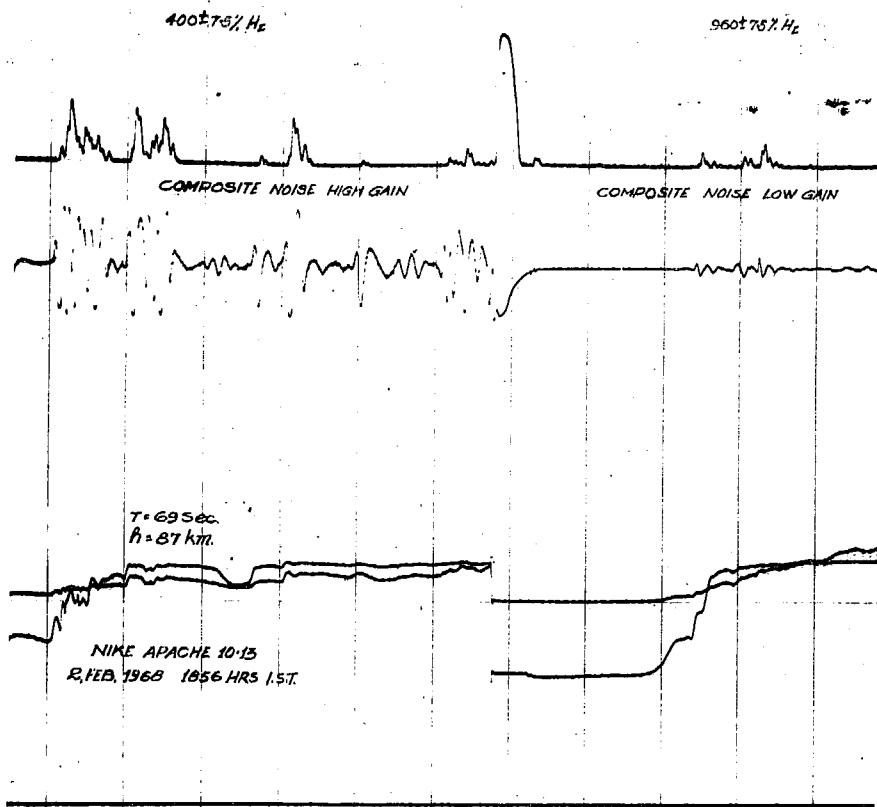


Figure-47a : Telemetry record obtained at 87 Km.

The large scale fluctuations greater than 30 meters can be seen directly on Langmuir probe current record, and their amplitude are as high as 30% as can be seen in figure 47a,b of Langmuir probe current outputs. On examining the record, we can see that at 87 Km the noise in 1-15 meters occurs in bursts. While in the 96-97 Km, region, it is more or less continuous. Also at 96-97 Km, the amplitude of the small scale sizes is much more than large scale sizes. This feature is demonstrated by the spectrum analyser outputs in figure 48 a, b corresponding to the two altitudes under consideration. From top to bottom, the top channel shows the composite noise while rest of channels show the fluctuations in frequency ranges centred at 110, 170, 240, 400, 600 and 900 Hz each of bandwidth $\pm 20\%$ of the centre-frequency. We can see that in 87 Km region lower frequencies are dominating while at 96-97 Km region higher frequencies are dominant. The irregularities in this region occur in bursts which are randomly separated. Table 5 shows the burst size and separation between them for flight 10.13 (Satya Prakash et al 1969 a, b). Some of the burst amplitudes are more than 2% of the ambient value. Only samples for alternative sweeps where the plasma noise amplifier gain was high, were taken. Hence, the table does not contain all the bursts that are present in this altitude region. The table shows that the most probable sizes are around 100 meters which correspond to large scale irregularity sizes.

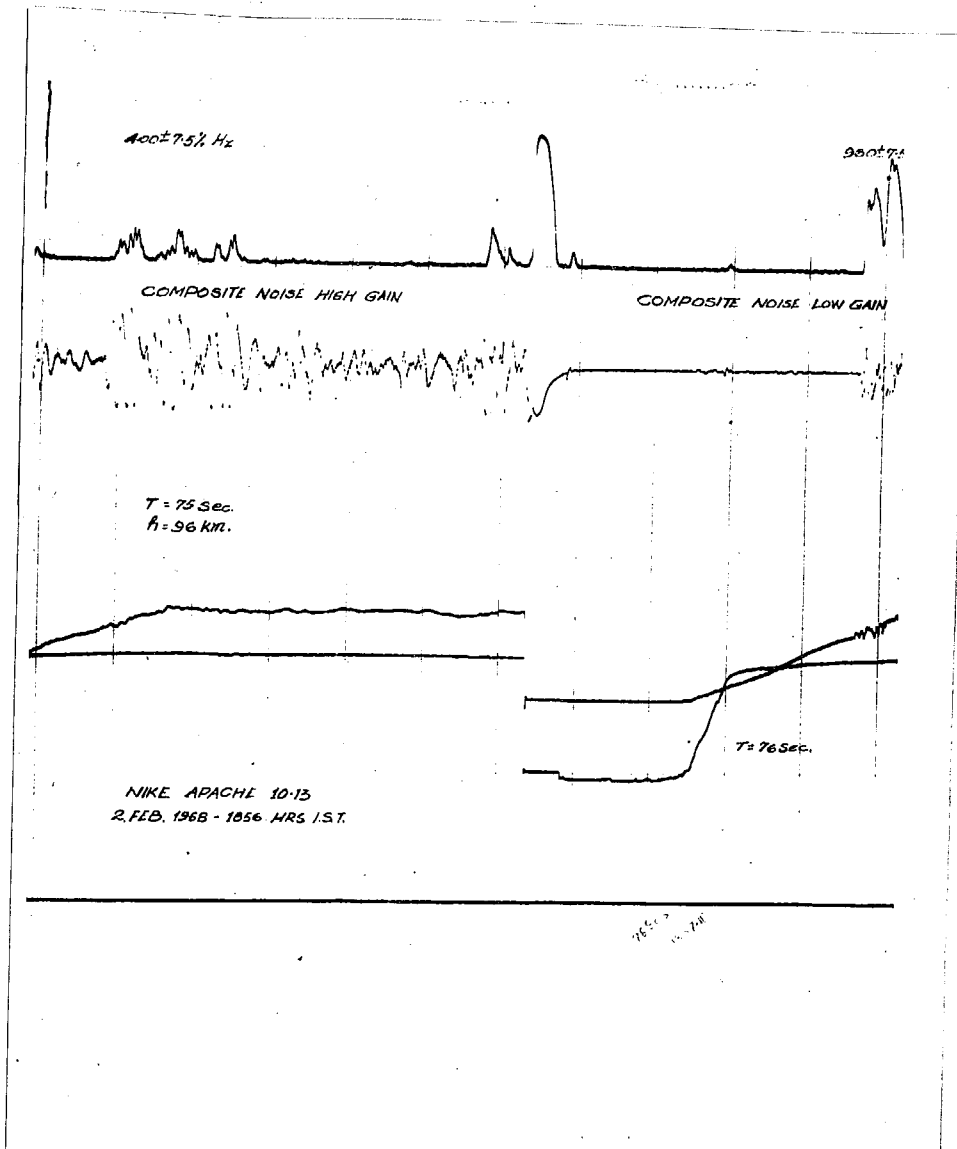


Figure-47b : Telemetry record obtained at 96 Km.

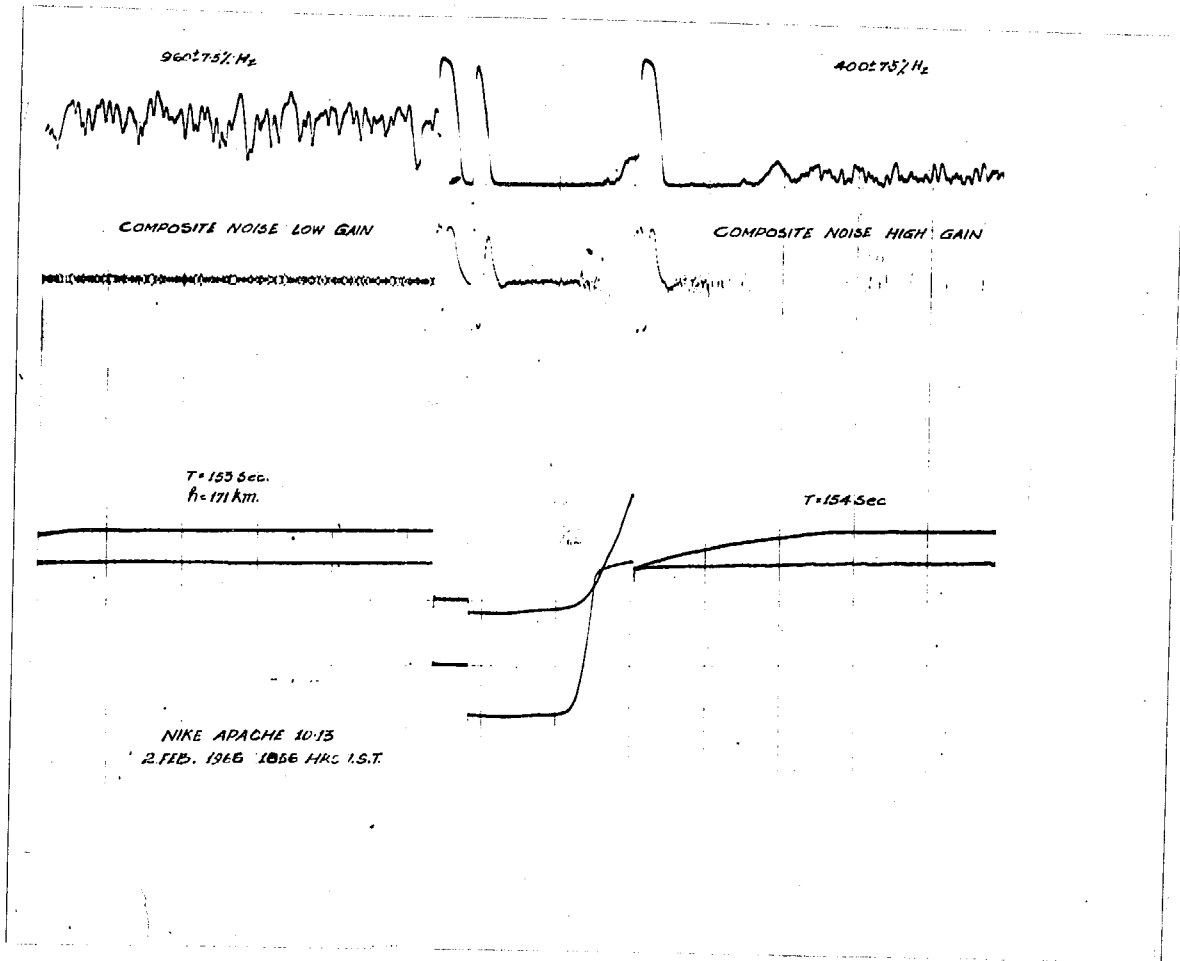


Figure-47b : Telemetry record obtained at 171 Km.

6.1.3 Irregularities in the 90-120 Km region

This region is characterised by high wind shears. This region coincides with electrojet height where various ionospheric irregularities are encountered. The irregularities in this region over geomagnetic equator give rise to Q_y type E_s . The small scale irregularities of 3 meter size have been studied by back scatter radar at Jicamarca.

On the afternoon flight 20.07, small scale irregularities were studied and found to occur more or less continuously. For the large scale irregularities observed in this region, the scale sizes are much larger than the mean free path of neutral particles. While for the small scale irregularities, the sizes are of the order of or even less than the mean free path.

a) Large scale irregularities (30-300 meters)

Figure 42 shows the electron density profile for the mid-night flight. There is a general agreement between the ascent and descent profiles. They exhibit the following major features. The three major peaks in the electron density profile are observed at (92,96) Kms, (101.5, 102) Kms, (109, 110.5) Kms. Above 120 Km there is a deep valley where the electron density falls by two orders of magnitude (to a few hundreds per cc). Above 140 Km there is a general rise in the electron density upto the rocket apogee of 175 Km.

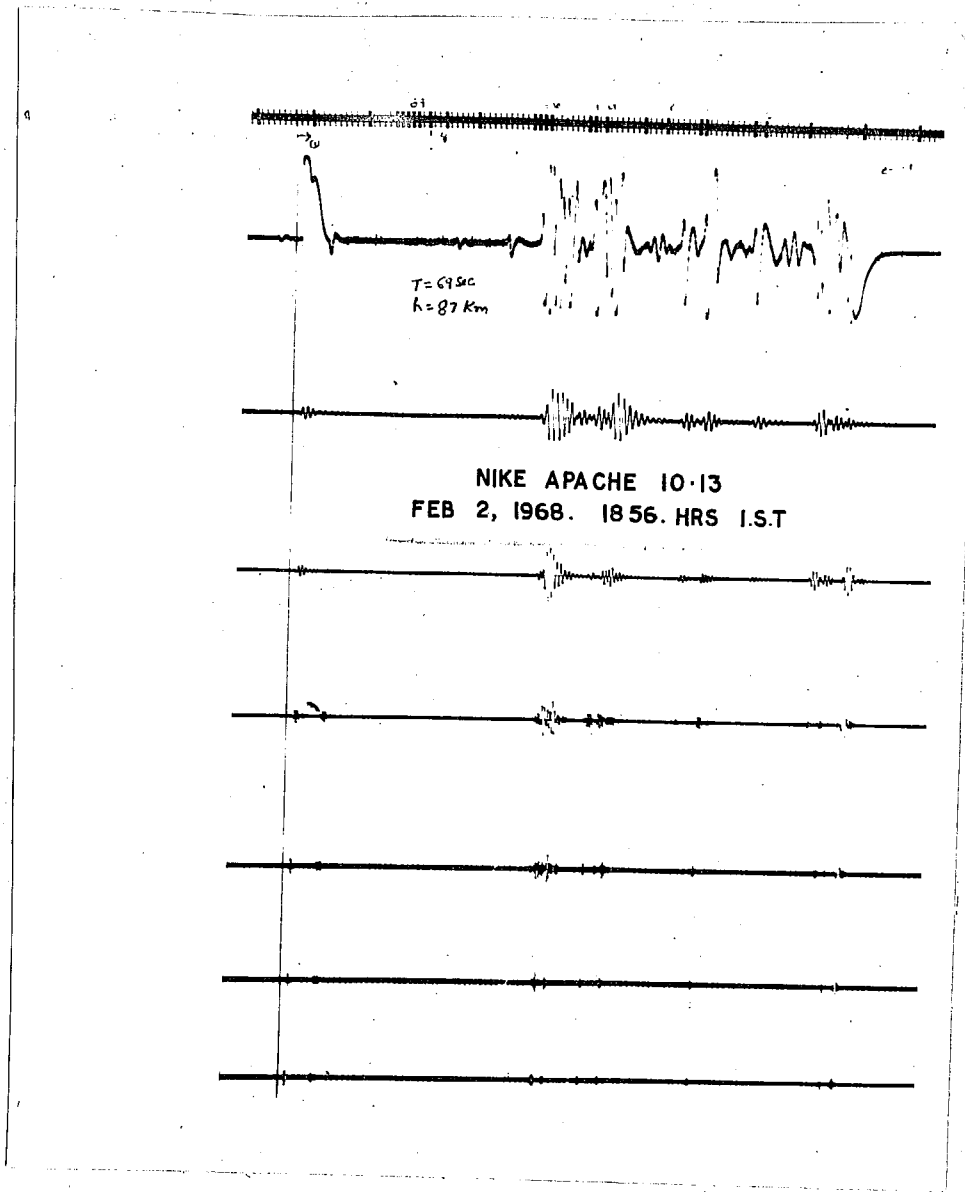


Figure-48a : Spectrum analyser output record at 87 Km.

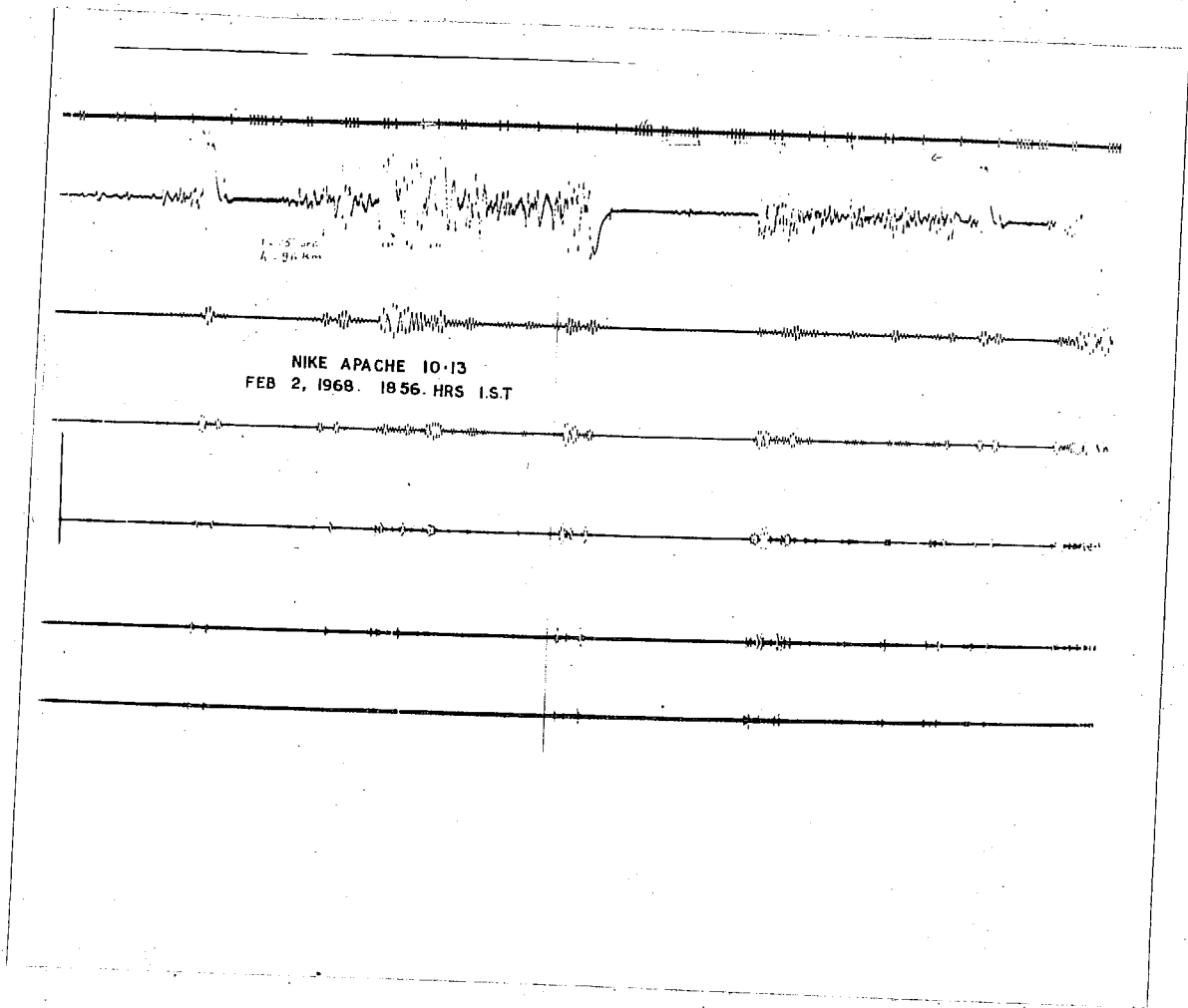


Figure-48b : Spectrum analyser output record at 96 Km.

Both the ascent and the descent profiles are characterised by the presence of large scale structures. The vertical scale size of these structures is a few Kms and they can be seen throughout the profile. But they are markedly present in the height region 90-120 Kms. In the more striking of these structures, the ionisation density varies by a factor varying between 4 and 25 within the structure, thereby giving them the appearance of layers. The overlapping of these structures (layers) between the ascent and the descent profiles shows that they have a fairly large horizontal extent (the horizontal separation between the ascent and the descent profiles is about 60 Kms at an altitude of 100 Km).

Figure 44 a, b shows the amplitude of the large scale irregularities upto 130 Km as percentage fluctuations. In the same figure, the electron density profile is also shown. It can be seen that the irregularities have been observed mostly in these regions where the electron density gradients are negative in upward direction. Table 3 gives the amplitude of large scale irregularities versus altitude. There are a few exceptions where the irregularities were observed in the region of positive density gradient. The exceptions are around 101 and 104 Kms during descent. The amplitude of the irregularities around 101 Km is small and hence can be ignored. Hence, it may be concluded that the irregularities of large scale sizes (30 to 300 m) mostly lie in the region of negative ionization density gradients.

On both the evening flights large scale irregularities were observed around 100 Km region where electron density

TABLE - V

Flight 10.13

Characteristics of plasma noise bursts during ascent

Altitude (km)	Burst width (m)	*Burst interval (m)
86.90	112.0	141.0
87.04	94.0	262.0
87.30	122.0	347.0
87.65	103.0	
89.4	94.0	478.0
89.88	103.0	103.0
89.93	108.0	
92.6	131.0	131.0
92.79	122.0	141.0
92.87	75.0	159.0
93.03	56.0	75.0
93.1	75.0	
95.3	65.0	169.0
95.47	75.0	94.0
95.55	103.0	122.0
95.68	141.0	131.0
95.81	112.0	384.0
96.19	94.0	

* Burst interval was measured between the centres of two consecutive bursts.

TABLE - 6

Flight 10.11: 12th March 1967
18.57 Hrs. IST.

Flight 10.13: 2nd February 1968
18.56 Hrs. IST.

Ascent		Descent		Ascent	
Altitude Km	-1 Km	Altitude Km	-1 Km	Altitude Km	-1 Km
90	0.105	88	0.293	80	0.428
100		90		90	
100	0.053	90	0.293	90	0.066
110		100		100	
125	0.137	100	0.021	100	0.0394
135		110		110	
140	0.0446	125	0.20	110	0.0126
145		135		115	
		140	0.024	125	0.0283
		150		130	
				135	0.0604
				145	

$$\lambda = \left(\frac{\text{Grad Ne}}{\text{Ne}} \right)$$

TABLE -7.

Flight 20.07: 29th Aug. 1968
14.15 Hrs.I.S.T.Flight 20.08: 29th Aug. 1968
23.00 Hrs.I.S.T.

Ascent		Descent		Ascent		Descent	
Altitude Km	\angle Km	Altitude Km	\angle Km	Altitude Km	\angle Km	Altitude Km	\angle Km
75		75		86		87	
80	0.11	80	0.098	90	1.13	89.5	0.61
80		80		95		92	
85	0.185	85	0.244	99	0.403	96.5	0.39
85		85		100.5		96.5	
90	0.157	90	0.213	102	0.91	98	1.3
90		90		102		99	
95	0.11	95	0.148	104	0.98	101.5	0.98
95		95		104		101.5	
100	0.185	100	0.125	105.5	0.67	103.5	1.6
100		100		107		103.5	
105	0.138	105	0.086	109	0.46	106.0	0.5
				109		106	
				111	0.52	107.5	0.32
				111		108.0	
				114	0.36	110.5	0.5
				115		110.5	
				119	0.48	111.5	1.05
				120		116	
				121	2.13	117	1.05
				123		117.5	
				124	1.09	119	1.05
						121.0	
						122.5	0.403
						123	
						123.5	1.25

$$\angle = \left(\frac{\text{grad Ne}}{\text{Ne}} \right)$$

gradients are positive in upward direction. The value of which is a measure of electron density gradients is shown in table 6. It can be seen that electron density exhibits large gradients. The large scale fluctuations can be illustrated from the telemetry record of evening flight. In figure 47 b the 2nd channel from bottom to top is the telemetry record at 96 km which illustrates the large scale fluctuations in the Langmuir probe current. The irregularities occur randomly in space and suggest that they are due to some form of instability or turbulence in the medium. These fluctuations are likely to have nearly same dimensions in the plane perpendicular to the earth's magnetic field, i.e., in vertical as well as in east-west direction over geomagnetic equator, especially for small scale sizes.

b) Small scale irregularities (1-15 meters)

The percentage amplitude of small scale irregularities in frequency range 70 Hz to 1 KHz (1-15 meter scale size) is plotted for flights 10.13, 20.07 and 20.08 in figure 35, figure 41 and figure 45, respectively. On flight 10.11, the signals were studied in frequency range 740-1025 Hz and the observed amplitudes are shown in figure 33. The values of the electron density fluctuations are plotted on the right hand side of the diagram for the same scale sizes. On midnight flight irregularities of 1-15 meters were observed in regions where electron density exhibits negative gradients in upward direction, figure 45. Table 4 shows the percentage amplitude in various scale sizes versus altitude.

Figure 36 shows the amplitude of irregularities in arbitrary units of scale sizes for the flight 10.13 in the range 1 to 15 meters. The factor along the abscissa when multiplied by 7 will give the density fluctuations as electrons per cc in scale size shown in the figure.

The spectral index 'n' values for flight 10.13 and 20.08 are shown in fig.38 and fig.46 respectively. In both the figures, we find that the value of 'n' is about -3.5 at lower height and increases with height to a value of -1.8.

6.1.4 Small scale irregularities around 140 Km

On both the evening flights 10.11 and 10.13, small scale irregularities were observed around 140 Km. Figures 33 and 35 gives the amplitude of irregularities in this region. The electron density exhibits positive gradient in upward direction around 140 Km as is evident from figures 30 and 34. The spectral index for 10.13 is about -2.0 around 145 Km, which gradually increases and becomes positive above 160 Km. This is due to the fact that above 150 Km, the irregularities due to rocket motion itself are also detected by the probe along with the ambient irregularities. The spectral index for the rocket induced irregularities is positive as only the lower end the spectrum is observed. The rocket induced irregularities will be discussed in the later part of this Chapter.

6.2 Summary of the results

1. On the afternoon flight 20.07, the irregularities in

the scale size (1-15 meters) were observed in altitude region 60-100 Km and their nature was found to be more or less continuous.

2. The occurrence of irregularities of the scale size 1-15 meters and 30-300 meters in the 80-90 Km range on both the evening flights are random in nature. On mid-night flight, very few large scale irregularities were seen below 90 Km and small scale irregularities were completely absent below this altitude. Below 90 Km, the electron density gradients are positive for all the flights.

3. The 30 to 300 meters size irregularities in the altitude range 90 to 110 Km. occur randomly on both the evening flights. In the same height region small scale irregularities 1-15 meters were also observed. The spectrum of small scale irregularities shifts to higher frequencies with altitude. In this height region the electron density exhibits a positive gradient in upward direction. Irregularities on the mid-night flight were observed in the regions where electron density gradients are negative. They occur randomly in altitude. The small scale (1-15 meters) irregularities also occur in the same regions where large scale irregularities are observed.

4. Irregularities on both the evening flights were also observed around 140 Km. On 10.13 the scale sizes studied were 1-15 meters while on 10.11 the size studied was 1.5 m, to 2.0 meters.

5. The spectral index of the 1-15 m irregularities observed on evening flight 10.13 in the altitude region 90-105 Km increases from -3.5 to -1.8. The spectral index exhibits a large scatter. Similar features are observed on mid-night flight in altitude region 95-120 Km. For the evening flight 10.13, the value of the spectral index around 140 Km is -2.0 and does not show much scatter.

6. The spectral index for the irregularities observed near the rocket apogee have a positive value. These irregularities are produced due to rocket motion. The observed positive spectral index arises from the fact that only the lower end of the spectrum of these irregularities was studied by the present instrument.

6.3 Discussion

It was pointed out in Chapter II that the ionospheric irregularities can be produced by neutral turbulence, cross field instability, two stream instability and plasma turbulence. Neutral turbulence can arise due to the unstable configuration in the neutral atmosphere or due to large disturbances like those due to wind shears. The eddies produced by neutral turbulence have a spectral index of $-5/3$ for an incompressible fluid. The turbulence in presence of an electron density gradient can give rise to ionisation irregularities through collisions with positive ions. By this mechanism only the irregularities of scale size larger than a few times the mean free path of neutral particles can

be produced. Sizes smaller than the mean free path cannot be accounted for by the neutral turbulence. Table 1 of page 28 shows the values of the mean free path of neutral particles at different heights in the atmosphere.

The cross-field instability operates when the gradients in the electron density are in the same direction as the ambient electric field. The scale sizes produced by cross field instability are a few times larger than the mean free path of neutral particles at the altitude under consideration. The study of large scale irregularities (30-300 meters) can be effectively employed to study cross field instability in the absence of neutral turbulence. While the study of 1-15 meters irregularities can help in understanding the nature of other instabilities like two stream instability and plasma turbulence.

The two stream instability can give rise to irregularities when the electron drift velocity exceeds the ion thermal velocity. The drift velocity is given by : $V_e = -3.8 \times 10^4 \times \frac{\sigma_2}{\sigma_1} E_y$ meters/sec., where σ_1 and σ_2 are the Pedersen and Hall conductivities respectively. E is ambient electric field in east west direction. The maximum value of $\frac{\sigma_2}{\sigma_1}$ is realised around 100 Km. The threshold condition will therefore, depend on the value of E which is presently not known. Therefore, it is difficult to predict when the mechanism is likely to be most effective. From the back scatter observations at Jicamarca, the threshold conditions are satisfied

around noon hours near 100 Km region (Balsley 1969 a, b). This mechanism can produce scale sizes even lower than one meter.

The plasma turbulence concept was first introduced by Balsley (1964, 1965, 1967) to explain the bifurcation of the equatorial electrojet irregularity regions. It will be most effective in the regions where Hall conductivity exhibits maximum gradients. These regions are 90 to 100 and 100 to 110 equispaced on either side of the nominal peak of the conductivity profile at 100 Kms. Like two stream instability, the plasma turbulence may produce scale sizes as low as a few meters. Balsley believes that Plasma turbulence mechanism is operative during all the time of the day and night.

The scale size of the irregularities studied below 90 Km is many times larger than the neutral mean path and hence, their production can be explained by the neutral turbulence and the cross field instability. Neutral turbulence in the 60-80 Km region can arise due to decrease in neutral gas temperature with altitude. This makes the atmosphere unstable and small disturbances like vertical gradients in neutral wind can give rise to convective overturning which results in neutral turbulence. This turbulence is imparted to the Plasma through collisions with positive ions.

The above mentioned irregularities were first invoked to explain the origin of weak partial reflections from

D region by Gardner & Pawsey (1953). They estimated a value of 2% for the amplitude of irregularities, for scale sizes about 18 meters. The amplitude of irregularities detected in the present study is about 1% in the scale size 1-15 meters. The present results are therefore roughly in agreement with that of Gardner and Pawsey and support the theory of production of these irregularities due to convective overturning.

The region between 80 to 90 Km is characterised by large wind shears, which give rise to turbulence. Wind shears have been observed around 90 Km over Thumba by Bhavsar and Ramanuja Rao(1965). The diurnal behaviour of these shears is not known yet. Hines (1963) believes that internal atmosphere gravity waves play dominant role in this altitude region. These waves are physically similar to tidal and planetary waves in which earth's gravity plays important role. Hines suggested that gravity wave oscillations lead to density variations of the neutral atmosphere which would give rise disturbances in Plasma. Wind shears produced by the gravity waves could lead to turbulence and turbulence in the presence of ionisation gradients will produce ionisation irregularities. First large scale eddies are produced and these in turn produce small scale eddies till viscous dissipation sets in.

The amplitude of the irregularities produced by neutral turbulence can be estimated from the following equation:

$$\left(\frac{\Delta N_e}{N_e} \right)^2 \approx \frac{1}{3} l_0^2 \left(\frac{\text{grad } N_e}{N_e} \right)^2 \approx \frac{1}{3} l_0^2 \times \alpha^2 \quad (22)$$

where 'Ne' is background electron density and l_0 is size of largest eddy. The factor $\frac{\Delta Ne}{Ne}$ gives half the peak to peak amplitude used in the present analysis.

On night time flight 20.08 the irregularity size of 240 meters at 87 Km had an amplitude of about 15%. The value of α is tabulated in table 7. The value of α around 87 Km is 1.13 Km^{-1} . Amplitude of about 30% in present study can be accounted from the above formula. The results are thus in fair agreement with the theory. No small scale size irregularities were observed below 90 Km. On this flight the irregularities observed above 90 Km are of different type and will be discussed later.

During evening flights 10.11 and 10.13, both large scale and the small scale irregularities were observed. The irregularities of scale size 30-40 meters have amplitudes as large 20%. Such large amplitudes can't be explained by neutral turbulence. The scale sizes 1 to 15 meters have been observed both in 100 Km as well as 140 Km regions. These scale sizes being much smaller than the neutral mean free path, their production cannot be explained by neutral turbulence.

During evening hours, the small scale irregularities were observed along with large scale irregularities in 85 to 95 Km region. They occur in bursts. Table 5 shows the amplitude of bursts and their sizes. The bursts are randomly separated. In the 95 to 105 Km region, the occurrence of the

small scale irregularities become continuous. Also the smaller scale sizes dominate over the larger one with increasing altitude, which is contrary to what would be expected for neutral turbulence. As discussed in Chapter II, the Kolomogorov microscale i.e., size of the smallest eddy should increase with altitude. Scale sizes as low as 1 meter which is even less than the electron mean free path have been observed around 100 Km. Such features cannot be accounted by the neutral turbulence.

The spectral index of -3.5 is much smaller than what would be expected from neutral turbulence. The spectral index due to neutral turbulence has a value of $-5/3$. This may indicate that either the efficiency of production of the small ionization irregularities from neutral eddies is smaller or that the attenuation of small scale size is much larger. The occurrence of small scale irregularities in large amplitudes and more or less continuous manner support the idea that the production of the small scale irregularities from neutral turbulence is less efficient than the large scale ones.

Another form of instability, a cross field instability which requires the presence of D.C. electric fields and a background gradient in the electron density has been recently considered by Tsuda et al (1966, 1969) and by Reid (1968) with a view to explain the formation of sporadic E and spread F irregularities. This mechanism needs a specific relation-

ship between the direction of the applied electric field and the sign of the background electron density gradient. With a negative electron density gradient the direction of the ambient horizontal electric field needs to be westwards. It is expected that the electric field in the equatorial E region which is eastward during daytime becomes westward during night time (Balsley 1966, 1969 a, b; Romero et al 1968). Balsley experimentally demonstrated this reversal from the movements of the small scale irregularities of scale size of 3 meters. It has been observed that the reversal takes place late in the evening (Romero et al 1968).

The vertical field arises due to Hall polarisation and its magnitude is a function of σ_2/σ_1 , where σ_1 and σ_2 are the Pederson and Hall conductivities respectively. This factor σ_2/σ_1 increases from 9 to 28 in altitude region 90 to 100 Km. and again decreases to about 10 at 110 Kms. Around 85 Km, this factor is about 4. The eastward electric field gives vertically upward directed Hall polarisation field while the westward field produces Hall field in downward direction.

The vertically upward electron density gradients need the electric field to be in upward direction if the cross-field instability is to become operative. If either of them reverse direction, the medium will be stable and the cross-field instability will be inhibited.

The electron density gradients below 90 Km are always in upward direction and hence, the cross-field instability is operative during afternoon and evening periods, while it will be inhibited during mid-night below 90 Km.

The experimental results of present study below 90 Kms are in agreement with cross-field instability theory. It is not evident whether the scale sizes of (1-15) meters can be explained by this mechanism. In the height region below 90 Km, no irregularities (1-15 meters) were seen during nighttime while they have been observed during day and evening times. The absence of large scale irregularities (30-300 meters) below 90 Kms during nighttime may be due to the absence of wind shears.

The results of irregularities in the 90-120 region of mid-night flight 20.08 has been ideal for the study of the cross-field instability. As already mentioned, the electron density profile on this flight exhibits large structures, a few Kms in vertical extent, giving rise to positive as well as negative electron density gradients in this altitude region. Since Hall polarisation field is directed vertically downward during night, the occurrence of irregularities of scale sizes 30-300 meters in this region of negative gradients of electron density confirms qualitatively the production of these irregularities due to cross-field instability mechanism.

The irregularities associated with cross-field instability were found to occur randomly and hence have some similarity with those produced by neutral turbulence.

For a given gradient in background electron density and applied electric field, there is a lower limit λ_{min} for the scale sizes of the irregularities that can exist in a given region of the ionosphere. This limit is proportional to

$$\sqrt{\frac{1}{\alpha E}}$$

where α and E have usual meanings. With $E=1$ mv/m and $\alpha = 1 \text{ Km}^{-1}$, the analysis of Tsuda et al (1969) gives a lower limit of 100 meters for the irregularities in the 100-120 Km region. The factor for the major structures in the electron density profile range from 0.3 to 2.0 Km^{-1} and electric fields of the order of 1 to 2 mv are known to exist in the E region heights. Hence the 30-300 meter irregularities can be quantitatively explained by the cross-field instability mechanism.

The small size irregularities which are observed in the height range 95-120 Km in regions where there is a large negative gradient in electron density. This suggests some relationship with electron density gradients. The height range 95-120 Km where they occur suggests a relationship with the electric fields that are expected in that region (the region of the electrojet). It would be difficult to explain these irregularities on the basis of the presently known theory of the cross-field instability mechanism. Large electric fields will have to be assumed if the theory in

its present form is extended to these scale sizes.

Balsley (1967) has recognised the existence of two different types of irregularities in the electrojet region from the VHF radar echoes. One type which is seen only for a few hours around noon is due to the two stream mechanism and consists of plane wave irregularities with a wavelength of a few meters. But this mechanism would not be related to the electron density gradients and would not distinguish between the signs of the gradients. The second type of irregularities recognised by Balsley occur both during the day as well as during the night. They are considered to be due to a form of plasma turbulence arising out of large shears in electron velocity. In the presence of an applied horizontal (east-west) electric field E , the horizontal electron velocities at E-region heights are due to (a) a Pederson mobility due to the ambient field and (b) a Hall mobility due to the vertical polarisation field $E_p = \frac{\sigma_2}{\sigma_1} E$. Where σ_1 and σ_2 are the Pedersen and Hall conductivities. In the entire height region under consideration, the Hall mobility is predominant. Therefore, if we assume the applied horizontal electric field to be constant in height, the profile of the horizontal electron velocities will follow the $\frac{\sigma_2}{\sigma_1}$ profile in this height regions. The conductivities σ_1 and σ_2 and hence the ratio $\frac{\sigma_2}{\sigma_1}$ is critically dependent on the values of the ratios $\frac{\nu_e}{\omega_e}$ and $\frac{\nu_i}{\omega_i}$, ν_e and ν_i are the electron and ion collision frequencies while ω_e and ω_i represent the gyro-frequencies for electrons and ions respectively. The ratios

$\frac{v_e}{w_e}$ and $\frac{v_i}{w_i}$ change rapidly in the height range of interest. While the gyrofrequencies are known fairly, accurately, the same cannot be said of the collision frequencies. The day time and the night time values of the collision frequencies, and their variation with height in the region the 90-120 Km are not known clearly from direct experiments. Computations based on a standard atmospheric model such as the CIRA 1965 do not give any difference between the day time and night time values of $\frac{\bar{v}_2}{\bar{v}_1}$ even though such variations probably exist. A height profile of $\frac{\bar{v}_2}{\bar{v}_1}$ has been worked out by several workers (for ex. Sugiure and Cain 1966). Their results show that $\frac{\bar{v}_2}{\bar{v}_1}$ (and hence the electron velocity) maximises around 100 Kms and large shears can be expected in the electron velocity on either sides of the 100 Km level in the entire height region of interest. Since the actual values of v_e and v_i may be different from the model values and since the ratios $\frac{v_e}{w_e}$ and $\frac{v_i}{w_i}$ undergo large variations in the height range of interest, (table 1 page 28), a meaningful quantitative analysis cannot be carried out. But qualitatively it can be seen that large shears in electron velocity are possible in the height regions where the irregularities with $\lambda < 15$ m have been observed. Hence, plasma turbulence can be expected at these heights. This however, does not explain why these irregularities exist only in regions of negative electron density gradient. The complete lack of these irregularities in regions of positive electron density gradient suggests that the negative gradient ^{how} some helps in generating these irregularities while a positive gradient inhibits it. Plasma turbulence

does not seem to play dominant role (if any) in the generation of these irregularities. Same is probably true of the two stream instability mechanism which will be effective in region where electron velocities are maximum i.e. around 100 Km. However, the possibility of more than one mechanism operating simultaneously cannot be completely ruled out.

The small scale as well as large scale irregularities were observed between 90-110 Km region on two evening flights and small scale on afternoon flight, where the electron density exhibits positive gradient in upward direction. Irregularities of 30-300 meters, therefore can be explained on the basis of cross-field instability on both the evening flights.

The spectral index of small scale irregularities was studied on two flights and needs some comments. This index was -2.5 around 87 Km on evening flight and increases to a value to a value of about -1.8 at 105 Km this increase is contrary to what is expected for irregularities produced by neutral turbulence. The large scatter in the spectral index value indicates that the irregularities of two different types co-exist in the medium. The increase of the spectral index with height indicate that irregularities less than a particular scale size may have longer life compared to large scale size irregularities. This is probably true for electron waves where positive ions do not play important role (Spitzer, 1962).

The irregularities of scale sizes less than 15 meters observed around 100 Km region for the evening flights and afternoon flights cannot be explained on the basis of cross-field instability, hence other mechanisms like two stream instability and plasma turbulence have to be invoked.

The value of spectral index of scale size 1-15 meter for night time flight are similar to the values obtained for the irregularities observed during mid-night. This suggests that the mechanism responsible for the generation of the irregularities is same at both these times. Since at the time of both these observations, the electron density gradients were large the importance of any competing mechanism can be assessed only by observing the nature and the spectrum of the irregularities at a time when the electron density gradients are small.

The irregularities in 1-15 meter size observed around 145 Km during evening flight have spectral index of -2.0 and does not show much scatter. Due to their small scale sizes, the production of these irregularities cannot be explained by the cross-field instability mechanism and some other mechanism is necessary to explain their production. The spectral index values of about -1.0 seen between 155-160 Km are due to overlap of spectra of the rocket produces irregularities and irregularities in the ambient medium similar to that of 145 Km. Only the lower end of the spectrum of the rocket induced irregularities was studied with the system and hence a positive spectral index observed for them.

6.4 Irregularities due to rocket motion

The disturbances produced by moving rocket were studied on two evening flights and on one mid-night flight between 155 to rocket apogee i.e. upto around 175 Km. On one evening flight 10.11 signals were studied in frequency band $880 \pm 15\%$ Hz while on rest two flights signals were studied in frequency band 70 Hz to 1 KHz.

The percentage amplitudes of irregularities produced due to rocket motion are shown in figures 33, 35, 45 for two evening and one mid-night flights respectively. The irregularities i.e. ion acoustic waves produced by vehicle motion were observed above 150 Km and upto the apogee where rocket motion is subsonic. The observed amplitudes were about 1% of the ambient medium. The observed frequencies were around 500 Hz and above. The noise amplitude during ascent was higher than during descent and varied with rocket spin. The noise amplitude was found to be dependent on (a) probe potential, (b) rocket velocity (c) rocket spin.

These fluctuations were observed when the sensor was kept at a positive potential with respect to ambient plasma and the fluctuation amplitude was found to increase with increase in probe voltage. The telemetry record at 171 Km in fig. 47c, (2nd channel from top) illustrates some of the features of this noise. It can be seen for the comparison of channel 2 and 3, that as the probe voltage

increases, the amplitude of noise also increases. The variation of the noise amplitude with rocket spin can also be seen from this figure. The above features can also be seen in the spectrum analyser output record Figure 48c. The first channel in figure 48c shows the composite noise while the rest of the channels show filter outputs in ascending order of frequency. From the record it is clear that only high frequencies are present at this height. The amplitude is maximum in the bottom channel whose frequency is $900 \pm 20\%$ Hz.

The values of the spectral index for the evening and night time flights (fig.38, 46) varies from +1 to +3 from 155 to 175 Km. The observed positive spectral index arises from the fact that only the lower end of the spectrum of these irregularities was studied by the present instrument. These fluctuations were observed around rocket apogee when it is moving nearly horizontally, with its axis in the vertical direction. In this case the angle of attack is about 90° . The rocket velocity around apogee is about 250 meters/sec. The size of the body in this case is equal to the diameter of the Apache body which is 18 cm. The ratio of the body velocity to its size is a measure of self frequency of oscillations of the body and the scale of expected frequency spectrum of waves excited in plasma by the moving rocket. The value in present case is 1.6 KHz.

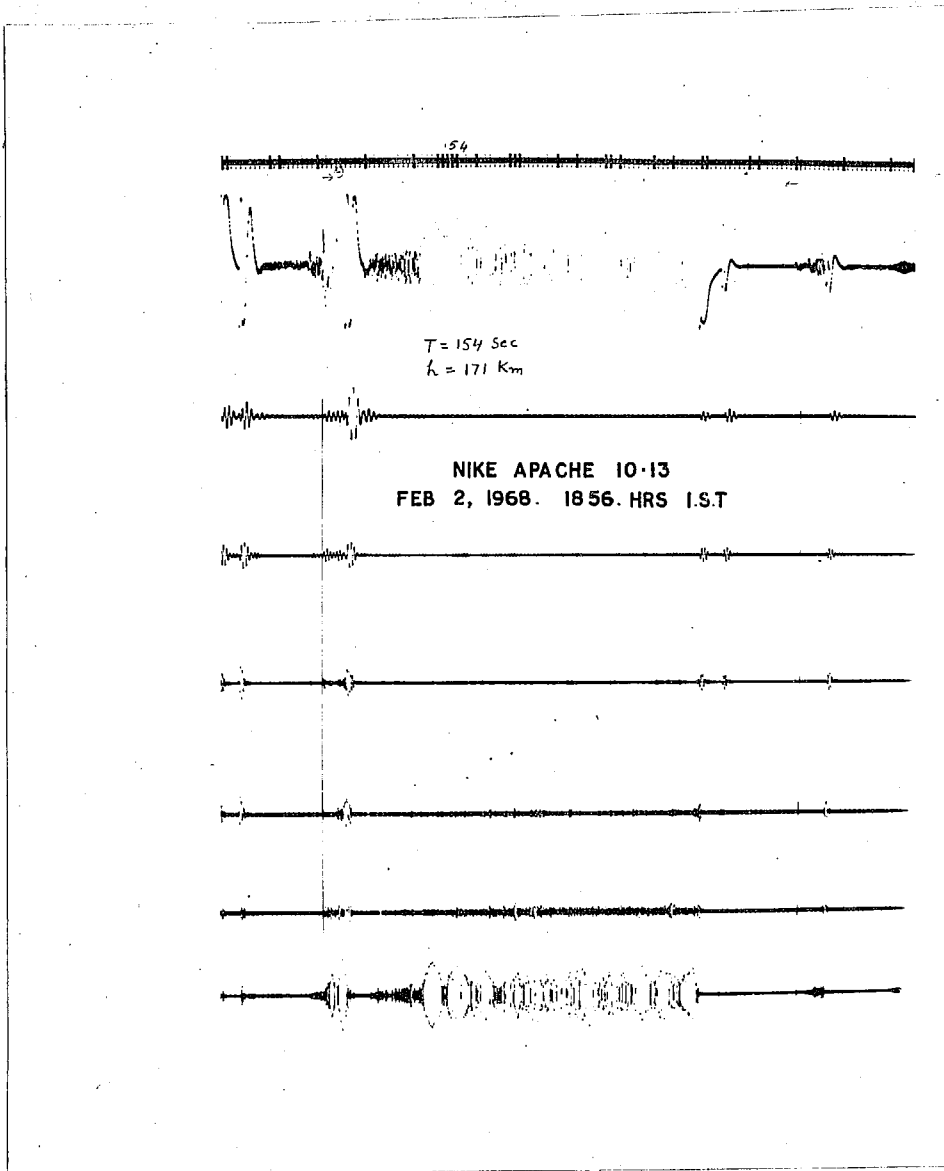


Figure-48c : Spectrum analyser output record at 171 Km.

6.4.1 Discussion

It is believed that in the wake region of the vehicle moving through the ionised media, ion acoustic waves are generated. For a supersonic motion this wake region can extend as long as ten times the dimensions of the body (Alpert 1965).

As already discussed in Chapter III, the frequency of the waves generated due to rocket motion lies in the range 0.1 to 1.0 ω_i . (Gurvich and Pitivesky 1965). The ion plasma frequency around 175 Km altitude during evening and night hours is about 5 KHz while during noon hours it is 18 KHz. Since the bandwidth of the amplifier was 70 Hz to 1 KHz these disturbances were studied only for the evening and mid-night flight.

Study of the disturbances produced around a body travelling through a plasma is of importance in many problems. Extensive theoretical analysis is carried out for supersonic speeds by Alpert et al (1965). A satellite moving with a velocity about 8 Km/sec at altitudes between 500 Km to 1000 Km has velocity about three times the ion thermal velocity. The present situation is quite different. Firstly the measurements were carried out with rockets whose velocity is comparable or even less than the ion thermal velocity. At these lower vehicle speeds electric fields will play a more important role because they have larger time to influence the motion

of the ions. Hence the theories developed for satellite motions cannot be applied to rocket motions. Secondly the shape of the satellite body is generally spherical while for rockets a cone cylinder configuration should be considered.

As already pointed out in Chapter III, a space-craft will detect the disturbances produced by its motion only when it is subsonic. Such conditions are realised by a rocket around its apogee and provide an ideal situation to study ion waves excited by the vehicle. The dimensions of the rocket are much smaller than the mean free paths of charged particles at heights above 150 Km. Thus the collisions between charged particles do not have any important influence on the disturbances to the concentration of the particles in the vicinity of the rocket.

The efficiency of the rocket to produce and detect the disturbance depends on its velocity. Around 100 Km the rocket is supersonic and its efficiency for producing ion waves is high. But here it is least efficient in detecting these waves as the waves are unable to reach the rocket body. On the other hand, when rocket is subsonic i.e. around apogee its efficiency for producing the disturbances is low but the probe will be most efficient to detect these disturbances.

For supersonic motion the amplitude of the disturbance can be as high as 50% - 100% of background medium. For subsonic motion the wave amplitude would be less by an order

of magnitude. The frequency of oscillations of the waves is likely to be less than the ion plasma frequency for both supersonic and subsonic motion. In present study the amplitude of the observed fluctuations was about 1%. As the efficiency of detection of these waves is not known, the ambient amplitude may be even an order of magnitude higher.

The ion plasma frequency around 170 Km is about 5 KHz in evening and has nearly the same value around midnight also. The observed frequencies of around 1 KHz are therefore in good agreement with Gurevich and Pitavsky's theory.

6.5 Equatorial D-region electron density profile

On examining the electron density profile between the heights 60 and 100 Km obtained on the afternoon flight (1415 Hrs, I.S.T.), figure 39 we find that the electron density increases more or less monotonically in this height region. There is no evidence of any layer or valley. This profile can be compared with that of Smiddy and Sagalyn(1967) for noon hours which was also obtained over the equator. Smiddy's profile shows a well defined layer at 75 Km and valley at 85 Km. The difference may partly be attributed to difference in solar activity. The solar flux index on 28th August 1968 was 119 while on 20th March, 1965 (corresponding to Smiddy's profile), it was 74. Moreover there was a short radio wave fadeout during the time of launch, 1415 hours I.S.T.

on 29th August, 1968. From these observations it can be inferred that due to relatively high solar activity the valley between 75 to 90 Km was filled up by enhanced ionisation which is attributed to increased X-ray flux.

The absolute values of electron density below 90 Km are uncertain since the Langmuir probe theory is not applicable in the D-region (see page 42). In the height range below 90 Km the actual electron density values are uncertain by a factor which gradually increases with decreasing height. This feature prohibits any serious attempt of a quantitative study of the data in terms of photochemical processes occurring in this regions. However the present electron density values can still be compared with those obtained by propagation experiment for a day on which solar activity was nearly same (Kane 1969). Table below gives the results of two techniques.

Langmuir probe measurement
over Thumba dip $0^{\circ}.47^{\circ}\text{S}$,
29th August, 1968.

Propagation technique Korokoni
(Greece) dip 34°N , May 1966.

14.15 Hrs. I.S.T.		13.00 Hrs. I.T.
Altitude	Ne/cc	Ne/cc
70	8×10^2	3×10^2
80	3×10^3	10^3
88	1.5×10^4	10^4

6.6 The equatorial E-region during afternoon hours

Referring to figure 39, we see that the electron density value increases monotonically from 85 Km to 110 Km and then remains more or less constant. No sporadic E layer has been observed around 105 Km. Ionograms taken during the flight by the C 4 recorder at Thumba show strong non-blanketing 'sporadic-E' layer of type E. It has been known (Bowles and Cohen, 1962) that the origin of the such 'sporadic-E' ionogram record is due to radio wave scattering from irregularities. Probe measurements conducted during 15.30 hrs, I.S.T. by Maynard and Cahill (1965) and ^{their} his group over Thumba do not indicate the presence of sporadic E layer in agreement with the present result. Langmuir probe experiments conducted by Aikin and Blumle (1968) over the coast of Peru around mid-noon did not report any enhanced ionisation at 100 Km. Our results are in agreement with Aikin and Blumle and Maynard & Cahill's results. The small scale irregularities observed in the height region 90 to 100 Km has been already discussed earlier.

6.7 The equatorial E region during evening twilight

The flights 10.11 and 10.13 took place during evening twilight on two days of low solar activity and high solar activity respectively, Figures 30 & 34.

A comparative study of the electron density profile shows that after sunset on extremely quiet days the electron

density increases by an order of magnitude within a few Km around 90 Km. Whereas on highly disturbed day for flight 10.13 there is a more gradual rise from 80 to 90 Km. In flight 10.11 no ionisation was observed below 85 Km while in 10.13 the ionisation has been observed even upto 78 Km. The region 78 to 85 Km is ionised by Lyman alpha and solar X-rays $2 - 8 \text{ \AA}^0$. The solar X-ray flux varies by a large factor from a quiet day to a disturbed day. The day (2nd Feb., 1968) was characterised as a highly disturbed day and a solar flare of importance two was reported at 1500 hrs, I.S.T. (Boulder Prediction Centre, USA). Solar activity remained high throughout the day. It is most probable that the pre-sunset electron density on 2nd Feb., 1968 was much more than on 12th March, 1967, so that the electron density took more time to decay after sunset.

Above 95 Km especially in the 100 to 120 Km region, the electron density profile on both the days are similar. This is due to the fact that the day time ionisation in this region is due to solar ultraviolet radiation in the Lyman beta and Lyman continuum from the sun and these radiations are relatively insensitive to solar activity. Both the evening time profiles show the presence of a valley around 125 Km. which becomes deeper during mid-night fig.42.

Comparison of the electron density profiles of 10.11 and 10.13 in an altitude region around 140 Km shows a layer in

both the flights. In 10.11 a clear layer is seen with an electron density of 2×10^4 ele/cc with a sharp increase within a few Km both in ascent and descent. This layer is known as E_2 layer in literature (for ex. Rastogi 1954). The profile of 10.13 shows a gradual increase in ionisation from 120 to 150 Km and then a nearly constant value afterwards. This difference may be possibly due to the difference in solar activity on these days. Sharp well defined E_2 layers may be more common on quiet day while broad E_2 layers may be characteristics of the high solar activity (Satya Prakash et al, 1969).

6.8 The E-region over Thumba around mid-night

The electron density profile for flight 20.08 (23.00 hrs.I.S.T.) is shown in figure 42. There is a steep rise in electron density from 85 to 90 Km region. Electron densities as high as 10^4 ele/cc have been observed both during ascent and descent at 102 Km height. This profile has some very interesting features. Between 95 to 120 Km region large variations in electron density (by a factor of 4 to 20) having a vertical scale of a few Kms have been observed. The maxima and minima in electron density coincide very well during ascent and descent indicating that such structures extend in east-west direction for more than 100 Kms. One or more layers of sporadic E with a fairly large value for ratio between the electron density within the layer to that outside

the layer have been detected earlier over mid-latitudes during the night time by rocket borne, Langmuir Probes (Smith 1966). Also the profile of fig.42. exhibits multiple layers. There is not enough experimental evidence to show whether the occurrence of such layers in the equatorial E region is a regular phenomenon or the present observation represent an exceptional case.

The most popular mechanism for the formation of dense thin layers in the E region is the mechanism of wind shears. But this mechanism in its present form does not operate successfully in the equatorial region. At present it is not possible to explain the observed layers on the basis of any other known mechanism.

A deep valley is observed both in ascent and descent between 115 to 140 Km, centered at 125 Km where the electron density goes down to a value as low as 10^2 ele/cc. The electron density increases monotonically from this value upto the rocket apogee at 175 Km.

6.8.1 Explanation for high electron density in the equatorial E region and the valley in the 120-140 Kms region during mid-night.

The likely sources of ionisation during mid-night over geomagnetic equator can be scattered solar Lyman alpha and Lyman beta. Galactic X-rays can also be a source of ionisation; however their intensity, as known today is too

small to produce any reasonable effect. Ogawa and Tohmatsu (1966) have used scattered Lyman alpha flux and a nitric oxide density of $5 \times 10^7/\text{cc}$ with a Lyman Beta flux 10^8 in a model of night time E layer which yields electron densities of the order of $10^3/\text{cc}$ around 100 Kms during night. Using these flux values, the maximum electron density of 10^3 ele/cc can be achieved during mid-night hours. The observed electron densities are higher by an order of magnitude. The scattered ultraviolet radiation cannot directly account for such high electron densities.

It has been suggested that in the equatorial E region there is a downward transport of ionisation during mid-night hours from F-region. Vertical drifts of magnitude about 5 meters/sec. have been observed in the F region over Jicamarca by Woodman & Hagfors (1969) and Falsley (1969 a,b) at 400 Km altitude. But no measurements have been made to find vertical drifts in the equatorial E region. If such drifts are present in the E region, they can give rise to electron densities that are observed in the present experiment.

Another interesting feature of the night time E region is the presence of a deep valley in the 120-140 Km region. The electron density at 125 Km is 10^2 ele/cc while at 100 Km, it is about 10^4 ele/cc. It may be noted that during evening twilight flights indications of such valleys have been observed (figures 30 and 34). The evening

time vallies are not so deep. As indicated earlier night-time vallies have been observed over equator by Satyaprakash et al (1967), Aikin and Elum'e (1968), and over mid-latitude by Smith (1966). From these results the presence of such a valley in the night-time E region can be taken as a common feature.

A possible explanation of the vallies would be the night time presence of a source of ionisation which has a production profile exhibiting a fairly sharp minimum around 120 Km. Ionisation due to scattered Lyman alpha during night has such features. It shows a maximum production rate around 100 Km and a minimum around 125 Km. With such a production profile and an allowable margin for the variation in the recombination coefficients, it is possible to reproduce an electron density similar to that shown in figure 42. In addition to Lyman alpha, scattered Lyman beta radiation is also present during night time hours. The production profile due to Lyman beta does not show the features required for a valley between 120 to 140 Km region.

Probably the presence of a night time source of ionisation together with the movement of ionisation from above can give rise to observed electron density profile.

6.9 Electron temperature in the equatorial E region

The electron temperature values of the mid-day, evening and mid-night flights are shown in figures 40, 32,

42 respectively. On the mid-night flight 20.08, there is a gap in the 120 to 140 Km height region. This is due to the low ambient electron densities. For comparison purposes, the neutral gas temperature is also plotted. Following are the main features of the observed electron temperatures in the equatorial E region.

1. The electron temperature; T_e is larger than the neutral gas temperature through out the height region 100 Km to 175 Km. Various workers have measured electron temperature in the E region over various latitudes at different times of the day and night. Their results have shown higher value of T_e compared to neutral gas in the E region (Smith 1969, Erace 1965, Satya Prakash 1969 a).
2. A common feature observed in all the flights was the ascent values of electron temperature were higher than descent values upto about 130 Km. This effect was first observed by Smith (1969) and he attributed it to aerodynamic heating of the tip sensor during ascent.

6.9.1 Discussion

The electron temperature T_e is an essential parameter of the ionosphere firstly because it reflects the sources of atmospheric heating which are present. Secondly it influences the rates of recombination and therefore

exercises a degree of control over the charged particle concentrations. In the forthcoming paragraphs, various sources of heat input to the electron gas are considered. The experimental results of Langmuir probe measurements over Thumba will be compared with the theory.

The equilibrium electron temperatures in the ionosphere are determined by the heat input to the electron gas and the various loss processes. Absorption of solar radiation produces a general heating of the atmosphere. But Joule heating due to ionospheric currents is also an important source for input energy.

The total photon energy available at 150 Km is about 1.2 Kev/cc/sec for H_e 304 \AA for noon conditions (Hanson and Johnson 1961). From the expression given by Dalgarno et al (1963) this much energy cannot raise the electron temperatures more than 100°K above the neutral gas temperature.

Other source of heat input in the equatorial E region is Joule heating due to the dissipation of electrojet currents. The heat flux available due to Joule heating is about 10 Kev/cc/sec., in the electrojet region during mid-noon hours when the electrojet current intensity is maximum. During other periods of the day and night this value will be much smaller than 1 Kev/cc/sec due to large decrease in current intensity.

The results of electron temperature of all the

flights show that even around 100 Km, the electron temperature is larger than neutral gas temperature by 500°K . An input energy of about 5 Kev/cc/sec. is needed to give rise to such high values. As already discussed the heat input due to solar radiation around noon is about 1 Kev/cc/sec. at 150 Km. The energy available from Joule heating is also less than 1 Kev/cc/sec. during the periods when flights took place. Neither the solar radiation nor the electrojet current can account for higher values of electron temperature compared to neutral gas temperature.

It is important to note that Langmuir probe electron temperature measurements are based on the assumption that the electron energy distribution is Maxwellian. But in practice only about a few percent of electrons (compared to electrons collected at space potential) are involved in determining electron temperature. The measurements could be in error if for example the electron distribution were very nearly Maxwellian around the most probable energy but deviated from the Maxwellian form in the 'tail'. Such condition might occur when electron to neutral collision frequency is a function of electron energy (Talbot 1960).

CHAPTER-VII

SUMMARY AND CONCLUSIONS

The equatorial ionosphere represents an ideal magnetoionic media to study plasma instabilities. The study of these instabilities in the laboratory, plasma becomes difficult as a field free plasma is difficult to realise in the laboratory. Some of the plasma instabilities are responsible for the production of ionospheric irregularities. These ionospheric irregularities are responsible for many ionospheric phenomena like non-blanketing type sporadic E and spread F in the equatorial ionosphere.

The rocket borne plasma noise probe incorporated with the Langmuir probe was employed by the author to study equatorial E region irregularities in the scale sizes 1-15 meters over Thumba (dip latitude 0.47°S). The system is capable of studying probe current fluctuations as low as 0.05%. The scale sizes greater than 30 meters were studied directly from the Langmuir probe outputs. The observed current fluctuations are due to electron density fluctuations in the neighbourhood of the probe.

The present system was also employed to study the local disturbances produced by the rocket itself. These disturbances are studied best when the rocket is subsonic,

i.e. around rocket apogee. The rocket borne Langmuir probe and plasma noise probe study carried out over Thumba have shown very interesting features of equatorial E region irregularities, electron density and electron temperature. Following is the summary of the main results :

- i) On an afternoon flight, the small scale irregularities (1-15 meters) with amplitude of about 0.5 - 1.5% were observed between 60 to 100 Km. No large scale (30 to 300 meters) irregularities were studied on this flight. The irregularities in the 60-80 Km region are probably due to convective overturning in the neutral atmosphere which gives rise to neutral turbulence.
- ii) The irregularities in 80 to 90 Km region observed on two evening flights and on the afternoon flight in scale size 1-15 meters with amplitudes about 1-2% are due to neutral turbulence. Neutral turbulence is effective even above this region. Large scale irregularities (30-300 meters) of amplitude as high as 20% observed in this region on two evening flights can also be attributed to neutral turbulence. Very few large scale irregularities were observed below 90 Km on the midnight flight while small scale irregularities were completely absent. On all the flights, the electron density profiles exhibit positive gradients upto 90 Km. The conditions existing in this region are also favourable to the growth of cross-

field instabilities for day and evening time.

iii) In 90-120 Km region large scale irregularities (30-300 meters) were observed on two evening flights in the region of positive electron density gradients. On midnight flight, the above irregularities were observed in the region of negative electron density gradients. Their occurrence can be explained on the basis of the cross-field instability mechanism.

iv) In the 90 to 120 Km region, the small scale irregularities 1-15 meters with amplitude 2-3% were observed in the same regions where large scale irregularities were observed. Their production cannot be explained on the basis of cross-field instability. From the height distribution of these irregularities, it is concluded that the two stream instability is not very effective for production of these irregularities during midnight hours. Same is true for plasma turbulence.

On two evening flights, small scale (1-15 meters) irregularities were also observed around 140 Km where electron density gradients were positive (in upward direction).

v) The spectral index for irregularities of scale size 1-15 meters increases from -3.5 to -1.8 in altitudes

region 90 to 105 Km, for evening flight. The spectral index exhibits a large scatter. Similar features were observed on midnight flight in altitude region 95 to 120 Km. The large scatter probably indicates the existence of more than one type of mechanisms operating simultaneously. For the evening flight the value of spectral index around 145 Km is -2.0 and does not show much scatter.

The increase of spectral index with height indicates that irregularities smaller than a particular scale size may have a longer life compared to that of the large scale sizes. This is probably true for the electron waves of scale sizes much less than the mean free path of neutral particles, where positive ions do not play important role in the propagation.

vi) The irregularities observed around rocket apogee i.e. 155 to 175 Km are due to ion acoustic waves generated by rocket itself. Their amplitudes are about 1-2% and frequency about 1 KHz. Their spectral index is +2.00 at 175 Km. The positive spectral index is due to the fact that only the lower end of the spectrum was studied. The frequency range lies well within the Gurvich and Pitavesky's dispersion relation.

vii) No enhanced electron density was observed in the 100 Km region during afternoon hours. The day time

configuration of equatorial sporadic E observed on the equatorial ionograms can only be explained from the scattering of radio waves from the small scale irregularities.

viii) The electron temperature values were higher compared to neutral gas temperature in the equatorial E region during afternoon, evening and midnight period. To explain the high values of electron temperature observed in the E region, heat sources with large energies are required. Solar radiation and electrojet current cannot account such high value of electron temperature.

ix) Around 100 Km., electron densities as high as 10^4 ele/cc were observed during midnight hours. Such high electron densities can be accounted by transport of ionisation from F region to E region if certain assumptions are made. Large structures in electron density were observed in altitude region 90 to 120 Km. Electron density varies by a factor of 4 to 20 within a few Kms within these structures. These structures may be as larger as 40-50 Km in the east-west direction. A valley was observed around 125 Km during midnight.

REFERENCES

- Aikin, A.C. and
L.J. Flumle (1968) Rocket experiments of the E region electron concentration distribution in the vicinity of the magnetic equator, J.Geophys.Res. 73, 1617-1625.
- Alpert, Y.L.(1965) Disturbances around a vehicle moving through the ionosphere, Aeronomy & Geomag. Vol.5 pp. 1-20.
- Alpert, Y.L.,
A.V.Gurvich and
L.P.Pitayvesky(1965) Space Physics with artificial satellite, Consultant Bureau, New York.
- Aiono, Y.,
K.Hirao and
S.Miyazki (1963) Rocket observations of ion density, electron density and electron temperature in the ionosphere, Radio Res. Laboratories 9, No.46.
- Balsley, B.B.(1964) Evidence of stratified echoing regions at 150 km region in the vicinity of magnetic equator during day light hours. J.Geophys.Res.69, pp.1925-1930.
- Balsley, B.F. (1965) Some additional features of radar returns from the equatorial electrojet, J.Geophys.Res.70, pp.3175-3182.
- Balsley, B.B. (1966) Evidence of the night time current reversal in the equatorial electrojet, Ann.Geophy.Vol.22, pp.460-462.
- Balsley, B.F. (1967) Evidence for plasma turbulence in the equatorial electrojet, Ph.D. Thesis, University of Colorado, Colorado, U.S.A.
Technical Memorandum IERTM, ESSA, USA, ITSA-89.
- Balsley, B.B. (1969a) Measurement of electron drift velocities in the night time equatorial electrojet, Jour.Atmos. Terr.Phys. Vol 3, pp.475-478.
- Balsley, B.B. (1969b) Night time electric fields and vertical ionospheric drifts near the magnetic equator, J.Geophy. Vol.74, pp.1213-1217.

(ii)

- Balsley, B.B., (1969c) Some characteristics of non two stream irregularities in the equatorial electrojet, Jour. Geophys. Res. Vol. 74, pp. 2333-2347.
- Fatchelor, G.K. (1956) The theory of Homogeneous turbulence. Cambridge University Press, Cambridge, England.
- Pettinger, R.T. (1965) An in situ probe system for the measurement of ionospheric parameters, Interaction of Space Vehicles with ionised atmosphere, Edited by S.F. Singer, Pergamon Press, New York, pp. 163-270.
- Bhavsar, P.D., and K. Ramanujarao (1965) A First study of atmospheric winds near the equatorial electrojet by Sodium Cloud technique. Space Research V pp. 986-996. Edited by P. Muller. (North-Holland Pub. Co., Amsterdam).
- Blamont, J.E., and DeJager (1961) Upper atmospheric turbulence near the 100 km level, Ann. Geophys. 17, pp. 134.
- Booker, H.G. (1956) Turbulence in the ionosphere with application to meteor trails radio-star scintillation, auroral radar echoes and other phenomena, J. Geophys. Res. 61, pp. 573-705.
- Bowles, K.L., E.B. Balsley and R. Cohen (1963) Field aligned E region irregularities identified with acoustic plasma waves, J. Geophys. Res. Vol. 68, pp. 2485-2501.
- Bowles, K.L., R. Cohen, G.R. Ochs and E.B. Balsley (1960). Radio echoes from field aligned ionisation above the magnetic equator, J. Geophys. Res. Vol. 65, pp. 1853-1855.
- Bowles, K.L., and R. Cohen (1962). A study of radio wave scattering from sporadic E near the magnetic equator - Ionospheric sporadic E, Edited by E.K. Smith Jr. and S. Matsushita, pp. 51-77, Pergamon Press, London.
- Bowles, K.L. (1964) Radio wave ^{scattering} in the ionosphere Advances in electronics and electron Physics. Academic Press N.Y. Vol. 19, pp. 55-176.

(iii)

- Bowen, P.L.,
R.L.F.Boyd,
C.L.Henderson and
A.F.Willmore(1964).
Proc. Roy. Soc. A, Vol. 281, pp.
514-525.
- Bourdean, R.E.(1963) Ionospheric Research from space
vehicles, Space Sci.Rev.1, pp.
683-728.
- Boyd, R.L.F.,(1968) Langmuir Probe on space crafts,
plasma diagnostics, Chapt.12,
Edited by Lochite-Holt-Greven,W
North Holland Pub.Co., Amsterdam.
- Boyd, R.L.F., and
A.F.Willmore(1962) A method of studying the energy
distributing of ionospheric ions
and electrons Space Research III,
Edited by W.Priester, North Holland
Pub.Co., pp.1168-1173.
- Frace, L.H. (1965) Electron temperatures in the lower
ionosphere, Aeronomy Report No.10,
Edited by C.F.Sechirst, Jr. & J.S.
Shirke, Department of Electrical
Engg. University of Illinois,
pp.8-14.
- Buneman, O.(1959) Dissipation of currents in ionised
media. Phy.Rev. 115, pp. 503-517.
- Buneman, O.(1963) Excitation of field aligned sound
waves by electron streams
Phy.Rev.letters, 10, pp.285-287.
- Cahill Jr.L.J.,(1959) Investigation of equatorial electro-
jet by rocket magnetometers, J.
Geophys.Res. 64, 484-503.
- Chapman, S., and
T.G.Cowling (1960) The mathematical theory of non-
uniform gases, Cambridge University
Press, Cambridge, England,
Chapter 18.
- Clamesha, B.R.(1963) The elongation of irregularities in
the equatorial ionosphere, J.Geophys.
Res.68, pp.2362-2366.
- Cohen, R.,
K.L.Bowles and
W.Calvert(1962) On the nature of equatorial slant
sporadic E, J.Geophys.Res.67,
965-972.

(iv)

- Cohen, R., and
K.L.Bowles (1963).
The association of plasma wave
electron density irregularities
with equatorial electrojet,
J.Geophys.Res. 68, 2503-2525.
- Cohen, R (1967)
The equatorial ionosphere,
Physics of geomagnetic phenomena
Vol.1, Chap.III, pp.561-613, Edited
by Matsushita, S., W.H.Campbell,
Academic Press, New York.
- Cohen, R., and
K.L.Bowles (1967)
Secondary irregularities in the
equatorial ionosphere, J.Geophys.
Res. 72, pp.885-894.
- C.I.R.A..(1965)
Cospar International Reference
Atmosphere, Compiled by the members
of the Cospar Group IV, North
Holland Pub.Co., Amsterdam.
- Dalgarno, A.,
McElory, M.E. and
Moffet, R.J.(1963)
Electron temperatures in ionosphere,
Planet.Space Sci., Vol.11, pp.
463-484.
- Davies, T.N.,
K.Burrows and
J.D.Stolark(1967)
A latitude survey of the equatorial
electrojet with rocket borne magneto-
meters, J.Geophys.Res.72,
pp.1845-1861.
- Davies, K., (1965)
Ionospheric Radio propagation, N.B.S.
Monograph, 80, Chapt.8.
- Deshpande, M.R.,
and R.G.Rastogi(1966)
Ionospheric horizontal drifts within
the equatorial electrojet region
in India, Ann.de.Geophy.Vol.22,
No.3, pp.418-421.
- Farley, D.T., Jr.
(1963)
A plasma instability resulting in
field aligned irregularities in the
ionosphere, J.Geophy.Res.68,
pp.6083-6097.
- Foster, L.E. (1965)
Telemetry systems, John Wiley & Sons,
Inc., Chapt.2, N.Y. USA.
- Gardner, F.F.,
and J.L.Pawsey (1953)
Study of the ionospheric D region
using Partial reflections.
J.Atmos and Terr.Phy.3 p.321.

(v)

- Gurevich, A.V., and L.P. Pitayveskey (1965) Hypersonic motion in rarefied plasma, *Phy. Rev. letter* 15, pp. 346.
- Hanson, W.B., and F.S. Johnson (1961). Electron temperature in the ionosphere, *Mem. Soc. Roy. Liege*, Vol. 4, pp. 390-424.
- Haerendel, G., R. Lust and E. Rieger, (1969) Preliminary results about Barium release near the magnetic equator at Thumba, Published in *Space Research IX*.
- Heikkila, W.J., (1965) Ionospheric probe. Auroral ionospheric report, South West Center for advanced studies, Dallas, Texas, U.S.A.
- Hines, C.O. (1963) Upper atmosphere in motion, *Quart. J. Roy. Met. Soc.* Vol. 89, No. 379, pp. 1-42.
- Hok, G., N.W. Spencer, and W.G. Dow (1953) Dynamic probe measurements in the ionosphere, *J. Geophys. Res.* 58, pp. 235-242.
- Maeda, K., T. Tsuda, and H. Maeda (1963) Theoretical interpretation of the equatorial sporadic E layers, Report of Ionosphere and Space Research in Japan, Vol. 17, pp. 147-158.
- Matsushita, S. (1962) Inter relations of sporadic E and ionospheric currents. *Ionospheric Sporadic E*, Edited by E.K. Smith Jr. and S. Matsushita, pp. 344-375, Pergamon Press, London.
- Maynard, N.C., and L.J. Cahill, Jr. (1965) Measurement of equatorial electrojet over India, *J. Geophys. Res.* 70, pp. 5925-5936.
- Mott-Smith, H.M., and I. Langmuir, (1926). The theory of collectors in gaseous discharges, *Phy. Rev.* 28, pp. 727-763.
- McNamara, A.G., (1965) Langmuir probe measurements of the auroral ionosphere at Churchill (Canada) Aeronomy report No. 10, Edited by Sechist Jr., C.F., and J.S. Shirke, University of Illinois, Urbana, pp. 22-25.

Kane, J.E. (1969)

D region electron density measurements during solar eclipse of May 20, 1966. *Plan and Space Sc.* 17 p. 609.

(vi)

- Penrose, O. (1960) Electrostatic instabilities of a non-maxwellian plasma. *Phy. of Fluids*, 258-265.
- Ogawa, T., and T. Tohmatsu. (1966) Photoelectric processes in the upper atmosphere. The hydrogen and Helium ultraviolet glow as an origin of night time ionosphere, Report on Iono. Res. in Japan, 20, pp.395-414.
- Ogbuechi, P.O., A. Onwumechilli and S.O. Ifedrli (1967) The equatorial electrojet and the world wide S_q currents. *J. Atmos. Terr. Phys.* 29, pp.149-160.
- Onwumechilli, A., (1967) Geomagnetic variations in the equatorial zone. *Physics of Geo. Mag. Phen.*, Edited by S. Matsushita and W.H. Campbell, Academic Press N.Y. pp.425-507.
- Oya, H. (1968) Ionospheric plasma disturbances due to a moving space vehicle, paper presented at COSPAR Symposium, Tokyo.
- Rastogi, R.G. (1954) Intermediate layers of ionisation between the E and F, layers of ionosphere over Ahmedabad, *Proc. Indian Acad. Sci. Vol. XL, Sec. A.* pp.158-166.
- Reid, G.C. (1968) The formation of small scale irregularities in the ionosphere, *J. Geophys. Res.* 73, pp.1627-1640.
- Romero, A.C., A.A. Giesecke and M.E.P. Oscar (1968) V.H.F. Ionospheric scatter propagation via the equatorial electrojet paper presented at symposium on propagation of radio waves, Oslo, Norway, August 19-22.
- Samir, U., and A.F. Willmore (1965) Distribution of charged particles near a moving spacecraft, *Plan. and Space Sci. Vol. 13*, pp.285-296.
- Sastry, T.S.G., (1968) Quiet day electrojet over Thumba, India, *J. Geophys. Res.* 73, pp. 1789-1794.

ya Prakash
• Subbaraya,
• Gupta (1967)

Rocket and Balloon studies published
by INCOSPAR.

(vii)

- Satya Prakash, and
B.H.Subbaraya(1967) Langmuir probe for the measurement
of Electron density and electron
temperature in the ionosphere,
Review of Sc.Inst.38, pp.1132-1136.
- Satya Prakash.,
B.H.Subbaraya, and
S.P.Gupta (1968) A study of equatorial E region during
evening twilight using Langmuir
probe, J.Atmos.and Terr.Phys. 30,
pp.1193-1202.
- Satya Prakash,
B.H.Subbaraya, and
S.P.Gupta (1969) a. A study of the lower ionosphere over
the geomagnetic equator Thumba using
a Langmuir and Plasma noise probe,
Space Research, IX.,pp.237-244,
Edited by Champion K.S.W.,
P.A.Smith and R.L.Smith Rose,
North Holland Pub.Co.
- Satya Prakash,
S.P.Gupta and
B.H.Subbaraya (1969.b) Irregularities in the equatorial
E region over Thumba, Radio Sci.
(new series, September issue). Vol 4 P 971
- Satya Prakash,
S.P.Gupta, and
B.H.Subbaraya(1970) Night time equatorial E region
irregularities ~~(to be published in~~
~~Planet and Space Science)~~.
Vol 18 P 1367
- Simon, A., (1963) Instability of a partially ionised
plasma in cross electric and magnetic
field, Thy.Fluid, 6, pp.382-388.
- Singer, S.F.,
E.Marle, and
W.A.Bowen (1951) Evidence for ionospheric currents
from the rocket experiments near the
geomagnetic equator, J.Geophys.Res.
56, pp.265-281.
- Singer, S.F., and
E.H.Walker (1965) Plasma compression effects produced
by space vehicles in a magnetoionic
medium (Interactions of space vehicles
with an ionised atmosphere) pp.
483-501, Edited by S.F.Singer,
(Pergamon Press, New York).
- Smiddy, M., and
R.C.Sagalyn (1967) Investigation of the electrical
phenomena in equatorial ionosphere,
Space Research VII, Vol.I,
pp.428-445, Edited by R.L.Smith Rose,
North Holland pub.Co.
- Smith, L.G. (1966) Rocket Observations of sporadic E
and related features of E region,
Radio Sci.1, pp.178-186.

(viii)

- Smith, L.G., (1967) Electron density and temperature measurements in the ionosphere, Revised version of Tech. Manual series COSPAR bulletin No.17, Edited by K.Maeda.
- Smith, L.G., (1969) Langmuir probes in the ionosphere, Small rocket instrumentation, North Holland Pub.Co., Edited by K.Maeda, pp. 1-15.
- Sptizer Jr., (1952) Physics of Fully ionised gases, Inter Science Publishers, New York.
- Stix, T.H., (1962) The theory of plasma waves, McGraw-Hill BookCo., INC.Chapter 2 and 9.
- Sugiura, M., and J.C.Cain (1966) A model equatorial electrojet 71, pp. 1869-1878.
- Subbaraya, B.H.(1968) Ph.D.Thesis, Poona Unive rsity, Poona, India.
- Talbot, L., (1960) Theory of Langmuir Probe. Physics of Fluids 3, pp.289-298.
- Tsuda, T., T.Sato and K.I.Maeda (1966) Formation of sporadic E layers at temperate latitudes due to vertical gradients in charge density. Radio Sc.(New series 1) pp.212-225.
- Tsuda, T., T.Sato, and S.Matsushita (1969) Ionospheric irregularities and cross field plasma instability, J.Geophys.Res. 74, pp.2923-2937.
- Untied, J. (1967) A Model of the equatorial electrojet involving meridional currents, J.Geophys.Res.72, pp.5795-5810.
- Weinstoke, J.(1968) Deducing the magnitudes of ionospheric irregularities from Backscatter, J.Geophys.Res. 73, pp.225-231.
- Watts, J.M., and J.N.Erown (1954) Some results of sweep frequency investigation in the low frequency band, J.Geophys.Res. 59, pp.71-86.
- Woodman, R.F., and T.Hagfors (1969) Methods for the measurement of vertical ionospheric motions near the magnetic equator, J.Geophys.Res. 74, pp.1205-1212.